THE KINETICS OF THE REDUCTION OF NICKEL SALTS BY HYDRAZINE

by

Michael Roy Edwards, B.Sc.(Eng.), A.R.S.M.

A Thesis submitted for the degree of Doctor of Philosophy of the University of London.

One Ring to rule them all, One Ring to find them,

One Ring to bring them all and in the darkness bind them

In the Land of Mordor where the Shadows lie.

ABSTRACT

The reduction of nickel chloride by hydrazine in aqueous solution on to a metallic substrate has been found to occur in a limited range of reagent concentrations. At other concentrations, the rate of reaction is very slow or the reaction takes place at any solid surface, depositing nickel as a metallic mirror. Using a rotating disc, the rate of reaction was found to be dependent on the chemical reaction at the disc, rather than the transport of reactants to the disc. The activation energy, over the temperature range 81 - 90°C, was found to be 18.3 $\pm$ 0.9 k.cals mole^{-1}. The rate of reaction was found to obey the pseudo-rate law:

$$\text{Rate of reaction} \propto \frac{[\text{total nickel concentration}]}{[\text{total ligand concentration}]\{H^+\}^2}$$

where ligand is the tartrate or malonate ion added to stabilise the solution. This equation is analysed semi-empirically to give an understanding of the reaction mechanism. The mechanism is postulated as the breakdown of a nickel-hydrazine complex at the substrate, electrons being transferred from the reducing agent via the substrate to the complex, thus producing nickel metal.

The nickel produced was analysed by X-ray diffraction to be an α-solid solution of hydrogen in nickel, with a maximum hydrogen content of H : Ni = 0.015. The deposits had no preferred orientation, whether deposited on single crystals or other substrates.

CONTENTS

CHAPTER 1 INTRODUCTION

In this work the reactions considered are those where an aqueous solution of metal ions is reduced by a reducing agent to metal at a substrate immersed in the solution. Thus the substrate is coated with a layer of metal. For this reaction to be of use, the deposition of metal on to the substrate should not be accompanied by homogeneous nucleation of metal powder, or a heterogeneous reaction, depositing metal on the walls of the reaction vessel. Substrates that will catalyse the reduction of metal ions are metal surfaces or non-metallic surfaces that have been sensitised with metal, for example by successive immersion in stannous chloride and a solution containing palladium ions (1). Once the first layer of metal has been produced, it acts as the catalyst for the following reaction. For this reason, this reaction is often called the autocatalytic deposition of metal. The reducing agents considered in this work are aqueous solutions, gaseous reductants such as hydrogen or carbon monoxide being ignored.

The first reaction of this type to be studied (2) was where nickel (II) ions were reduced by sodium hypophosphite in alkaline solution to produce a coating of nickel metal with a phosphorus content of about 3%.

1.1. Reduction of nickel (II) salts to nickel metal.

The first report of nickel salts being reduced to nickel metal was by Wurtz (3). He heated concentrated solutions of nickel ions and sodium hypophosphite together, and after prolonged heating, deposited metal as a mirror on the reaction vessel and also as powder. A simple method to obtain nickel as powder and a mirror on the container wall was discovered by Paal and Friederici (4). Using a 0.03 M solution of nickel sulphate with large excesses of sodium

acetate and sodium hypophosphite, and with 10 mg litre^{-1} of palladium chloride as a catalyst, they produced nickel metal within a few minutes on a steam bath. In none of these early experiments was there any attempt to deposit nickel on to a catalytically active substrate. The deposits of nickel contained amounts of phosphorus which varied from 2.7% for a bath containing an excess of ammonium salt as a complexing agent, to 13.1% for a bath using 2.5 M sodium hypophosphite as a reducing agent.

Consider the reaction (Symbols as in Appendix 1)

$$Ni^{2+} + H_2PO_2^- + H_2O = Ni^o + 2H^+ + H_2PO_3^- \qquad (1.1.)$$

Taking free energy data from Latimer (5):

$$\Delta G^c_{298} = -21.72 \text{ k.cals.} \qquad (1.2.)$$

$$\Delta G_{298} = \Delta G^o_{298} + RT \ln \frac{a_{H_2PO_3^-} \cdot (a_{H^+})^2}{a_{Ni^{2+}} \cdot a_{H_2PO_2^-}} \qquad (1.3.)$$

Let pH = 8 (2) and $a_{Ni^{2+}} = 10^{-2}$

$$\Delta G_{298} = -43.52 + 1.36 \log \frac{a_{H_2PO_3^-}}{a_{H_2PO_2^-}} \qquad (1.4.)$$

At equilibrium $\Delta G_{298} = 0$ and

$$\frac{a_{H_2PO_3^-}}{a_{H_2PO_2^-}} = 10^{32} \qquad (1.5.)$$

which means the reaction will continue even in the presence of a large excess of the oxidised phosphite species.

The assumptions made in this analysis are:

a) The calculations are made using data valid for 25°C, and the error in using this data is taken to be negligible.

b) The nickel is assumed to be in the form of uncomplexed Ni^{2+} ions.

c) The ammonium salts added act as a buffering agent only and do not interact with the nickel ions.

These assumptions are not strictly valid, but the calculation

generally shows that nickel ions will be reduced by hypophosphite ions, and that the reaction will take place, even in the presence of phosphite ions.

Since the process of reducing nickel ions to nickel metal was reported by Brenner (2), many variations of the process have been developed. They form two groups; the first being baths in which the deposition takes place at a pH of 8-9, of which the original B renner bath is one, and the second group uses acid solutions with a pH of 4.5-5.5. A typical bath of this second group is due to Giraud (6). Most deposition reactions take place at temperatures of 80 - 95°C., but one reported by Marton and Schlesinger (7) is operated at 25°C. In all these varied plating processes, the metal produced is always an alloy of nickel and phosphorus.

The structure of as-plated nickel-phosphorus alloy has been the subject of controversy. Goldenstein (8) postulated that alloys with 7 - 10 wt.% phosphorus had an amorphous structure, from his X-ray diffraction studies. The work of Marton and Schlesinger (9) on thin films grown at 25°C. on activated non-metallic substrates, suggests an as-plated liquid-like structure, which, when heat-treated, becomes a more crystalline solid structure. On the other hand, Graham (10) has suggested that the as-plated alloy is a crystalline solid, although it does contain a metastable supersaturated solid solution of phosphorus in nickel. On heat-treatment, the stable structure of α-nickel and nickel phosphide (Ni_3P) forms. These results applied to both acid and alkaline baths.

There is general agreement that deposits from hypophosphite baths, after heat treatment, consist of small particles of nickel phosphide in a matrix of α-nickel. The beneficial properties of this alloy coating are its high hardness and associated wear resistance, its corrosion resistance and its magnetic hysteresis loop characteristics (1). However, in certain applications, the

brittleness associated with the phosphorus is a serious disadvantage, and an alternative reducing agent has to be employed.

One such alternative is sodium borohydride, $NaBH_4$. In strongly alkaline solution it has been used to reduce nickel ions to nickel (11, 12). A very similar reducing agent is an alkyl borane, commonly diethylamineborane, $(C_2H_5)_2$. $NH.BH_3$, used by Lang (11) and McLeod (13). This is used in plating baths at a pH of 5 - 6 (11) and at a temperature of 55°C. In the following thermodynamic analysis, the standard borohydride reaction is considered, since more thermodynamic data is known of it, rather than the alkyl borane reaction. The same assumptions are made in the analysis, as were made for the similar analysis of the hypophosphite reaction in 1.1, with the same reservations, particularly as the complexing agent used, ethylenediamine, is a well-known chelating ligand.

Taking the overall reaction as:

$$BH_4^- + 4Ni^{2+} + 8OH^- \rightleftharpoons 4Ni^o + BO_2^- + 6H_2O \qquad (1.6.)$$

with free energy data from Latimer (5), except for the free energy of formation of the borohydride ion BH_4^- (aq.), taken as + 28.6 k.cal. $mole^{-1}$ (14), we get

$$\Delta G^o_{298} = -191.46 \text{ k.cal.} \qquad (1.7.)$$

$$\Delta G_{298} = \Delta G^o_{298} + RT \ln \frac{a_{BO_2^-}}{a_{BH_4^-} \cdot (a_{Ni^{2+}})^4 \cdot (a_{OH^-})^8} \qquad (1.8.)$$

Let pH = 13 $\quad a_{OH^-} = 10^{-1}$ and $a_{Ni^{2+}} = 10^{-2}$

$$\Delta G_{298} = -169.66 + 1.36 \log \frac{a_{BO_2^-}}{a_{BH_4^-}} \qquad (1.9.)$$

At equilibrium $\Delta G_{298} = 0$ and

$$\frac{a_{BO_2^-}}{a_{BH_4^-}} \sim 10^{120} \qquad (1.10.)$$

and the reaction will continue, even in the presence of a large excess of the oxidised metaborate species.

The product of the borohydride and alkyl borane reactions with nickel ions is an alloy of nickel with 5 - 7% boron. Structurally, the alloy resembles the nickel-phosphorus alloys described earlier, Winkler (15) describing it as an amorphous solid. The deposits harden after heat-treatment (11), and this would seem to suggest that the nickel-boron alloy is a metastable supersaturated solution of boron in nickel, similar to the metastable solution of phosphorus in nickel described by Graham (10). On heat-treatment, the stable state of α-nickel and nickel boride is formed.

The baths used have a tendency to decompose (13), forming both powdered nickel and a mirror of nickel on the container walls. Earlier work (16) had suggested that the product of reaction when nickel salts were reduced by borohydride, was nickel boride, Ni_2B. For a 6% boron alloy the proportion of boride, if all the boride is Ni_2B, is about 75%. Even if this is finely dispersed, the presence of boride will cause embrittlement.

Overall, the borohydride bath has some advantages, such as economy of reductant, over the hypophosphite bath, but the two major disadvantages of the hypophosphite bath remain. These are the impurity content of the nickel deposit and the tendency to brittleness.

A suggested reducing agent that should eliminate at least the first of these disadvantages is hydrazine, N_2H_4, and its use as a reducing agent will be considered in 1.2.

1.2. Hydrazine as a reducing agent.

The pure compound, hydrazine, N_2H_4, is a liquid at room temperature. Its vapour forms explosive mixtures with air or oxygen, and the liquid is also corrosive. For these reasons, reactions involving hydrazine are normally carried out using aqueous solutions of hydrazine or hydrazine salts. The most convenient form of hydrazine is the hydrate $N_2H_4 \cdot H_2O$, which is an equimolar mixture of

hydrazine and water. This may be further diluted with water if necessary.

1.2.1. Thermodynamics of hydrazine reduction reactions.

In alkaline solution, hydrazine is oxidised to nitrogen and water, according to the reaction:

$$4OH^- + N_2H_4 \rightleftharpoons N_2 + 4H_2O + 4e^- \qquad (1.11.)$$

Taking free energy data from Latimer (5):

$$\Delta G^o_{298} = -106.9 \text{ k.cals.} \qquad (1.12.)$$

Therefore, for the reduction of an ion M^{z+} to metal M to occur, the reaction:

$$M^{z+} + 4OH^- + N_2H_4 \rightleftharpoons M + N_2 + 4H_2O + (4 - z)e^- \qquad (1.13.)$$

should have a negative free energy. This means that the reaction:

$$M^{z+} + Ze^- \rightleftharpoons M \qquad (1.14.)$$

should have $\Delta G^o_{298} = +106.9$ k.cals., as a first approximation. This suggests that many metals can be reduced by hydrazine, and this is found to be the case. As an example, take the reduction of nickel (II) ions to nickel.

$$Ni^{2+} + 4OH^- + N_2H_4 \rightleftharpoons Ni + N_2 + 4H_2O + 2e^- \qquad (1.15.)$$

$$\Delta G^o_{298} = -95.43 \text{ k.cals. (5)} \qquad (1.16.)$$

$$\Delta G_{298} = \Delta G^o_{298} + RT \ln \frac{p_{N_2}}{a_{Ni^{2+}} \cdot (a_{OH^-})^4 \cdot a_{N_2H_4}} \qquad (1.17.)$$

Let pH = 11 $\quad a_{OH^-} = 10^{-3}$ and $a_{N_2H_4} = 1$

Since the nitrogen is being discharged into the atmosphere, $p_{N_2} = 1$ atm.

$$\Delta G_{298} = -79.03 + 1.36 \log \frac{1}{a_{Ni^{2+}}} \qquad (1.18.)$$

At equilibrium $\Delta G_{298} = 0$ and

$$\log a_{Ni^{2+}} = -58.2 \qquad (1.19.)$$

Therefore nickel salts will be reduced to metal until the activity of nickel ions is reduced to $10^{-58.2}$, that is, the reaction

will go to completion.

The assumptions made are the same as in the analysis of the hypophosphite reaction in 1.1. and have the same limitations. The thermodynamics of the reaction are so favourable that any hindrance to the reaction must be due to the activation energy of the reaction and other kinetic factors, rather than the thermodynamics, even when determined semi-empirically.

1.2.2. Production of metal powder using hydrazine.

The first work where hydrazine was used to reduce metal ions to metal, was that of Curtius and Schrader (17), who reduced a solution of gold (III) chloride to gold. Another use for hydrazine was in the determination of the atomic weight of selenium (18), where the ratio Se : SeO_2 was found by precipitating the selenium from a solution of selenium dioxide, using drop additions of hydrazine, according to the method of Jannasch and Muller (19). This reaction is so sensitive that it was used as a spot test for traces of selenium by Gutbier (20) and Montignie (21), and also for tellurium (22).

This use of hydrazine to precipitate metal as powder was later used as a gravimetric analysis for the elements of the platinum group. Platinum was precipitated by adding a dilute solution of hydrazine sulphate to a solution of potassium platinichloride by Jannasch and Stephan (23). For palladium (24), the same technique was used, except that palladium chloride was the source of palladium. Osmium (25) was produced by the action of hydrazine on a solution of potassium osmiate (K_2OsO_4) at 60 - 80°C. In all these reactions, the metal is first homogeneously formed as nuclei, which is the rate-controlling step, and the heterogeneous reaction at the metal nuclei takes place very fast, forming metal powder.

Mercury was produced in the form of black powder by Krauss and

Mählmann (26), who used a solution of iron (II) ions as a catalyst in the reduction of mercurous nitrate solution. This work was modified by Galatzky (27), who used a solution of mercurous oxide, without the use of the iron (II) catalyst.

Silver was produced, presumably as a powder, by Purgotti (28), who reduced an alkaline solution of silver nitrate to silver, with the liberation of nitrogen. Later work on gold and silver was concentrated on the precipitation of gold and silver from cyanide solutions (29) or the reclamation of gold from gold-antimony alloys (30). Both these methods produced powders free from base metals.

In the production of nickel, which should be thermodynamically possible according to 1.2.1., the initial work was done by Paal and Friederici (31). They used 0.15 M solutions of nickel (II) ions and a high concentration of palladium (II) ions as a catalyst (Pd : Ni = 0.06). On addition of a few drops of hydrazine hydrate, the solution decomposed to form a black powder or a mirror of metal. Since work described later in this thesis produced no powder, even at high temperatures, it is quite possible that the powder was formed by heterogeneous deposition of nickel on to palladium nuclei formed in the solution. The only production of nickel powder by reduction of nickel salts using hydrazine has been that reported by Sharov (32, 33). He used solid nickel hydroxide as his starting material, and added to it 92% pure anhydrous hydrazine, in the molar ratio $Ni(OH)_2$: N_2H_4 of 1 : 8. In the pulp the only reaction products were nickel and nickel hydroxide, both in the form of powder. Other than this, nickel has always been produced as a result of a heterogeneous reaction as will be described in 1.2.3.

Hydrazine, from this outline and its thermodynamics, is not a selective precipitant for metals and its main use is in the heterogeneous deposition of metals on surfaces, described in 1.2.3.

1.2.3. Heterogeneous deposition of metals by hydrazine.

As well as the deposition of metals from baths containing metal ions and hydrazine, there is also a method (34) of activating non-metallic surfaces with nickel or palladium by successively dipping a substrate into a hydrazine solution and a solution containing nickel or palladium ions. In essence, this is identical to the normal activation of substrates with stannous chloride and palladium ions (35) to produce catalytic nuclei of palladium atoms to start a heterogeneous reaction.

The first chemically deposited metal films using hydrazine as a reducing agent were the palladium deposits of Rhoda and Madison (36). They used a solution of palladium (II) ions, complexed by ammonia in an $[NH_3] : [Pd]$ ratio of greater than 10 : 1, to which a very dilute hydrazine solution was added. The baths had additional stabilising agents such as the sodium salt of ethylenediaminetetra-acetic acid (EDTA) to prevent the homogeneous production of palladium powder. Operating temperatures of these baths varied from 30°C. to 80°C., depending on the exact formulation of the bath. In this work, the substrates plated were all metallic, or non-metals sensitised with palladium. The baths were very prone to decompose, forming palladium powder, especially if the concentrations of palladium (II) ions or hydrazine were too great. A study of the decomposition of palladium plating baths has been made by Singh (37). Another process (38) to produce metallic palladium used unsymmetric dimethyl-hydrazine as a reducing agent. This bath operated at 75 - 80°C. and used a dilute solution of the reducing agent. The palladium (II) ions was with a large excess of ammonia, and the bath was as prone to decompose as the earlier bath of Rhoda and Madison (36).

Metals of the platinum group may also be deposited using hydrazine reducing agents (39). For the deposition of platinum, the platinum was in the form of sodium platinum (IV) hydroxide,

Na_2 $Pt(OH)_6$, and the bath was stabilised with EDTA. Hydrazine was added as a dilute solution and the platinum was deposited on a metallic substrate. By adding salts such as ammonium rhodium (III) chloride, $(NH_4)_3$ $RLCl_6$, ammonium iridium (III) chloride or ammonium ruthenium (III) chloride to the sodium platinum (IV) hydroxide of the bath, alloys of platinum with rhodium, iridium or ruthenium can be deposited. However the addition of excess hydrazine or metal ion will cause the bath to decompose, giving metal powder rather than a metal film on the substrate.

The heterogeneous deposition of gold from solution was noted by Gostin and Swan (40). They used a 3 g. $litre^{-1}$ solution of potassium gold (III) cyanide, K_3 $Au(CN)_6$, buffered with ammonium citrate and a 2×10^{-4} g. $litre^{-1}$ solution of hydrazine. This gave a thin coating of gold, but bath decomposition followed if the hydrazine concentration was increased. Levy (41) used a very dilute (10^{-3} M) solution of gold (III) chloride with a complexing agent such as ethylenediamine to reduce the activity of gold (III) ions even more, in conjunction with a concentration of hydrazine of 2 - 5 M. This bath operated at room temperature. No mention was made of bath stability. The same technique of using a dilute solution of gold (III) ions with a complexing agent, in this case an alkali sulphite, and a concentrated solution of hydrazine was used by Luce (42). She found that the bath was stable, except if the hydrazine solution was less than 1 M strength. In all probability, the activity of gold (III) ions in both Levy and Luce's formulations was reduced to such a low value that high hydrazine concentrations could be safely used.

The chemical deposition of copper and silver was studied by Owen (43). In his work, the reducing agents used were monohydrazine tartrate (N_2H_4) $C_4H_6O_6$ and dihydrazine tartrate $(N_2H_4)_2$ $C_4H_6O_6$. Using silver nitrate as the source of silver, a silver mirror may be deposited on to a glass substrate by reacting an ammoniacal solution

of silver nitrate with monohydrazine tartrate. Copper may be deposited either on to a non-conducting surface or preferably to an already silvered surface. For this, a copper sulphate solution was used. The solutions used were very unstable, and the metal ions and reducing agent were brought together just before deposition. In the case of copper deposition, an additional complexing agent, potassium sodium tartrate, was used to reduce the concentration of the free copper ion. For both silver and copper, the presence of tartrate ions from the reducing agent will reduce the concentration of free metal ions as the tartrate ion is known to form complexes with copper and other ions (44). Other work on the deposition of copper was carried out by Barmashenko and Voronin (45). They reduced a 0.05 M solution of copper sulphate in alkaline solution with a 0.09 M hydrazine sulphate solution at 96 - 98°C. Glass pretreated with silver was used as the substrate. In this work no mention is made of the stability of the solution.

The most frequently studied systems have been the reduction of nickel and cobalt salts to the metal. This is because the metal deposits from the hypophosphite process contain phosphorus as an impurity and those from the borohydride process contain boron. Thus a reducing agent which will give an essentially pure nickel or cobalt deposit would be useful. The reduction of nickel (II) salts by hydrazine on metal substrates was studied by Levy (46). He used concentrations of nickel (II) ions of 0.01 - 0.15 M, with a complexing agent of tartrate ions, and reduced these solutions with hydrazine of 0.5 - 1.5 M concentration. The reactions took place at a pH of 9 - 11 and at temperatures of approximately 90°C. In this work, the deposition rates are $1 - 3 \times 10^{-8}$ grm. moles. sec^{-1}. cm^{-2}. The results can be summarised as:

a) At concentrations of nickel > 0.05 M, the rate of deposition is independent of the nickel ion concentration, if the ratio of [nickel]

to [tartrate] is kept constant.

b) At concentrations of hydrazine higher than 0.6 M, the deposition rate is independent of hydrazine concentration. Below 0.6 M, the deposition rate increases with increasing hydrazine concentration.

c) The deposition rate increases with increasing pH.

d) Considering equal concentrations of complexing agent, the deposition rate using malonate ions is the greatest, followed by tartrate and citrate ions. A similar effect applies to the anion of the nickel (II) ions used.

e) Mechanical stirring made no difference to the deposition rate.

f) The effect of temperature on deposition rate was not measured quantitatively, although it seemed to increase exponentially with temperature. The similar cobalt-hydrazine system followed the Arrhenius rate law and gave an activation energy of 15.9 k.cal. $mole^{-1}$ (47).

g) The deposits were substantially pure with traces of hydrogen, nitrogen and oxygen as impurities.

The work does not mention bath stability and no estimates of its occurrence can be made.

The experiments of Levy were repeated by Dini and Coronado (48). Instead of an optimum deposition rate of 3×10^{-8} g. mole. sec^{-1}. cm^{-2}, they found the deposition rate to be about 1×10^{-9} g. mole. sec^{-1}. cm^{-2}. In their work, they used nickel acetate as a source of nickel ions, glycollic acid and the tetrasodium salt of EDTA as complexing agents, and hydrazine hydrate as reducing agent. The baths ran at 85 - 95°C. and at an approximate pH of 11. Their deposition rates were in the range $0.5 - 2.5 \times 10^{-8}$ grm. moles sec^{-1}. cm^{-2}, and their results may be summarised as:

a) Increasing the concentration of complexing agent decreased the deposition rate. There must be a minimum concentration of complexing agent, otherwise the bath will decompose. The authors

do not state whether the product of bath decomposition is a nickel mirror or nickel powder.

b) Increasing the concentration of nickel acetate increased the deposition rate. If the concentration of nickel acetate was above 80 g. litre^{-1}, the bath decomposed.

c) A certain minimum concentration (45 ml. N_2H_4. litre^{-1}) of hydrazine is required for a stable bath. Above this minimum, increasing the hydrazine concentration has no effect on deposition rate.

d) An Arrhenius plot for the reaction gives an estimated activation energy of 11 k.cal. mole^{-1}, over the temperature range 68 - 93°C.

e) At a pH of less than 10.3, the deposition rate is negligible; higher than 10.3, it increases rapidly with increasing pH.

f) The deposits had principal impurities of hydrogen, oxygen and nitrogen, all at less than 0.5 wt %.

The work of Dini and Coronado suggests that the heterogeneous deposition of nickel on to a catalytic substrate takes place only in a narrow range of reagent concentrations. At other times, there will be no measurable reaction or the reaction will take place at any substrate. This seems to correlate much more with work on other systems, than does Levy's work (46), as he does not mention bath stability at all.

Latatnev et al. (49, 50) used solutions of nickel sulphate of 0.1 - 0.2 M and hydrazine sulphate 0.2 M, operating at 8C - 85°C. and a pH of 8 - 10. Apart from ammonia, which was added to make the solution alkaline, there is no mention of any complexing agent or any remarks about the problem of bath stability. The deposition rates quoted are of the same order as those of Dini and Coronado (48).

Another study of nickel deposition was done by Koslova and Korovin (51). They used potassium sodium tartrate as a complexing agent and studied the stability of the baths and the kinetics of

deposition. They found that bath stability was dependent on pH and concentration of complexing agent, while the deposition rate was dependent on pH, temperature and inversely with concentration of complexing agent. According to them, the concentration of nickel salt makes no difference to the reaction kinetics.

Compared to the published work on nickel reduction, there has been little work published on cobalt reduction. Koslova and Korovin (52) found that baths remained stable in a narrow pH range (11.4 - 12.2) and at high concentrations of potassium sodium tartrate as complexing agent. The deposition rate was a function of hydrazine concentration and of pH. Operating temperatures were around 95°C. and the deposition rates were comparable to the deposition rates obtained for nickel (51). Alloys of cobalt and nickel were produced by substituting nickel salts for part of the cobalt salt.

Takano et al. (53, 54) used similar baths to Koslova and Korovin (52) to obtain deposits of pure cobalt. They claimed that 2 parts per million of thiourea would stabilise baths, containing 0.05 M cobalt (II) chloride, 0.4 M sodium tartrate, 1 M hydrazine at a pH of 12. This, however, according to Koslova (52), should be stable in the absence of thiourea.

1.3. This Work.

The objects of this work were to take deposition solutions of the same type as Levy (46), and to attempt to find the rate law describing the reduction of nickel ions to nickel metal. By considering the rate law and the activation energy of the reaction, an attempt was made to suggest a reaction mechanism. In addition, the deposits of nickel were examined to determine some physical properties, notably the development of preferred orientations and the absorption of gases into the crystal lattice of the metal.

The substrate was in the form of a rotating disc, since the

rotating disc is one of the few configurations where the diffusion of ions to the substrate has been studied and analysed (55).

Since the concentration of gases in the nickel metal was likely to be low, X-ray diffraction was used to analyse the nickel metal. The search for preferred orientations was done by depositing nickel on to substrates that were either particular cut faces of a single crystal or polycrystalline aggregates.

From these experiments, an understanding of the overall reaction and the problems in using such plating baths may be arrived at.

CHAPTER 2 EXPERIMENTAL METHODS

2.1. Investigation of the reaction mechanism.

The reduction of nickel ions to nickel metal in the reaction:

$$Ni^{2+} + N_2H_4 + 4OH^- = Ni + N_2 + 4H_2O + 2e^- \quad (2.1.)$$

is a slow reaction. Preliminary experiments showed that the rate of reaction was linear with time until about 5% of the nickel ions had been converted to nickel metal. Thus, when the length of the experiment was such that less than 5% of the nickel ions were converted, the average rate of nickel deposition in the experiment could be equated to the instantaneous rate of nickel deposition at the initial experimental conditions.

The rate of nickel deposition was measured as a function of the speed of rotation of a rotating disc, and as a function of temperature to determine whether the reaction was controlled by the transport of reactants to the disc surface or by the chemical reaction at the disc surface.

To determine the rate equation for the reaction, the rate of nickel deposition was measured as a function of the main reaction variables. These were the total concentrations of nickel, complexing agent (in this case, either tartrate or malonate ion) and hydrazine, and the solution pH. All these were varied in turn, the others being held constant in the usual way.

2.1.1. Experimental Apparatus.

The apparatus was as in Fig. 2.1. The reaction vessel was a 500 ml. "Quickfit" round-bottomed flask with a clip-on lid. To prevent evaporation of reactants, the lid was fitted with a condenser. Both flask and contents were placed in a thermostatically controlled bath, the temperature of which could be controlled to $0.1^{\circ}C$. Because of the poor heat transfer characteristics of the reaction

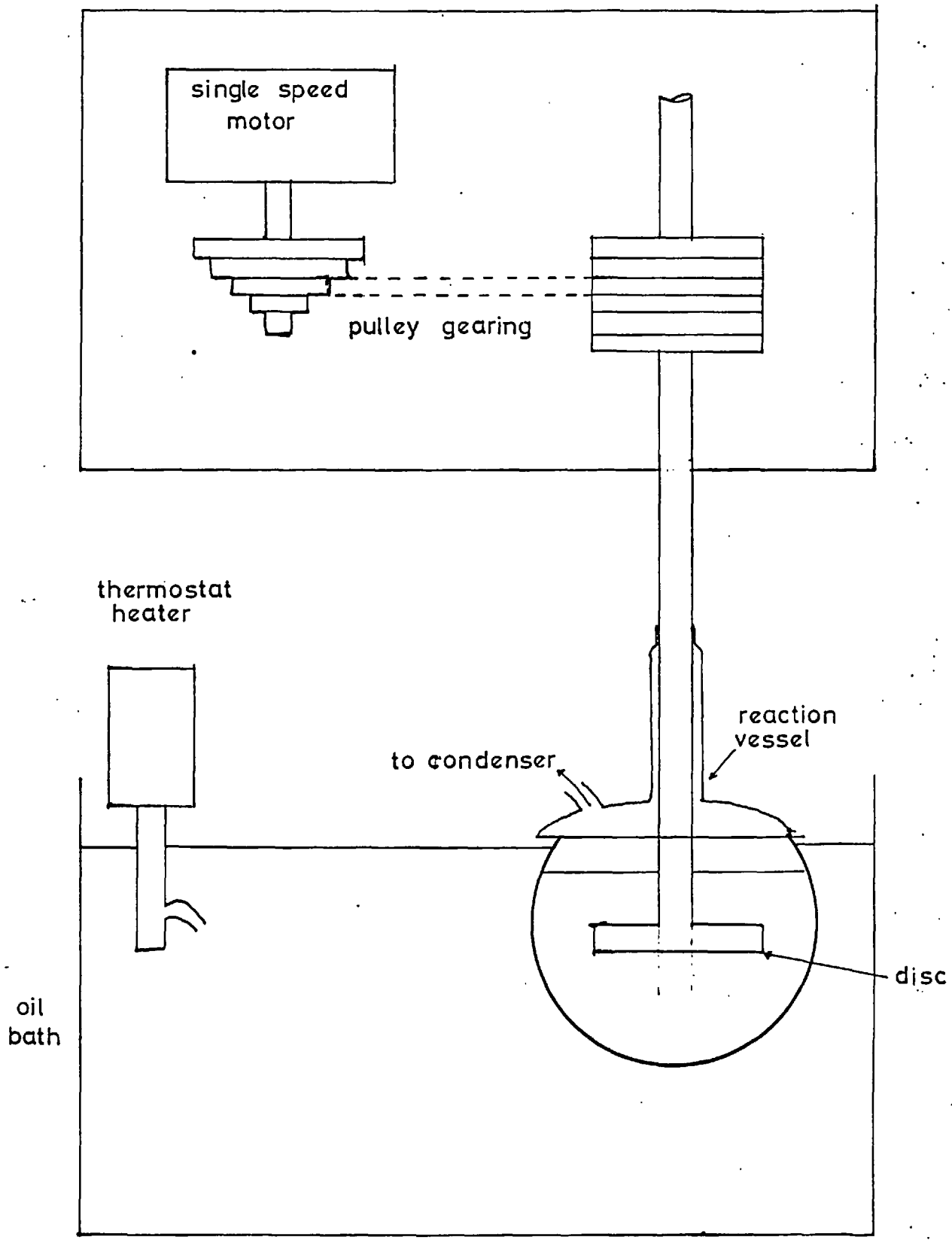

FIG. 2.1 EXPERIMENTAL APPARATUS

vessel and the rotating disc, there was a temperature difference between the bath and the reaction vessel. A calibration curve of reaction vessel temperature against bath temperature was therefore constructed (Fig. 2.2.).

The rotating disc used in these experiments was made of stainless steel, as was the stirrer rod. The diameter of the disc was 3.80 cms., giving a surface area of 11.34 cm^2. All parts of the disc assembly, shown in Fig. 2.3., were lacquered with a water-repellant spray, except for the reaction site, which was a ground surface of the stainless steel.

The disc was powered by a 1500 r.p.m. single speed a.c. motor, driving through a set of pulleys. This gave five possible constant speeds, which could be measured on a stroboscope.

As the reaction at the metal surface involved the possible transfer of electrons, and the apparatus was substantially made of metal; it was important that stray induction currents picked up from the motor should not find their way to the disc. Accordingly, the motor was insulated from the framework by inserting non-conducting gasket sheet between the two. Similarly, the pulley and stirrer rod assembly were insulated from the framework with the same non-conducting gasket sheet.

The chemicals used were as follows:

a) Nickel chloride : $NiCl_2.\ 6H_2O$ Analar grade, supplied by Hopkin and Williams.

b) Potassium sodium tartrate : $KNaC_4H_4O_6.\ 4H_2O$ Analar grade, supplied by Hopkin and Williams.

c) Sodium malonate : $Na_2C_3H_2O_4$. Analar grade, supplied by Hopkin and Williams.

d) Hydrazine hydrate : $N_2H_4.\ H_2O$, approximately 20 M. G.P.R. grade, supplied by Hopkin and Williams.

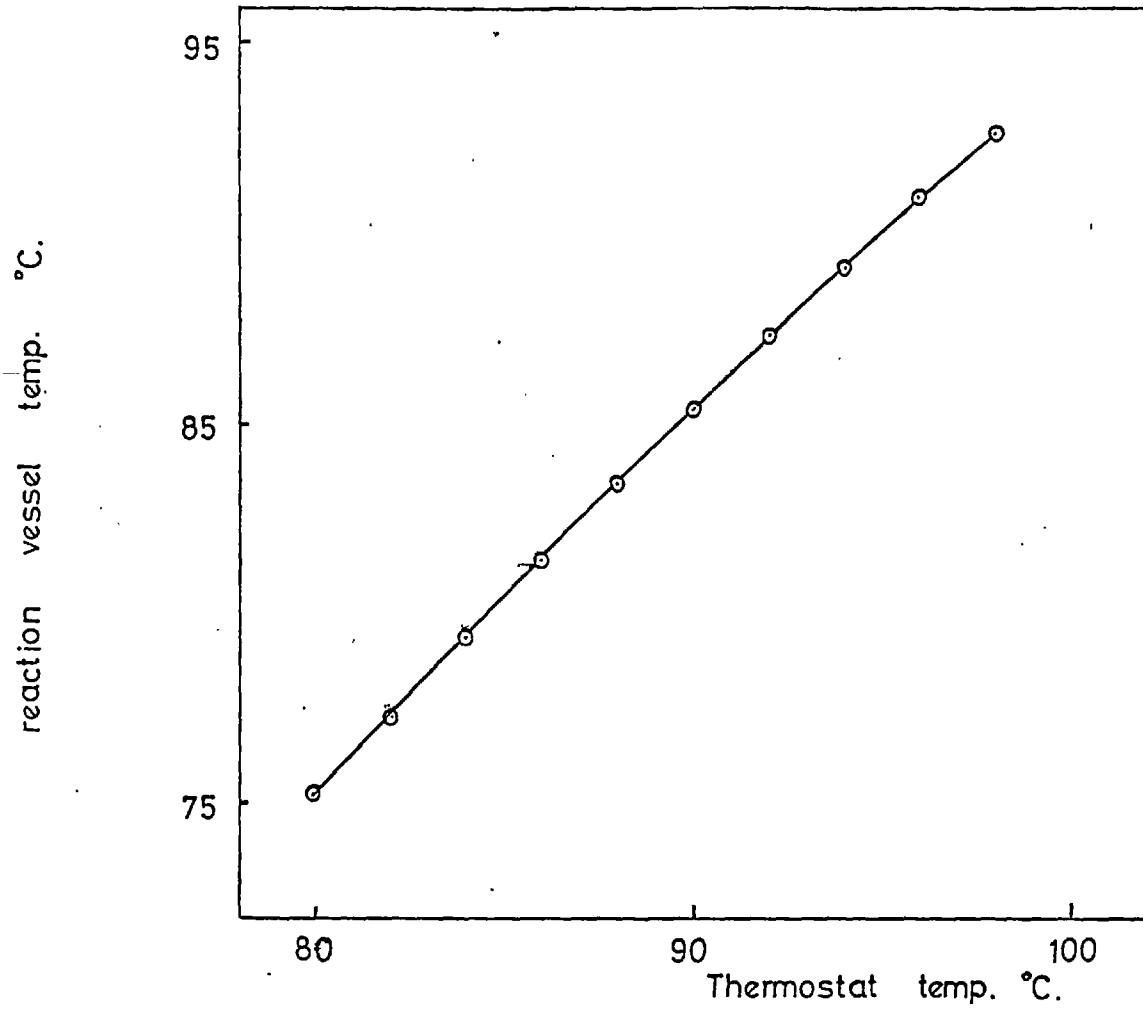

FIG. 2.2 CALIBRATION OF THERMOSTAT

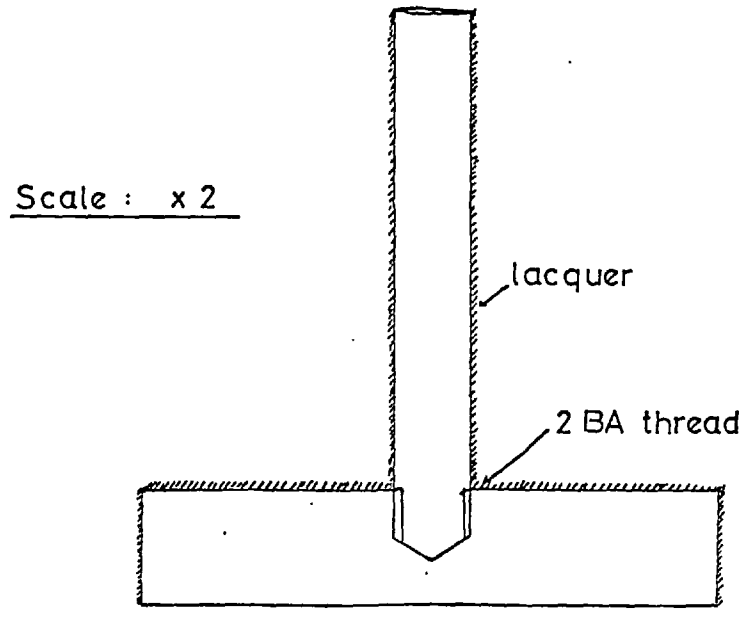

FIG. 2.3 ROTATING DISC ASSEMBLY

2.1.2. Experimental Procedure.

The solutions were made up at room temperature in the following way. First the nickel chloride was dissolved in about 400 ml. distilled water. To this solution, the sodium potassium tartrate crystals were added. After the tartrate had all dissolved, the required volume of hydrazine hydrate was added, and the solution stirred until it was a clear blue colour. The pH of this solution was about 10 and was adjusted to its final value with sodium hydroxide. After this, the solution was made up to 500 ml. In the runs where sodium malonate was used, it was added in the place of the tartrate crystals.

The disc had been ground to remove all traces of nickel, washed and dried before weighing. It was then sprayed with lacquer and screwed on to the stirrer rod.

Before each run, the reaction vessel was boiled with concentrated nitric acid to remove any traces of nickel metal on the walls that could catalyse the reaction. After washing and drying, the flask, disc and stirrer were set up as in Fig. 2.1., with the disc above the solution surface. The reactants were then transferred from the volumetric flask to the reaction vessel. The whole lot was then left to equilibrate for 1½ hours after the bath reached its preset temperature. The disc was then lowered into the solution, the motor and the clock started. After two hours, the motor was stopped and the disc raised above the reaction solution. When the apparatus was cool enough to dismantle, the disc was removed, washed in water and alcohol, and then left overnight in acetone to dissolve off the lacquer. The disc was then dried and reweighed. After the achievement of constant weight, the difference of weight was recorded.

2.1.3. Analytical techniques.

a) Nickel

The rate of nickel deposition was measured by weighing the disc before and after plating; the difference in weight being the weight of nickel deposited. To ensure that this represented the true weight of nickel, the disc was washed in acetone to remove the protective lacquer and dried in an air blast. This procedure was repeated until there was constant weight.

The metal deposited was initially analysed for purity by the standard technique for estimating nickel as the dimethylglyoximate $Ni(C_4H_7O_2N_2)_2$ (56). Another check was to compare it in the electron-probe microanalyser with a specimen of pure nickel. Both these methods showed that the metal could be regarded as pure nickel.

The alternative method of taking samples during a run, measuring the concentration of nickel in the solution, and by subtraction, finding the weight of nickel metal deposited at given times was not used. This was because, in the time of the experiment, only about 3% of the nickel is deposited as metal. In this case, the relative error of a spectrophotometric method (57) being measured as $\pm$1.1%, the scatter of the sampled results would be about 35%, which is unsatisfactory.

b) Hydrazine

Just before the reaction was allowed to start, a sample of reaction solution was taken from the reaction vessel and cooled. This sample was then analysed for hydrazine volumetrically, according to the method cited in Vogel (58). The method is based on the fact that hydrazine reacts with potassium iodate, in concentrated (3 - 9 M) HCl, according to the equation:

$$IO_3^- + N_2H_4 + 2H^+ + Cl^- \equiv ICl + N_2 + 3H_2O \quad (2.2.)$$

from which it can be seen that:

$$IO_3^- \equiv N_2H_4 \quad (2.3.)$$

Nickel ions and tartrate ions do not interfere.

Hydrazine was analysed every ten runs.

2.2. X-ray diffraction.

2.2.1. Debye-Scherrer photographs.

In all the powder photographs, a Philips 5.73 cm. radius camera was used. The radiation was copper K_{α}, with a voltage of 35 kV and a tube current of 20 mA. Depending on the sample, exposure times varied from 1 to 3 hours.

Nickel was deposited from solution on to a glass substrate, which had been sensitised with palladium, using Marton and Schlesinger's method (7). The foil was removed from the glass, dried at 110°C. and ground in a mortar to -325 mesh. Since this powder was heavily stressed, it was stress-relieved by vacuum annealing at 550°C. for 2 hours. The powder was then put in a 0.3 mm. capillary, and a powder photograph taken.

Palladium may be deposited from solutions containing hydrazine, either as the product of a homogeneous chemical reaction or of a heterogeneous reaction on a catalytically active substrate. Deposits corresponding to both methods were produced. For the heterogeneous reaction, a glass substrate as the one used for nickel was employed. Palladium was deposited from a solution cited as Example IV in the work of Rhoda and Madison (36), and the powder was made from the foil in the same way as before. The palladium produced by homogeneous reaction came from a solution identical to the previous one, except for the addition of 1 ml litre^{-1} of hydrazine hydrate. The powder was filtered from solution, dried and passed through a 325 mesh sieve. This fine fraction was placed in the X-ray camera and photographed. For this, there was no need to vacuum anneal.

2.2.2. Pin-hole photographs.

A polycrystalline iron substrate was plated from solution with nickel. Back-reflection pin-hole photographs were taken, using filtered molybdenum K_α radiation, at a voltage of 30 kV. and a tube current of 25 mA. The photographs were taken of the sample at various thicknesses of deposit on the iron substrate.

2.3. Electron diffraction.

In all this work, the camera used was an A.E.I. E.D.C.2. diffraction camera, operating at a voltage of 100 kV. The photographs taken are all reflection diffraction photographs, where the electron beam is at grazing incidence to the specimen. In this way, the diffraction pattern obtained is representative of the first few atomic layers of the specimen, rather than the much larger depths of penetration of the back-reflection Laue method of X-ray diffraction.

The substrates used were all of pure copper. The first was a polycrystalline disc of 99.99% spectroscopically pure copper, supplied by Johnson Matthey. The flat surfaces, on which the nickel was deposited, were cut, ground, polished and etched until the cold-worked layer had been removed from the surface. For the other work, the (100) and (110) faces of a single-crystal of copper, 99.99% pure, supplied by Metals Research Ltd., were used. These were cut with a slitting wheel, and the worked layer was ground, polished and etched until it was removed. On these faces nickel was deposited, the other curved surfaces being blanked off with lacquer.

Since the surface layers are the source of the diffraction pattern, it is important that the surface of the specimen is very clean before it is put in the camera. Thus the nickel deposits were washed in distilled water, acetone and rectified spirits, and dried in an air-blast. All the time, the specimens were handled with tweezers.

After the specimen had been loaded into the camera, the diffraction pattern was recorded on a photographic plate.

The deposition conditions used were: (Symbols - see Appendix 1):

$[Ni]_t$ = 0.02 M $[tar]_t$ = 0.02 M

$[N_2H_4]_t$ = 1.0 M pH = 11.0

Temperature = 80°C.

This ensured a slow rate of deposition, which would increase the possibility of epitaxial growth in the deposits.

2.4. Scanning electron microscope studies.

For a full account of the theory of the scanning electron microscope, one may refer to Thornton (59). The instrument used in this work was a "Stereoscan", supplied by Cambridge Instruments.

The specimens were nickel foils deposited on to previously sensitised glass discs. Since the scanning electron microscope has a greater depth of focus than either the transmission electron microscope or the standard optical microscope, there is no need to section or polish the foils. The foils, after drying, are examined directly in the microscope.

2.5. Electron probe microanalysis.

Copper plated with nickel was transversely sectioned and mounted in plastic. The specimen was then polished and examined using a JEOL electron probe microanalyser. First, the specimen was traversed for the presence of nickel and the results photographed through a green filter. The specimen was similarly traversed for the presence of copper, and the result photographed through a red filter. The resultant composite photograph may be seen on Plate 5.1. As a comparison, pure nickel and copper standards were run through the probe to check the purity of the deposits.

CHAPTER 3 EXPERIMENTAL RESULTS

The measured weight gain of the disc may be taken, after conversion into the appropriate units, as the rate of formation of nickel metal per unit area of substrate $\left[\frac{d(Ni^{o})}{dt}\right]^{11}$ (Symbols, see Appendix 1). As the nickel all comes from the solution, it may be related to the rate of loss of nickel ion concentration $-\left[\frac{d(Ni^{2+})}{dt}\right]^{11}$ by the following equation

$$\left[\frac{d(Ni^{o})}{dt}\right]^{11} = -\left[\frac{d(Ni^{2+})}{dt}\right]^{11} \times V \qquad (3.1.)$$

where V is the volume of the solution.

In all the following tables, the rate of loss of nickel ion $-\left[\frac{d(Ni^{2+})}{dt}\right]^{11}$ is plotted against various reaction parameters.

3.1. Rotation speed

Table 3.1. Effect of varying rotation speed of disc.

$[Ni]_t$ = 0.02 M $[tar]_t$ = 0.02 M

$[N_2H_4]_t$ = 0.982 M pH = 11.0

w = Variable Temperature = 87.7°C.

w r.p.m.	log w	$-\left[\frac{d(Ni^{2+})}{dt}\right] 11$ moles l^{-1} sec^{-1} cm^{-2}	$\log -\left[\frac{d(Ni^{2+})}{dt}\right] 11$
335	2.525	9.84×10^{-9}	- 8.007
700	2.845	1.11×10^{-8}	- 7.957
1060	3.023	9.68×10^{-9}	- 8.014
1320	3.121	1.03×10^{-8}	- 7.986
1575	3.197	1.04×10^{-8}	- 7.983

These are plotted in Fig. 3.1. The slope of the graph is

$- 0.045 \pm 0.06$

This shows that the rate of nickel deposition can be taken as independent of the rotation speed of the disc.

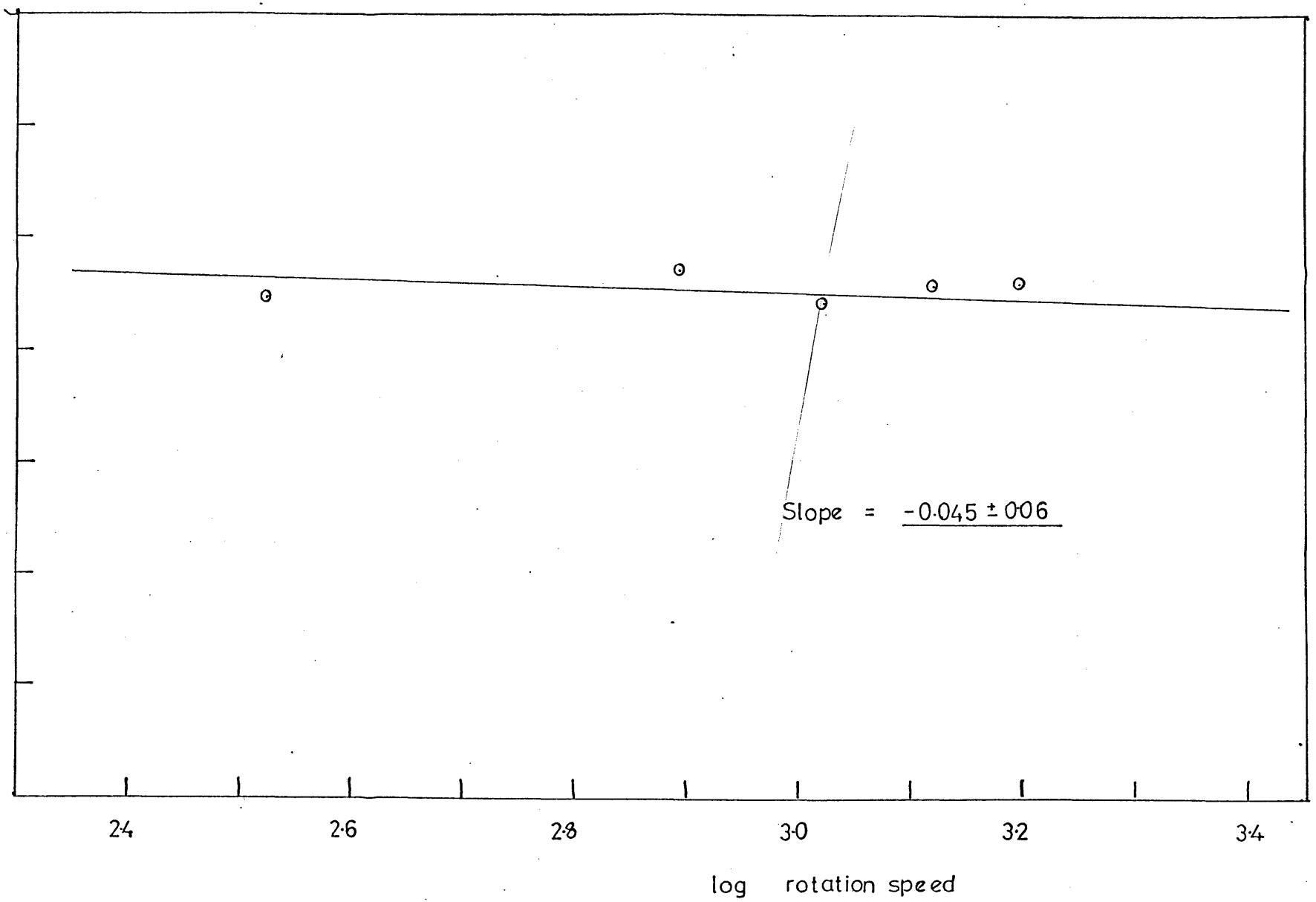

FIG. 3.1 EFFECT OF ROTATION SPEED

3.2. Temperature

Table 3.2. Effect of varying temperature.

$[Ni]_t$ = 0.02 M $[tar]_t$ = 0.02 M

$[N_2H_4]_t$ = 0.986 M pH = 11.0

w = 700 r.p.m. Temperature = Variable

T ^oK	$\frac{1}{T}$ $^oK^{-1}$	$-\left[\frac{d(Ni^{2+})}{dt}\right]11$ moles l^{-1} sec^{-1} cm^{-2}	$\log -\left[\frac{d(Ni^{2+})}{dt}\right]11$
349.5	2.861×10^{-3}	3.12×10^{-9}	- 8.506
352.2	2.839×10^{-3}	4.30×10^{-9}	- 8.367
355.4	2.814×10^{-3}	6.96×10^{-9}	- 8.158
356.6	2.804×10^{-3}	7.48×10^{-9}	- 8.126
358.1	2.792×10^{-3}	8.14×10^{-9}	- 8.089
359.5	2.782×10^{-3}	8.92×10^{-9}	- 8.049
360.9	2.771×10^{-3}	1.01×10^{-8}	- 7.996
362.7	2.757×10^{-3}	1.24×10^{-8}	- 7.906

These are plotted in Fig. 3.2. This gives the activation energy at higher temperatures as 18.3 ± 0.9 k.cals. $mole^{-1}$. At lower temperatures, the activation energy is 34 ± 5 k.cals. $mole^{-1}$. This latter value is only an estimate as there is considerable scatter in the experimental measurement of such small weights of nickel.

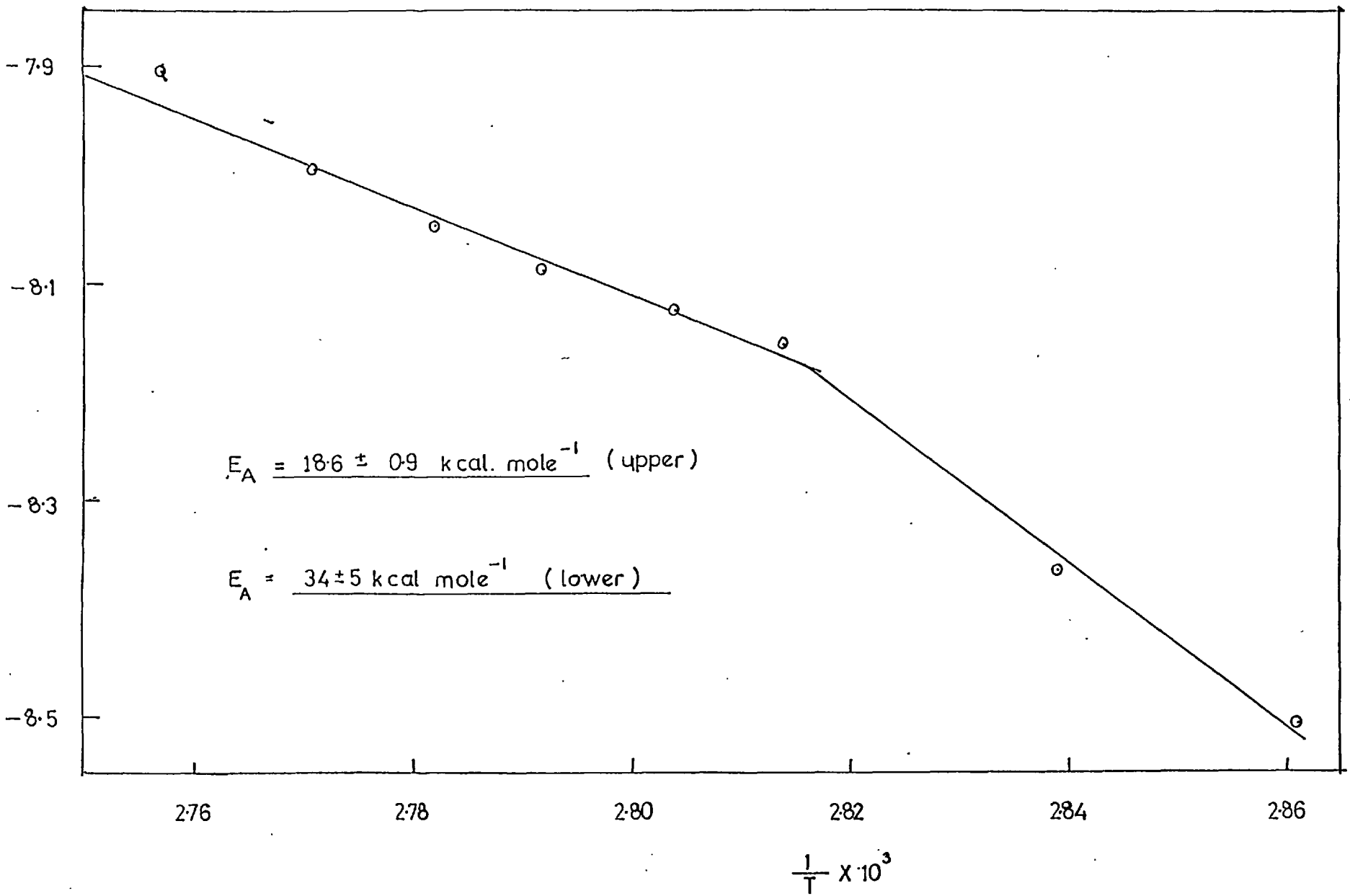

FIG 3.2 EFFECT OF TEMPERATURE

3.3. Nickel concentration.

Table 3.3. Effect of varying nickel concentration.

$[Ni]_t$ = Variable $[tar]_t$ = 0.02 M

$[N_2H_4]_t$ = 0.984 M pH = 11.0

w = 700 r.p.m. Temperature = 87.9°C.

$[Ni]_t$ moles. l^{-1}	$\log[Ni]_t$	$-\left[\frac{d(Ni^{2+})}{dt}\right]11$ moles. l^{-1} sec^{-1} cm^{-2}	$\log -\left[\frac{d(Ni^{2+})}{dt}\right]11$
0.01	- 2.000	4.38×10^{-9}	- 8.359
0.015	- 1.824	6.78×10^{-9}	- 8.169
0.02	- 1.699	1.03×10^{-8}	- 7.987
0.025	- 1.602	1.24×10^{-8}	- 7.908
0.03	- 1.523	1.47×10^{-8}	- 7.834
0.035	- 1.456	1.80×10^{-8}	- 7.745

These are plotted in Fig. 3.3. The slope of the graph is 1.12 ± 0.036.

At $[Ni]_t > 0.04$ M, the deposition of nickel takes place on the walls of the container as well as on the disc. There is no production of nickel powder.

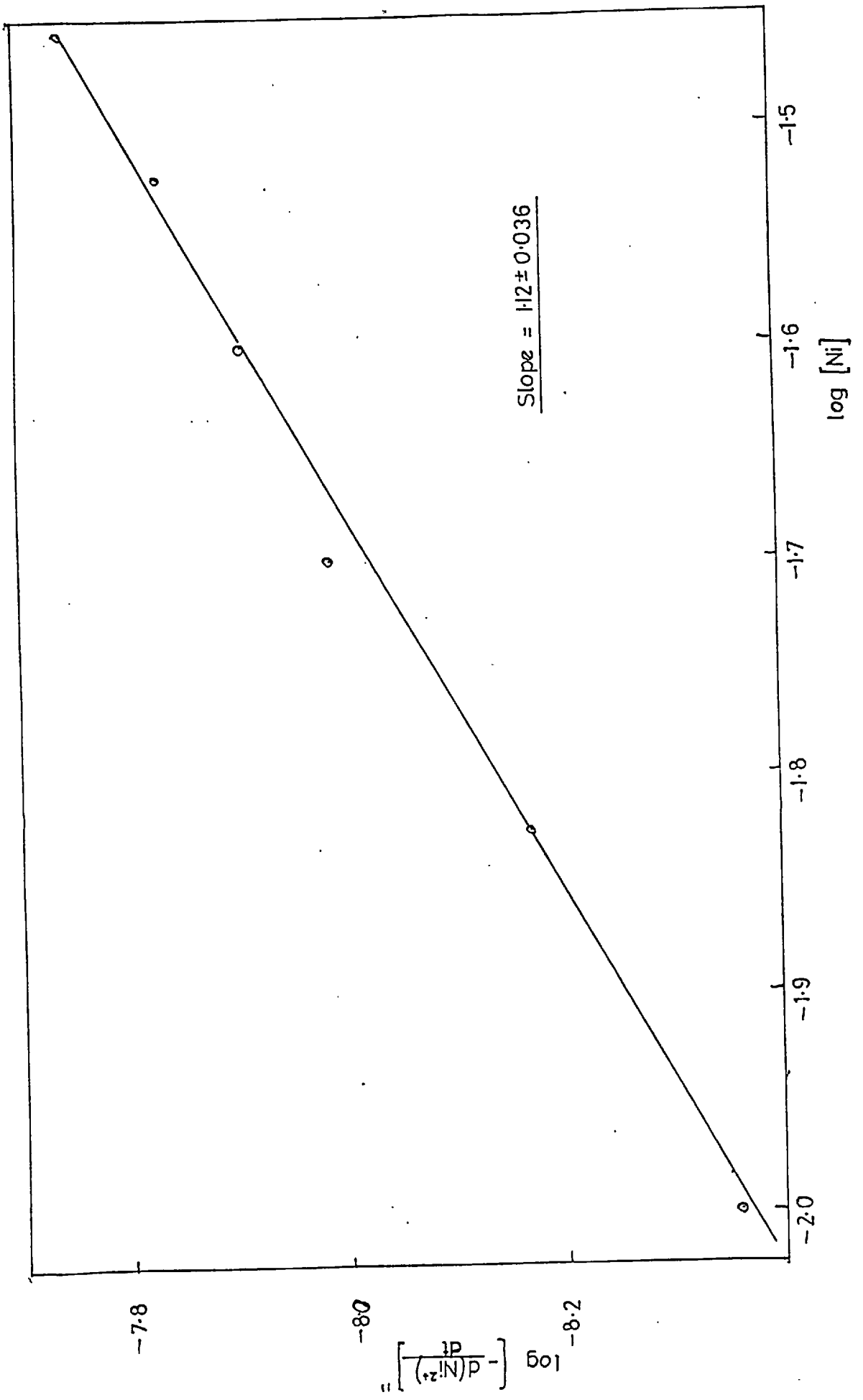

FIG 3.3 EFFECT OF NICKEL CONCENTRATION

3.4. Tartrate concentration.

Table 3.4. Effect of varying tartrate concentration.

$[Ni]_t$ = 0.025 M $[tar]_t$ = Variable

$[N_2H_4]_t$ = 0.984 M pH = 11.0

w = 700 r.p.m. Temperature = 87.9°C.

$[tar]_t$ moles l^{-1}	log $[tar]_t$	$-\left[\frac{d(Ni^{2+})}{dt}\right]$ II moles l^{-1} sec^{-1} cm^{-2}	log $-\left[\frac{d(Ni^{2+})}{dt}\right]$ II
0.015	- 1.824	1.63×10^{-8}	- 7.788
0.02	- 1.699	1.24×10^{-8}	- 7.908
0.025	- 1.602	9.88×10^{-9}	- 8.005
0.03	- 1.523	8.18×10^{-9}	- 8.088
0.04	- 1.398	5.48×10^{-9}	- 8.261
0.05	- 1.301	4.16×10^{-9}	- 8.342

These are plotted in Fig. 3.4. The slope of the graph is -1.14 ± 0.046.

At $[tar]_t < 0.0125$ M, the deposition of nickel takes place on the container walls, as indicated in 3.3.

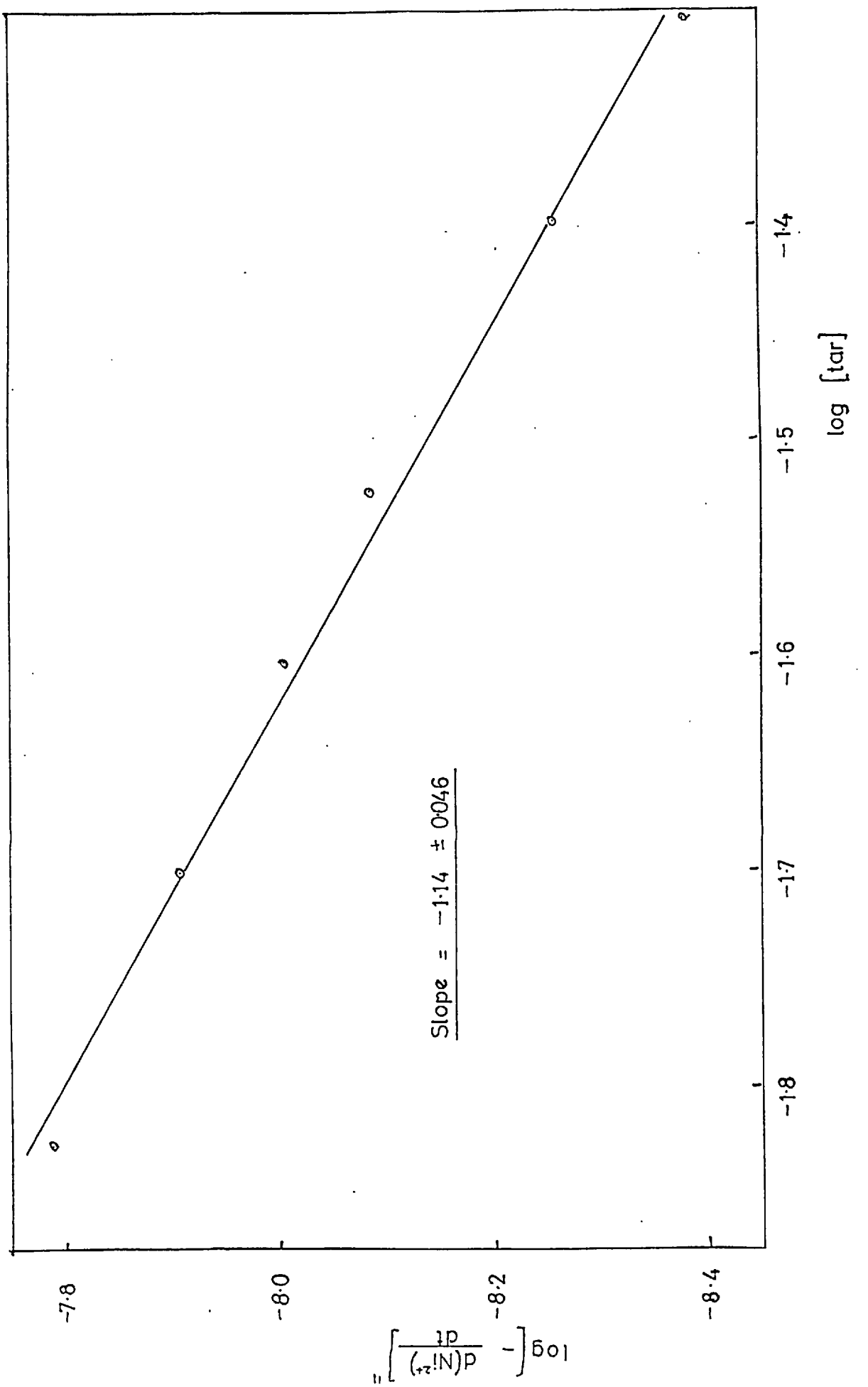

FIG 3 4 EFFECT OF TARTRATE CONCENTRATION

3.5. The ratio of tartrate concentration to nickel concentration.

Table 3.5. Effect of varying $[tar]_t : [Ni]_t$

$[Ni]_t$: Variable $[tar]_t$: Variable

$[N_2H_4]_t$: 0.984 M pH = 11.0

w = 700 r.p.m. Temperature = 87.9°C.

$\frac{[tar]_t}{[Ni]_t}$	$\log \frac{[tar]_t}{[Ni]_t}$	$-\left[\frac{d(Ni^{2+})}{dt}\right] 11$ moles l^{-1} sec^{-1} cm^{-2}	$\log -\left[\frac{d(Ni^{2+})}{dt}\right] 11$
0.500	- 0.301	1.79×10^{-8}	- 7.748
0.571	- 0.243	1.80×10^{-8}	- 7.745
0.600	- 0.222	1.63×10^{-8}	- 7.788
0.667	- 0.176	1.47×10^{-8}	- 7.834
0.750	- 0.125	1.29×10^{-8}	- 7.889
0.800	- 0.097	1.24×10^{-8}	- 7.908
1.000	0.000	8.74×10^{-9}	- 8.058
1.000	0.000	1.03×10^{-8}	- 7.987
1.000	0.000	9.88×10^{-9}	- 8.005
1.200	0.079	8.18×10^{-9}	- 8.088
1.333	0.125	6.78×10^{-9}	- 8.169
1.500	0.176	6.62×10^{-9}	- 8.179
1.600	0.204	5.48×10^{-9}	- 8.261
2.000	0.301	4.38×10^{-9}	- 8.359
2.000	0.301	4.16×10^{-9}	- 8.382

These are plotted on Fig. 3.5. The slope of the graph is -1.08 ± 0.036.

At all $[tar]_t : [Ni]_t < 0.5$, the solution decomposes, and nickel is deposited on the container walls.

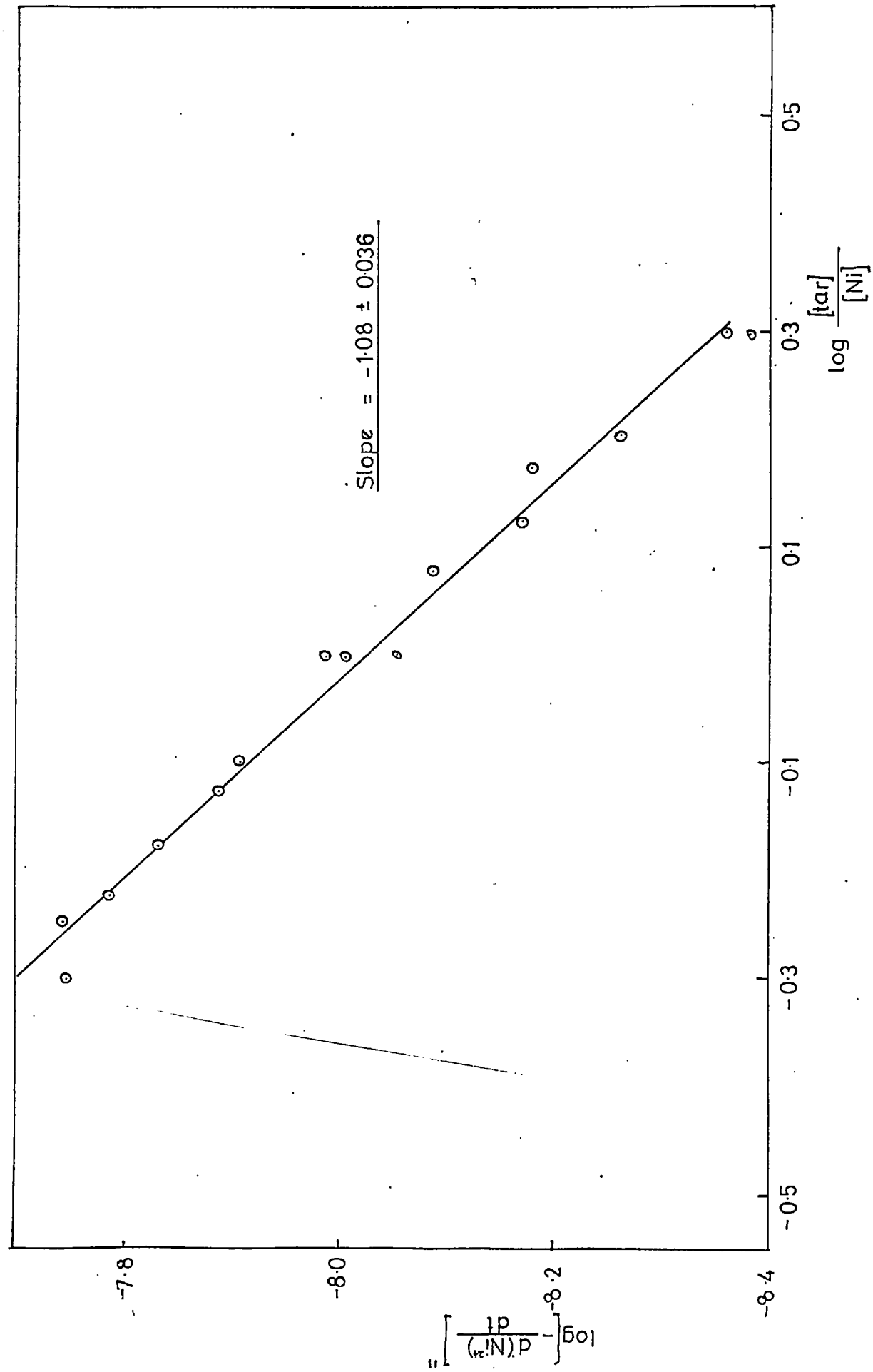

FIG. 3.5 EFFECT OF TARTRATE : NICKEL RATIO

3.6. Effect of pH.

In this work, the pH is measured with a glass electrode and represents the difference in the potential of a glass electrode when immersed in a solution and when immersed in a standard buffer solution, given a pH of 9.15. The true hydrogen ion activity is not actually measured.

Table 3.6. Effect of pH.

$[Ni]_t$ = 0.02 M $[tar]_t$ = 0.02 M

$[N_2H_4]_t$ = 0.981 M pH : Variable

w = 700 r.p.m. Temperature = 87.9°C.

pH	$\log \{H^+\}$	$-\left[\frac{d(Ni^{2+})}{dt}\right] 11$ moles l^{-1} sec^{-1} cm^{-2}	$\log -\left[\frac{d(Ni^{2+})}{dt}\right] 11$
10.7	- 10.7	2.78×10^{-9}	- 8.558
10.8	- 10.8	4.16×10^{-9}	- 8.381
10.9	- 10.9	6.06×10^{-9}	- 8.217
11.0	- 11.0	1.03×10^{-8}	- 7.986
11.1	- 11.1	1.40×10^{-8}	- 7.853

These are plotted in Fig. 3.6. The slope of the graph is -1.76 ± 0.06.

At a pH of $\geq$ 11.15, the solution decomposes, and nickel metal deposits on the container walls.

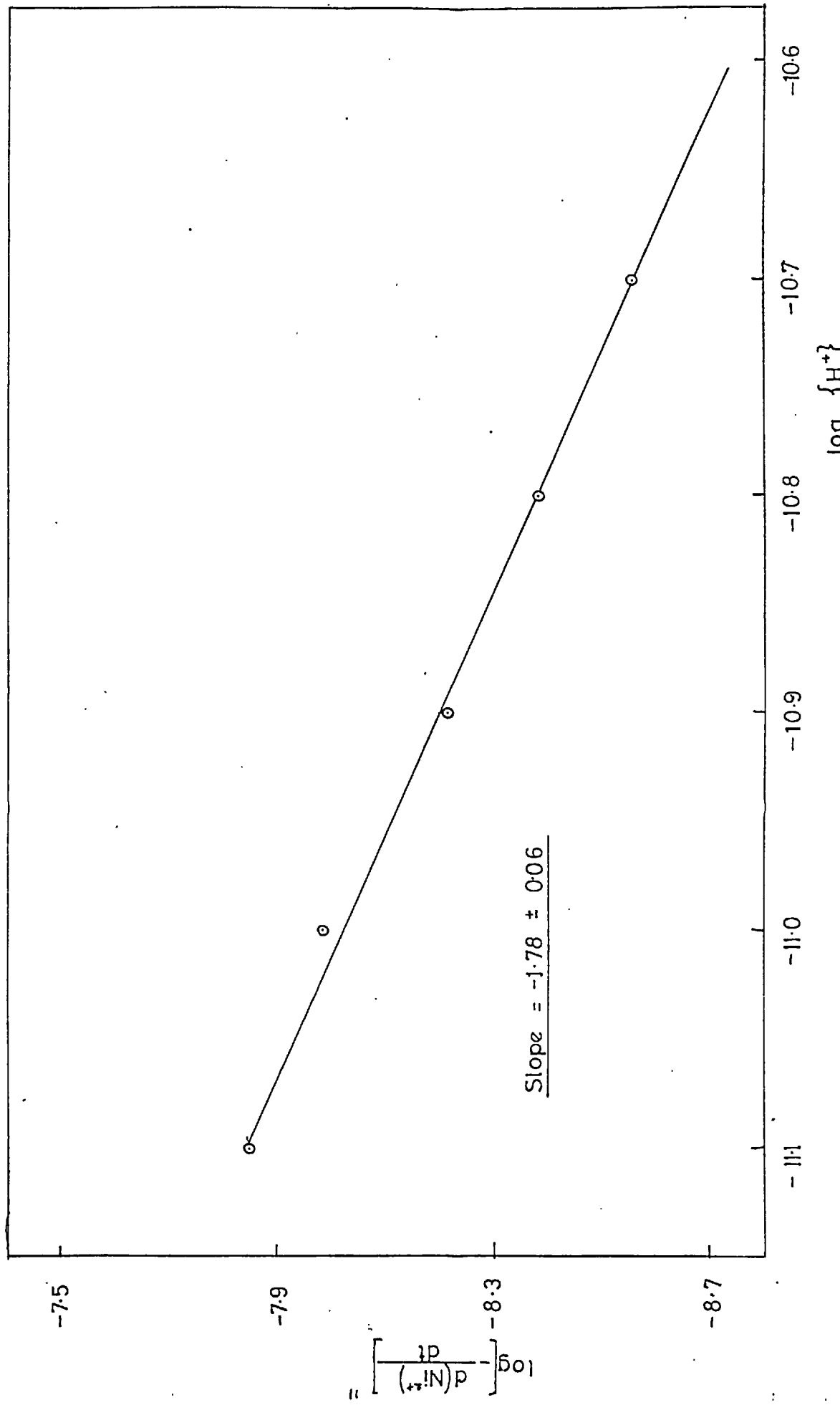

FIG 3.6 EFFECT OF pH

3.7. Hydrazine concentration.

Table 3.7. Effect of varying hydrazine concentration.

$[Ni]_t$ = 0.02 M $[tar]_t$ = 0.02 M

$[N_2H_4]_t$: Variable pH = 11.0

w = 700 r.p.m. Temperature = 87.9°C.

$[N_2H_4]_t$ moles l^{-1}	log $[N_2H_4]_t$	$-\left[\frac{d(Ni^{2+})}{dt}\right]$ 11 moles l^{-1} sec^{-1} cm^{-2}	log $\left[-\frac{d(Ni^{2+})}{dt}\right]$ 11
1.00	0.000	1.01×10^{-8}	- 7.996
1.20	0.079	1.04×10^{-8}	- 7.983
1.60	0.204	1.04×10^{-8}	- 7.982
2.00	0.301	9.84×10^{-9}	- 8.007
3.00	0.477	1.01×10^{-8}	- 7.996

These are plotted on Fig. 3.7. The slope of the graph is -0.02 ± 0.03. This shows that the rate of nickel deposition is independent of hydrazine concentration, in the ranges of hydrazine concentration considered.

At $[N_2H_4]_t < 0.85$ M, nickel deposits on the walls of the container.

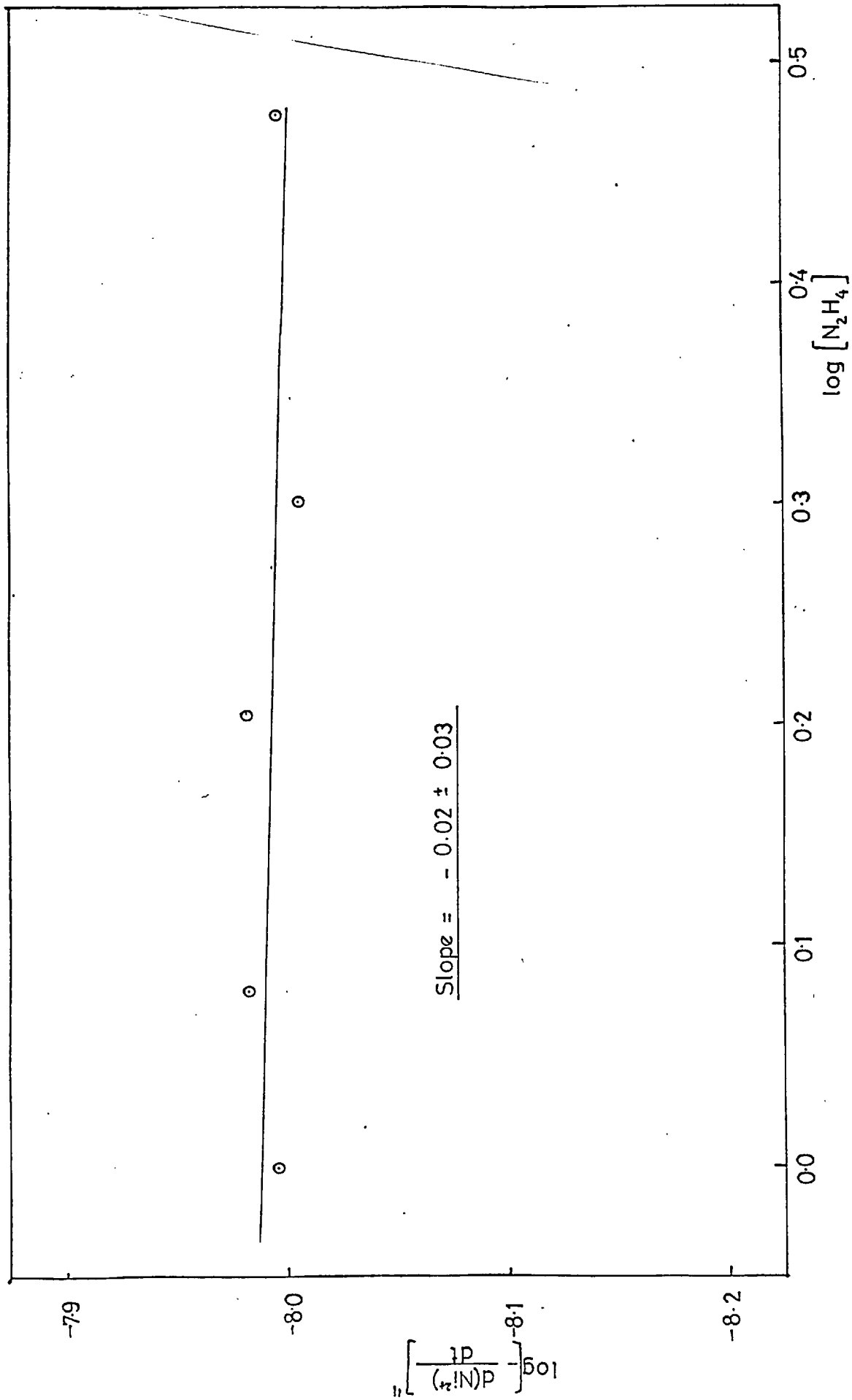

FIG. 3.7 EFFECT OF HYDRAZINE CONCENTRATION

3.8. Malonate concentration.

Table 3.8. Effect of malonate concentration.

$[Ni]_t$ = 0.005 M $[mal]_t$ = Variable

$[N_2H_4]_t$ = 0.982 M pH = 11.0

w = 700 r.p.m. Temperature = 87.9°C

$[mal]_t$ moles l^{-1}.	log $[mal]_t$	$-\left[\frac{d(Ni^{2+})}{dt}\right]_{11}$ moles l^{-1} sec^{-1} cm^{-2}	log $\left[-\frac{d(Ni^{2+})}{dt}\right]_{11}$
0.050	- 1.301	7.16×10^{-9}	- 8.245
0.0625	- 1.204	5.82×10^{-9}	- 8.235
0.075	- 1.125	4.64×10^{-9}	- 8.333
0.0875	- 1.058	4.10×10^{-9}	- 8.386
0.100	- 1.000	3.62×10^{-9}	- 8.442
0.150	- 0.824	2.46×10^{-9}	- 8.609

These are plotted on Fig. 3.8. The slope of the graph is - 0.98 ± 0.022.

The solutions used in this series have $[mal]_t$: $[Ni]_t$ ranging from 10 - 30 compared to the 0.6 - 2 range for the tartrate ion. At lower $[mal]_t$: $[Ni]_t$, the solution decomposes and nickel is deposited on the container walls.

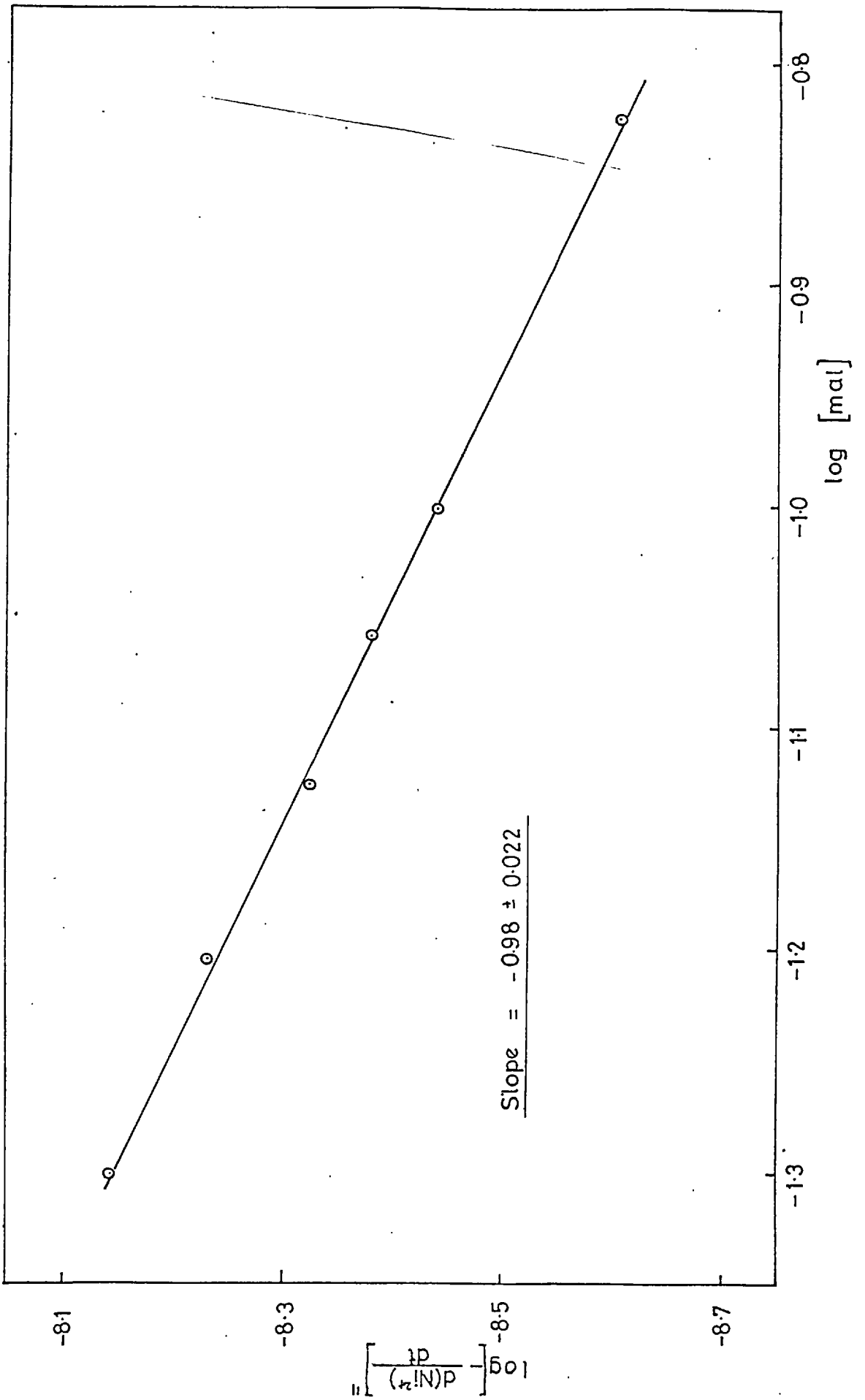

FIG. 3.8 EFFECT OF MALONATE CONCENTRATION

3.9. The heterogeneous deposition of nickel on the reaction vessel.

As has been noted in previous sections, deposition of nickel metal takes place on the walls of the reaction vessel. This occurs under certain experimental conditions rather than randomly, which would be the case if dust or extraneous grease was acting as a nucleating agent. The important factor seemed to be the ratio of $[L]_t : [Ni]_t$ below which decomposition occurred, where L represented tartrate or malonate. This ratio was therefore plotted against other parameters.

3.9.1. Rotation speed.

This had no effect on the mode of decomposition.

3.9.2. Temperature.

In the range of temperatures studied, 76.3 - 89.5°C., temperature did not affect the critical ratio. At higher temperatures there was a tendency for the solution to boil, and so no measurements could be taken.

3.9.3. Nickel concentration.

There was a slight increase in the critical ratio with increased nickel concentration. The results are tabulated in Table 3.9. and shown in Fig. 3.9.

Table 3.9. Effect of nickel concentration on mode of decomposition.

Temperature = 87.9°C. $[N_2H_4]_t$ = 0.98 M

w = 700 r.p.m. pH = 11.0

$\frac{[tar]_t}{[Ni]_t}$	$\log \frac{[tar]_t}{[Ni]_t}$	$[Ni]_t$ moles l^{-1}	$\log [Ni]_t$
0.45	- 0.347	0.01	- 2.000
0.48	- 0.319	0.015	- 1.824
0.50	- 0.301	0.02	- 1.699
0.50	- 0.301	0.025	- 1.602

3.9.4. Tartrate concentration.

There was a slight increase in the critical ratio with increased tartrate concentration. The results are tabulated in Table 3.10 and shown in Fig. 3.10.

Table 3.10. Effect of tartrate concentration on mode of decomposition.

Temperature = 87.9°C. $[N_2H_4]_t$ = 0.98 M

w = 700 r.p.m. pH = 11.0

$\frac{[tar]_t}{[Ni]_t}$	$\log \frac{[tar]_t}{[Ni]_t}$	$[tar]_t$ moles l^{-1}	$\log [tar]_t$
0.45	- 0.347	0.005	- 2.301
0.47	- 0.328	0.01	- 2.000
0.49	- 0.310	0.015	- 1.824
0.50	- 0.301	0.02	- 1.699

FIG. 3.9 EFFECT OF NICKEL CONCENTRATION

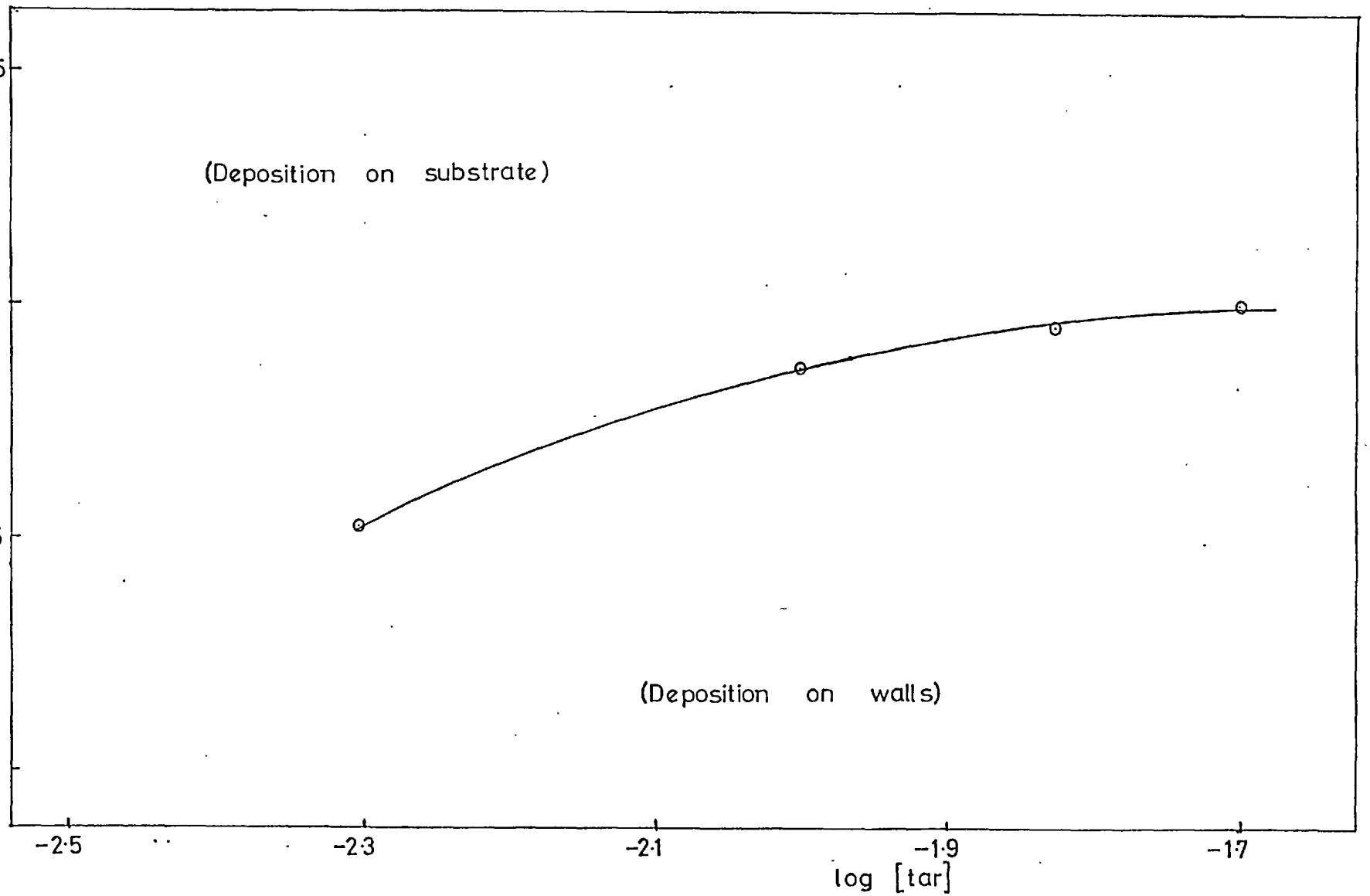

FIG. 3.10. EFFECT OF TARTRATE CONCENTRATION

3.9.5. Hydrazine concentration.

All solutions, irrespective of their $[tar]_t : [Ni]_t$ ratio, decomposed on to the reaction vessel if the concentration of hydrazine was less than 0.85 M.

3.9.6. Effect of pH.

The critical ratio was increased with increasing pH of the solution. The results are tabulated in Table 3.11. and shown in Fig. 3.11.

Table 3.11. Effect of pH on mode of decomposition.

Temperature = 87.9°C. $[N_2H_4]_t$ = 0.98 M

w = 700 r.p.m.

$\frac{[tar]_t}{[Ni]_t}$	$\log \frac{[tar]_t}{[Ni]_t}$	$\log \{H^+\}$
0.50	- 0.301	- 11.00
0.65	- 0.187	- 11.05
0.80	- 0.097	- 11.10
1.00	0.000	- 11.15

The slope of the graph is - 2.0.

3.9.7. Malonate concentration.

There was a small increase in the critical $[mal]_t : [Ni]_t$ ratio with increased malonate concentration. However the absolute values of the $[mal]_t : [Ni]_t$ ratio are about 20 times those of the $[tar]_t : [Ni]_t$ ratio in earlier sections. The values for the $[mal]_t : [Ni]_t$ ratio are tabulated in Table 3.12. and shown in Fig. 3.12.

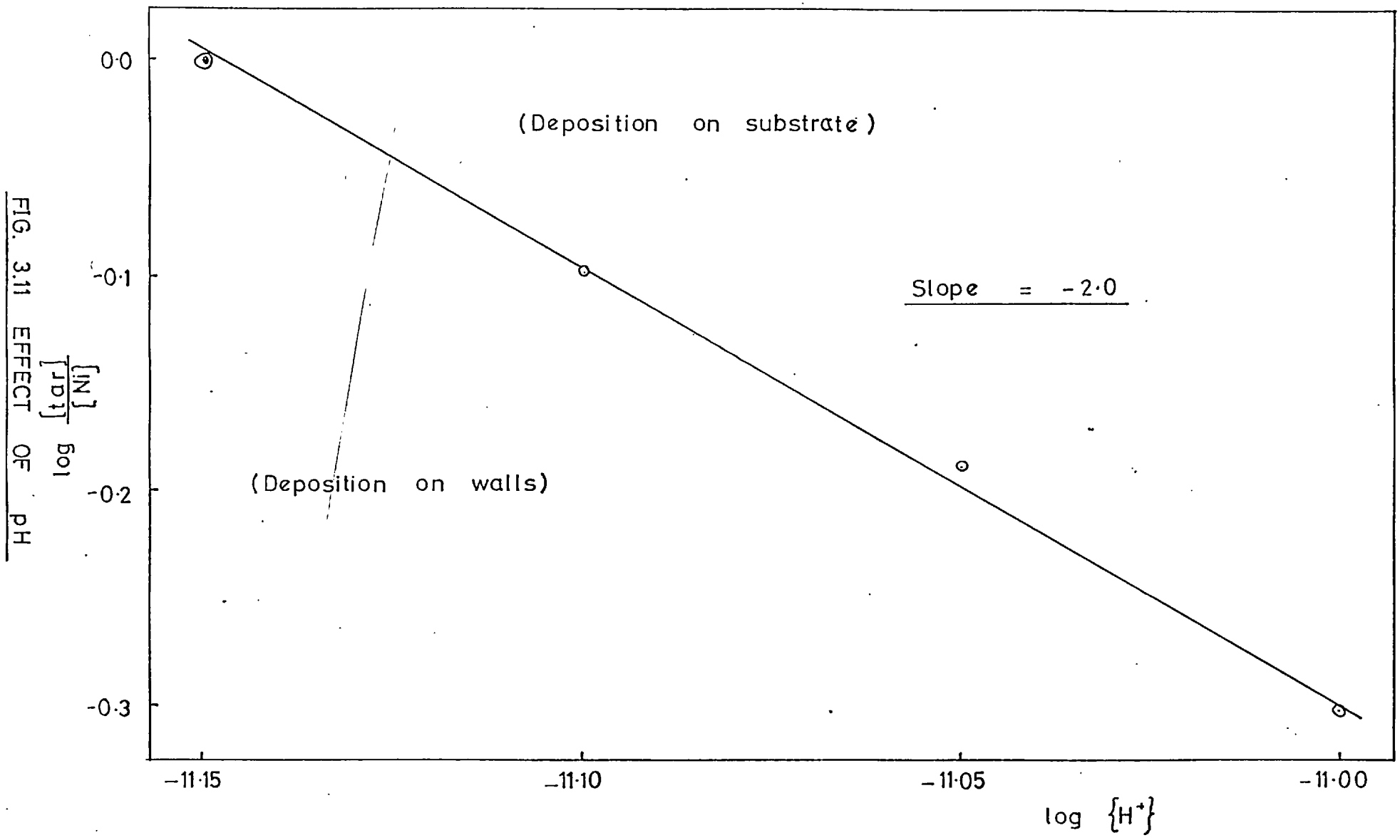

FIG. 3.11 EFFECT OF pH

Table 3.12. Effect of malonate concentration on mode of decomposition.

Temperature = 87.9°C. $[N_2H_4]_t$ = 0.97 M

w = 700 r.p.m. pH = 11.0

$\frac{[mal]_t}{[Ni]_t}$	$\log \frac{[mal]_t}{[Ni]_t}$	$[mal]_t$ moles l^{-1}	$\log [mal]_t$
10.0	1.000	0.05	- 1.301
11.0	1.041	0.1	- 1.000
11.5	1.061	0.2	- 0.699
12.5	1.097	0.4	- 0.398

3.10. Spectra.

The visible and ultraviolet spectra in the system $NiCl_2$ - $KNaC_4H_4O_6$ - N_2H_4 were measured over the range 225 - 700 mμ on a Unicam SP 800 spectrophotometer.

A 2 x 10^{-2} M solution of nickel chloride gave a small peak at 390 mμ When 2 x 10^{-2} M sodium potassium tartrate was added the 390 mμ peak was enlarged and shifted to 395 mμ On the further addition of 1 M hydrazine to simulate a working solution, the peak at 395 mμ was enlarged and shifted to 360 mμ A peak appeared at 576 mμ which explained the change in colour of the solution from green to blue. The main feature of the spectrum was a large peak at 244 mμ With only nickel chloride and hydrazine, the peak at 244 mμ is unaffected and the original 390 mμ peak of nickel chloride is hardly noticeable.

The spectra are plotted as Fig. 3.13. in the form of $\frac{dA}{d\lambda}$ against λ, since some peaks are very small and broad.

To determine the formula of the nickel-hydrazine complex whose peak is at 244 mμ the method of continuous variations was used. The wavelengths used were 245 mμ and 250 mμ but in neither case were

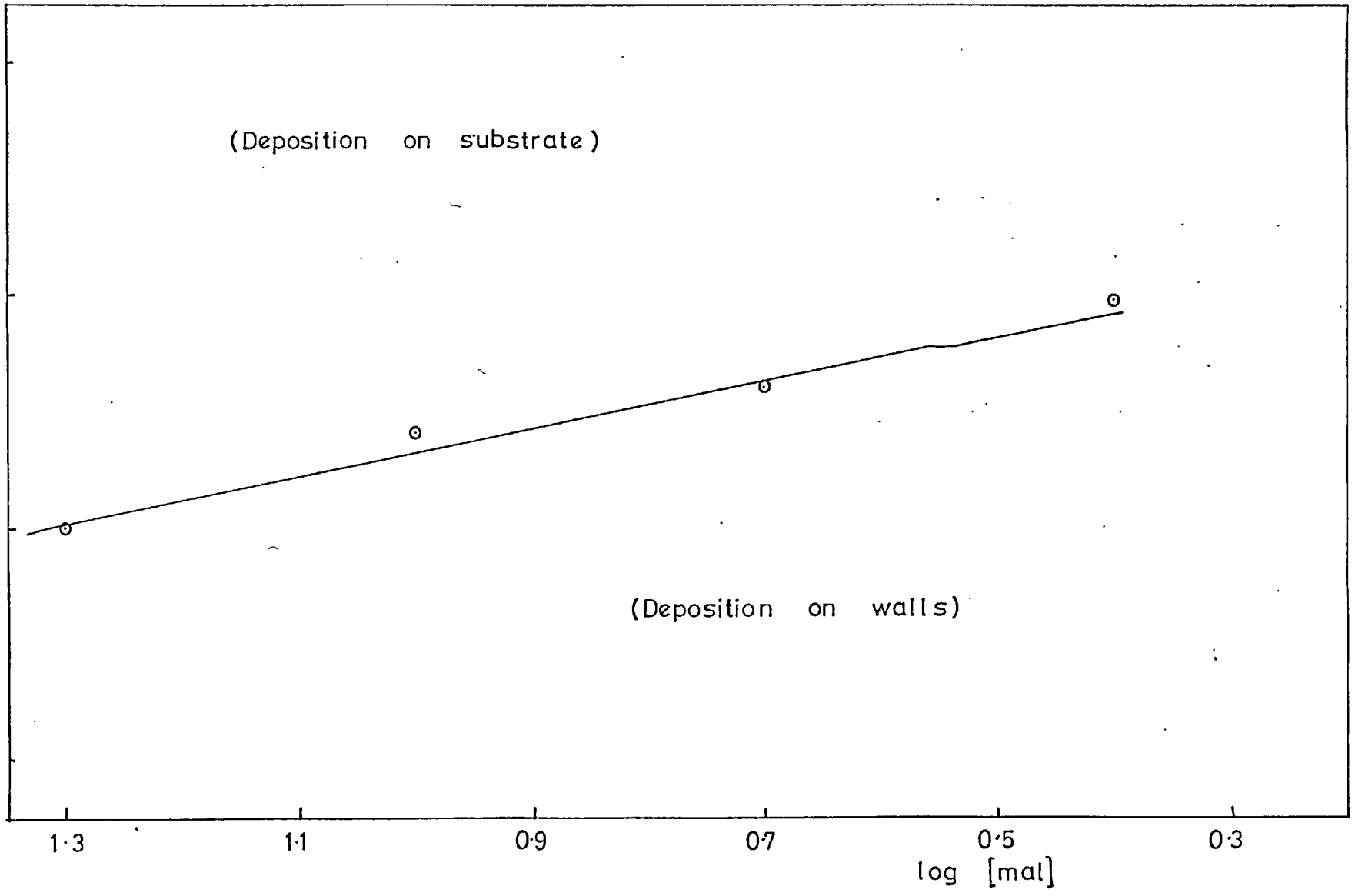

FIG. 3.12 EFFECT OF MALONATE CONCENTRATION

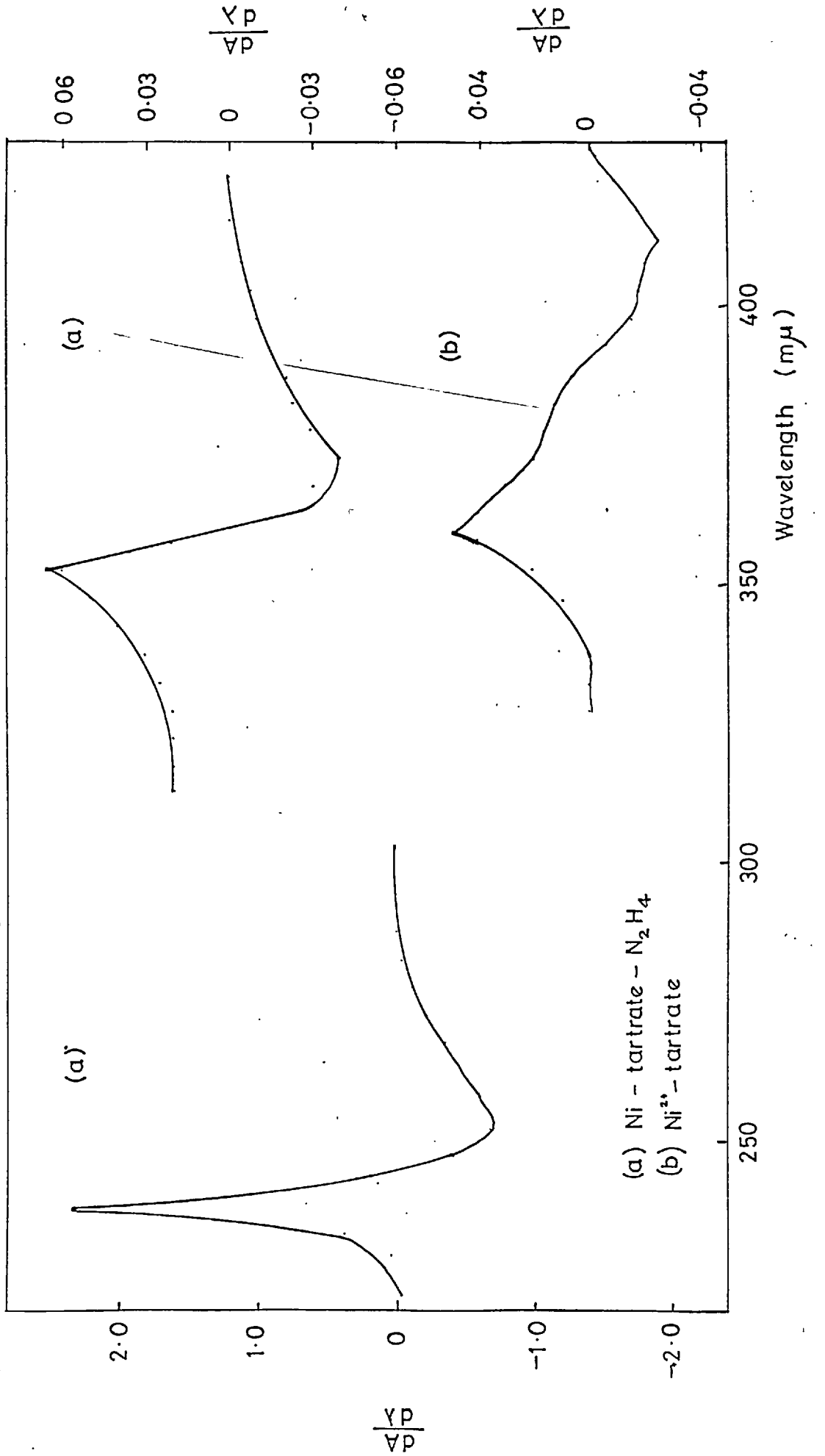

FIG. 3.13 SPECTRA IN THE NICKEL- TARTRATE — HYDRAZINE SYSTEM

there any conclusive results. This seemed to indicate that there was no single complex $\left[Ni_x(N_2H_4)_y\right]^{2+}$ responsible for the peak at 244 mμ

CHAPTER 4 X-RAY DIFFRACTION RESULTS

4.1. Debye-Scherrer photographs of nickel deposits.

The powder pattern obtained from the nickel sample is shown on Film 1.

Film 1. Nickel deposited from solution.

From the position of each line, the lattice parameter of nickel was found, using the following wavelengths for the incident radiation: Cu K_{α} = 1.5418 A^{o}, Cu $K_{\alpha 1}$ = 1.5406 and Cu $K_{\alpha 2}$ = 1.5444 A^{o}. These lattice parameters were plotted against the Nelson-Riley (60) extrapolation function $f(\theta) = \frac{1}{2}\left(\frac{\cos^2\theta}{\sin^2\theta} + \frac{\cos^2\theta}{\theta}\right)$ and may be seen on Fig. 4.1. The true lattice parameter is the lattice parameter when the Nelson-Riley function is zero, which corresponds to a value of the Bragg angle (θ) of $\pi/2$ (see Appendix 2).

From Fig. 4.1., it can be seen that the lattice parameter of hydrazine reduced nickel is 3.5282 $\pm$ 0.001 A^{o}. This compares with lattice parameters of 3.5238 A^{o} (61) for pure nickel and 3.5236 - 3.5240 A^{o} for nickel reduced by hydrogen (62), which are also shown on Fig. 4.1.

An attempt to estimate the grain size of the fresh nickel deposit by measuring the line broadening (B) (Symbols: see Appendix 1), according to the Scherrer formula:

$$D = \frac{0.9\,\lambda}{(B_o - b)\cos\theta} \qquad (4.1.)$$

where B_o is the measured broadening of a peak occurring at a Bragg angle , and b is the instrumental broadening of the instrument used. This latter is found by measuring the broadening of a sample containing grains larger than 3000 A^{o}, where $B_o \sim b$. These

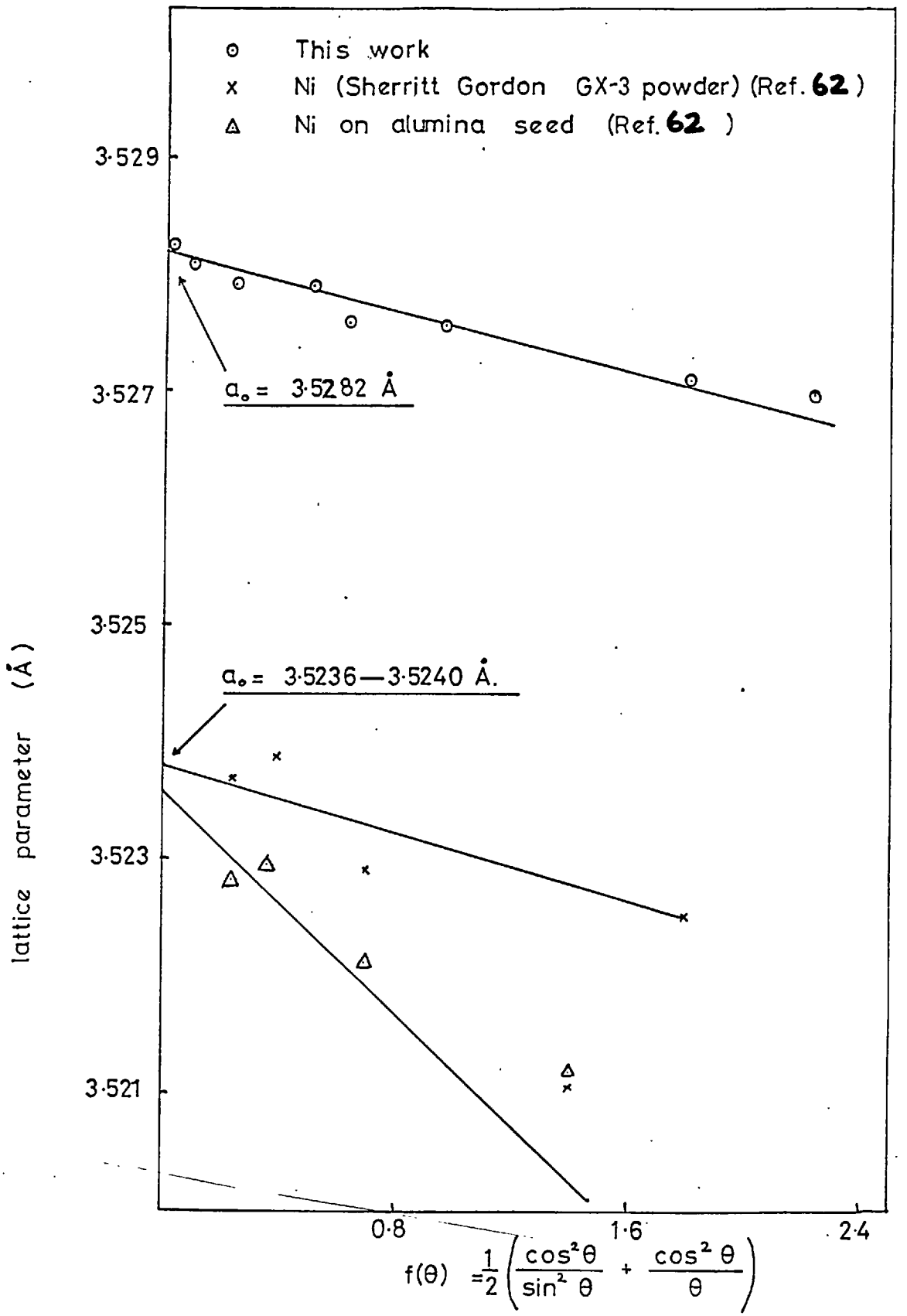

FIG. 4.1 EXTRAPOLATION OF MEASURED LATTICE PARAMETERS AGAINST THE NELSON-RILEY FUNCTION

broadenings, by convention, are taken to be the width of the peak in radians at half peak height above background. Since the presence of stresses broaden the peak as well, results for deposited nickel were of no significance, as the material was heavily stressed in the process of reducing it from foil to 325 mesh. The anneal at 550°C. had the effect of permitting recrystallisation and grain growth, so making any estimate of original grain size meaningless.

4.2. Debye-Scherrer photographs of palladium deposits.

These powder patterns are shown in Films 2 and 3. Film 2 is of palladium powder, homogeneously deposited, while Film 3 is of heterogeneously deposited palladium.

Film 2. Homogeneously deposited palladium.

Film 3. Heterogeneously deposited palladium.

Extrapolating the lattice parameters against the Nelson-Riley function as outlined in 4.1., gives the results plotted in Fig. 4.2. Fig. 4.2. shows that the lattice parameter of homogeneously deposited palladium is 3.8893 ± 0.001 A°, while palladium deposited heterogeneously has a lattice parameter of 3.8962 ± 0.001 A°. For comparison, the lattice parameter (61) of pure palladium, 3.8901 A°, is also shown on Fig. 4.2.

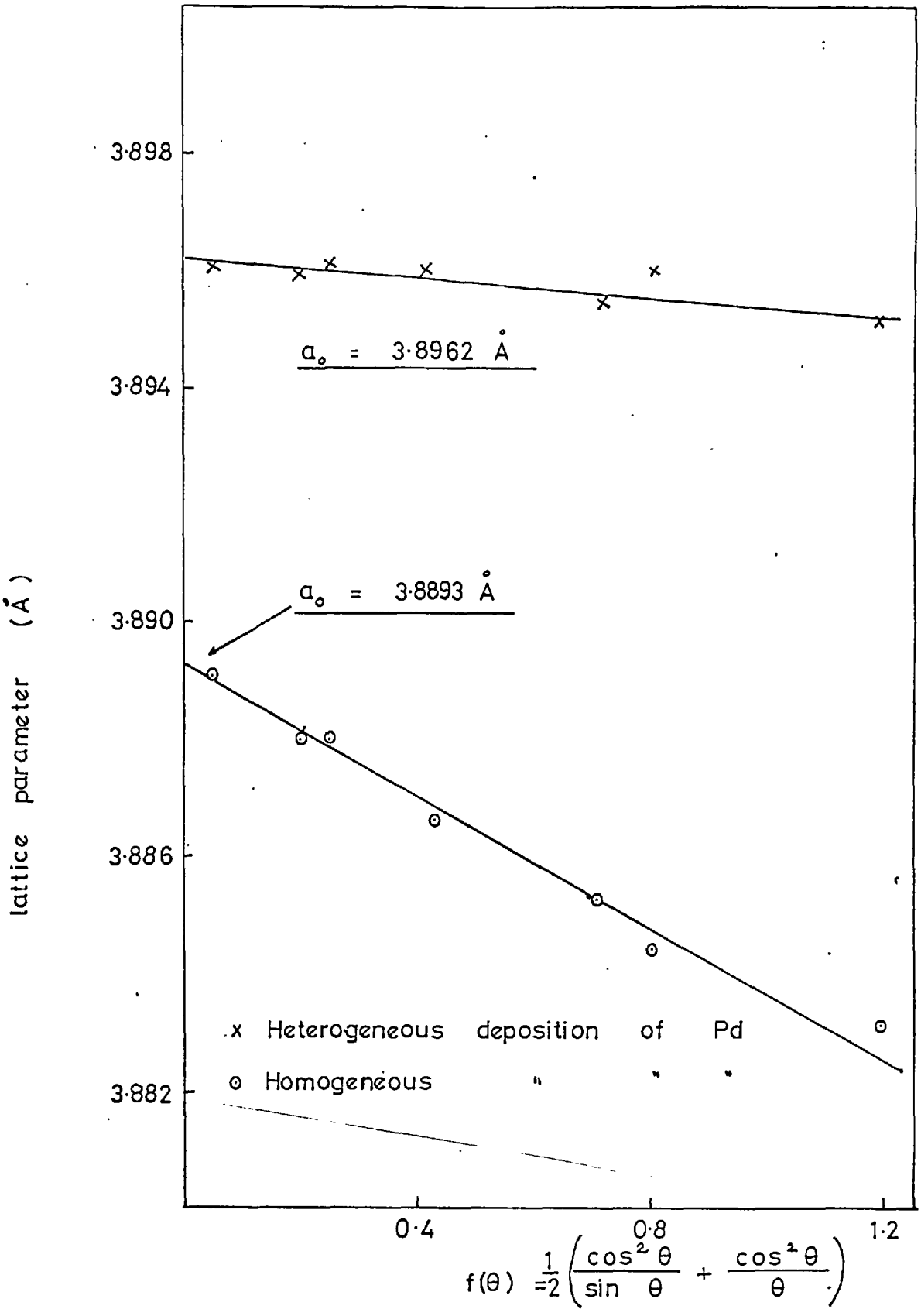

FIG. 4.2 EXTRAPOLATION OF MEASURED LATTICE PARAMETERS AGAINST THE NELSON-RILEY FUNCTION

4.3. Pin-hole pictures of nickel deposits.

The photographs taken with the filtered molybdenum K_α radiation showed that for thick deposits of nickel, the characteristic rings of the f.c.c. structure were comprised of a fine series of spots, although a few were continuous narrow rings. This indicated that the grain size of the nickel was about 10^{-4} - 10^{-5} cms. However the depth of penetration of the X-rays was so great that only very thick deposits gave pin-hole patterns that were characteristic of the deposit, rather than the substrate. In these thick deposits, there were no signs of any preferred orientation, since altering the orientation of the specimen, relative to the X-ray beam, had no effect on the diffraction pattern.

Thus the deposits of nickel on polycrystalline iron were randomly oriented, with an average grain size of 10^{-4} - 10^{-5} cms., as far as could be deduced from these studies on thick deposits.

CHAPTER 5 PHYSICAL PROPERTIES OF NICKEL DEPOSITS

5.1. Preferred orientations in deposited films.

In a polycrystalline material, the orientation of the deposit is said to be "preferred", when more grains than the statistical average are oriented in a particular direction. For a deposit of one substance on another where the deposit has one orientation only, the deposit is known as an epitaxial deposit.

Deposits are produced by the formation of nuclei on the substrate. These nuclei normally grow in three dimensions and the growing nuclei then coalesce to form a continuous thin film. Isolated three-dimensional nuclei have been observed (63), when the average thickness of the film has been less than one monolayer. A special case of islands of essentially monolayer thickness was noted (64, 65) for the case of lead, deposited on the (111) face of silver.

The conditions for the occurrence of epitaxy have been reviewed by Pashley (66). He states that there is no need for a small misfit in lattice parameter, citing the work of Schulz (67,68) on vacuum evaporation of alkali halides on to alkali halide substrates. For metals that have been electrodeposited, Pangarov (69) came to the conclusion that a lattice parameter misfit of 15% was all that could be permitted.

An important factor in the nucleation and growth of thin films is the amount of contamination on the surface of the substrate. Matthews (70) found that the epitaxial growth of gold on rock-salt was affected by whether the rock-salt surface was cleaved in air or cleaved at a vacuum of 10^{-8} torr , since this affected the number and size of gold nuclei. Compared with vacuum evaporation, whether under high or ultra-high vacuum, electrodeposition is a far less clean method of depositing metal, since the scope for contamination from the liquid phase is greater than from the vapour phase. This additional contamination may well be the reason why metals with a

large lattice parameter misfit do not show epitaxy when electrodeposited.

For the case of electrodeposited metals, Pangarov (71,72) has proposed a theory to explain the preferred orientations. In the initial stages of deposition, the deposit will be affected by the substrate. This means that a polycrystalline or amorphous substrate will produce a randomly oriented polycrystalline deposit and an (hkl) face of a single crystal substrate will produce a deposit with its (hkl) face parallel to the substrate. Later on in the deposition, the deposition conditions and current densities used become more important. His theory bases itself on the fact that the work involved in building a two-dimensional nucleus depends on the orientation of the two-dimensional nucleus and the overvoltage. Taking an example of the face-centred cubic structure (71) we have:

$$w_{hkl} = \frac{B_{hkl}}{\frac{1}{mN}(\mu - \mu_o) - A_{hkl}} \qquad (5.1.)$$

For a derivation see Appendix 3, and the symbols used are listed in Appendix 1.

For low overvoltage, i.e. when $(\mu - \mu_o)$ is small, w_{hkl} will depend on A_{hkl} and thus

$$w_{(111)} < w_{(100)} < w_{(110)} \qquad (5.2.)$$

and so the preferred orientation will be (111) planes parallel to the substrate.

For high overvoltage, μ_o and A_{hkl} may be ignored. Thus w_{hkl} will depend on B_{hkl} and

$$w_{(110)} < w_{(100)} < w_{(111)} \qquad (5.3.)$$

and the (110) planes will be parallel to the substrate.

For extremely high overvoltages, μ is very large compared with B_{hkl} and A_{hkl} and $w_{(110)} \sim w_{(100)} \sim w_{(111)}$ (5.4.)

and the orientation should be random.

This analysis, predicting the change in orientation as a function of overvoltage has been calculated for b.c.c. (71,73), c.p.h. (74) and tetragonal tin (75) structures. Examples of its usefulness can be seen in the case of electrodeposited nickel (76) and vapour deposited zinc (77). For substrates that are not inert, such as single crystals, the theory suggests that a certain proportion of substrate nuclei are inert, and that as the deposit gets thicker, the number of inert sites will increase, thus reducing the influence of the substrate with increasing deposit thickness.

The major shortcomings in the theory are its use of two-dimensional nuclei building up the deposit layer by layer, rather than by three-dimensional growth, and that it is assumed that only in exceptional circumstances can there be a randomly oriented structure. Another difficulty is that the effect of surface contamination has been ignored, while, as has been shown earlier, even in vacuum evaporation methods, care has to be taken to eliminate contamination as a cause of a particular mode of growth in the deposit.

5.1.1. Preferred orientation in chemically deposited films.

Compared with electrodeposits and vapour-deposited films, very few preferred orientations of chemically deposited metals have been reported. In the work of Graham (10), the as-plated nickel-phosphorus alloy had no preferred orientation, though a 111 fibre axis appeared on heat treatment. Fisher and Koopman (78), in their study of a cobalt-phosphorus alloy, found the preferred orientation was $[10\bar{1}0]$ parallel to the substrate, but with increasing hypophosphite concentration, the secondary texture $[11\bar{2}0]$ began to appear. This work was done using a sensitised Mylar substrate. The work of Frieze (79) on the same cobalt-phosphorus alloy showed that the $[10\bar{1}0]$ preferred orientation applied to thick deposits of alloy with a phosphorus content of more than 2%. This confirmed

Fisher's (78) work. For very thin non-continuous deposits and for lower phosphorus contents, Frieze (79) found a [0001] preferred orientation. The effect of substrate was investigated by Morton and Fisher (80). They found the same $[10\bar{1}0]$ orientation on Mylar but on a nickel-phosphorus substrate they found an initial [0002] orientation with $[10\bar{1}0]$ as a secondary texture. As the film got thicker the 0002 gave way to $[10\bar{1}0]$. The preferred orientations got more pronounced on the metal substrate.

For nickel deposited by hydrazine, Levy (46) reported that the deposits were randomly oriented.

In general, cobalt seems to have a $[10\bar{1}0]$ preferred orientation while there seems to be no data on the preferred orientation of nickel deposits.

5.2. Electron probe microanalysis.

The plated specimens examined with the electron probe microanalyser gave results shown in Plate 5.1. This shows a substrate of pure copper with a layer of pure nickel on top, approximately 3 μm. thick. The layers are separate, and there is no detectable diffusion of copper into the nickel deposit or nickel into the copper substrate. Adhesion between the deposit and the substrate was good, since very few discontinuities were created along the length of the composite, even when sectioned and polished prior to examination in the electron probe. As can be seen in Plate 5.1., the coating laid down is quite smooth and even in thickness over the whole substrate area.

5.3. Scanning electron microscopy.

The films of nickel deposited on the glass cover slides were a dull black colour with no metallic lustre. Most were continuous over the whole area of the cover slide, but one or two slides were

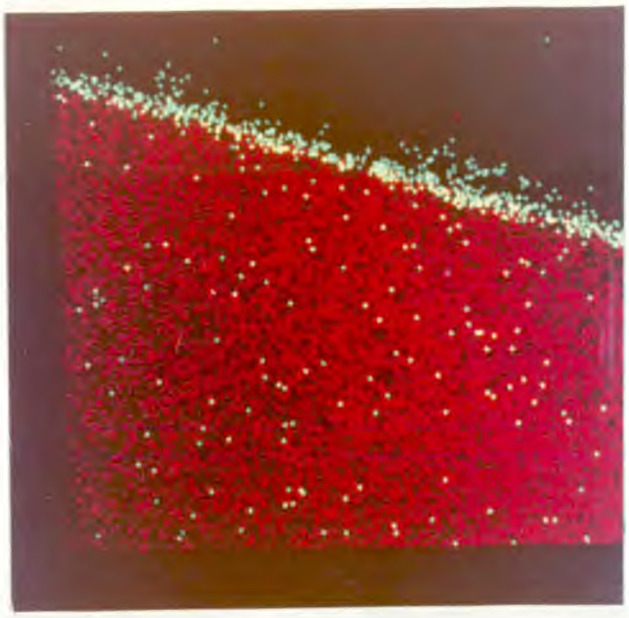

Green - Nickel

Copper - Red

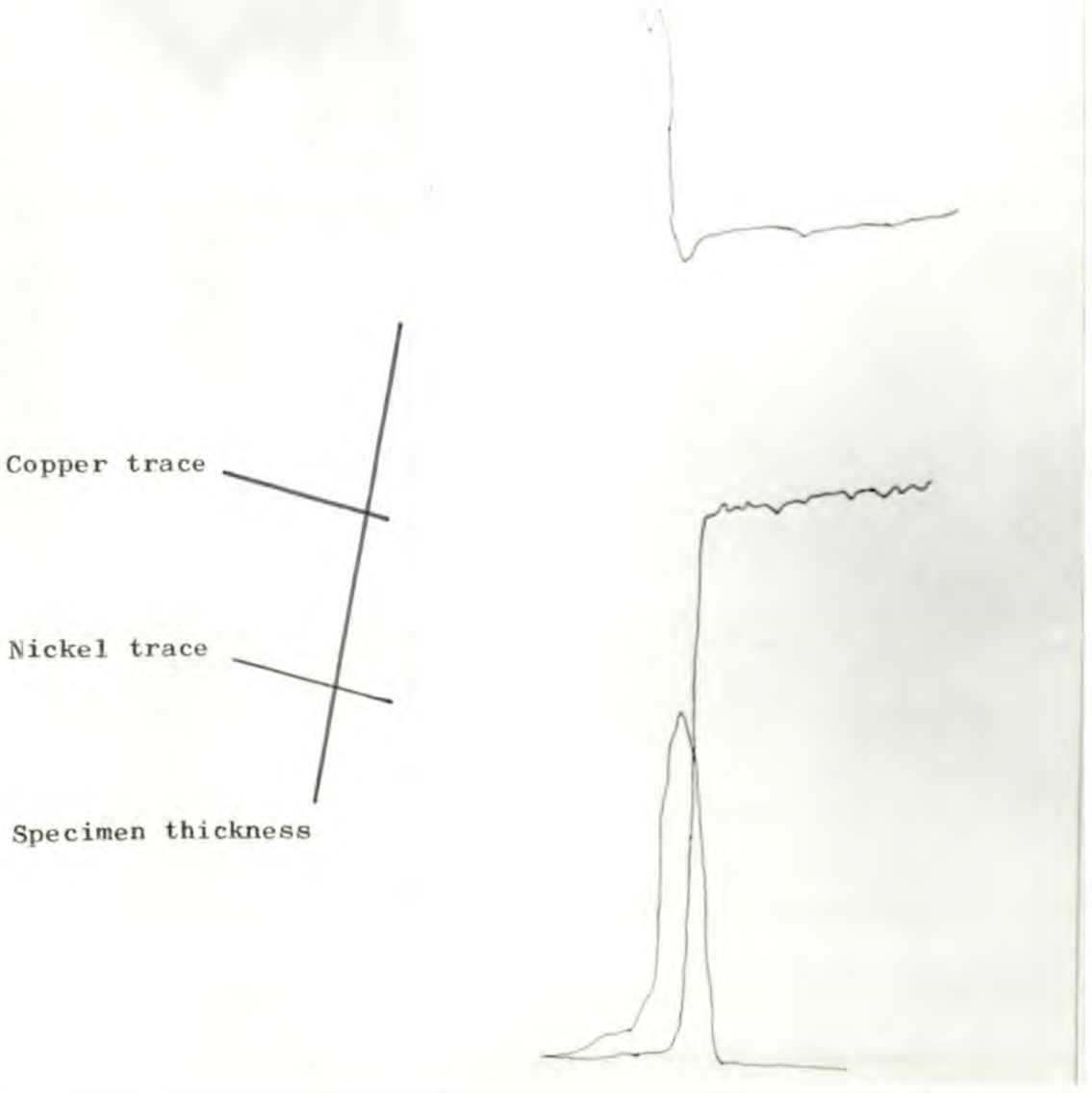

Plate 5.1. Electron probe microanalysis.

(a) x 71

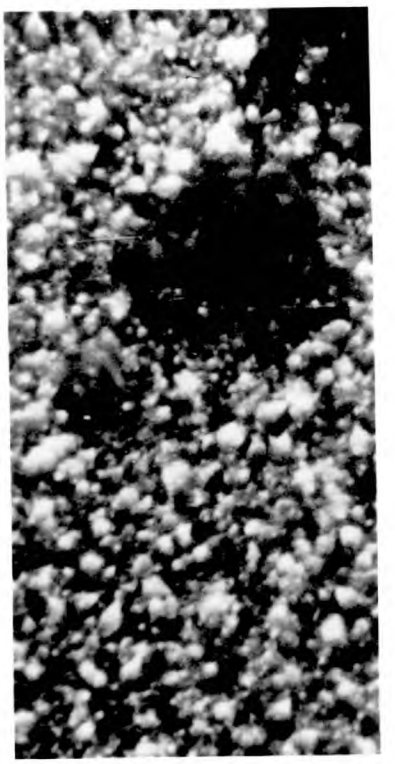

(b) x 14,200

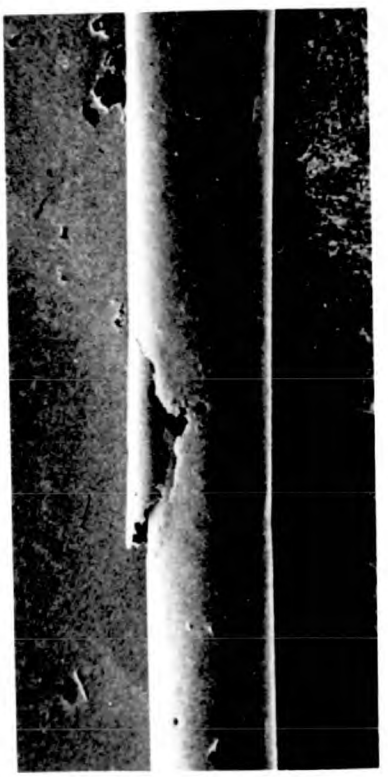

(c) x 81

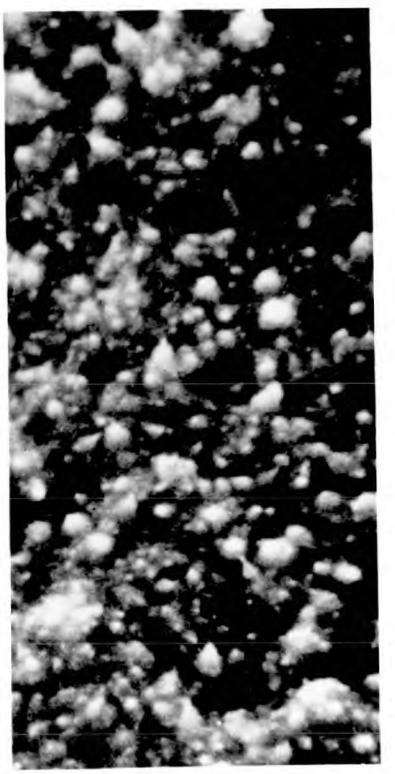

(d) x 15,700

PLATE 5.2 SCANNING ELECTRON MICROGRAPHS

only partly covered, giving a discontinuous jagged appearance to the film. These cases were probably due to incomplete activation of the glass by the palladium activation solutions. In contrast to the black surface in contact with the nickel plating solution, the surface in contact with the glass and all freshly cut surfaces, showed the characteristic silver lustre of metallic nickel.

Examples of scanning electron micrographs can be seen in Plate 5.2. Specimens (a) and (b) are nickel foils deposited on a palladium activated glass slide, while specimens (c) and (d) are foils taken from the walls of the container, which had not been previously activated.

Under low magnification, specimen (a) can be seen as a thin foil, which has a tendency to curl up and separate from the substrate. This curling exposes the fresh silver appearance, characteristic of newly cut nickel foil, rather than the dull black of the nickel deposits. Other specimens that had been deposited at lower deposition rates, showed less curling and were flat and dull black in colour.

Specimen (b) is taken from the same area of the specimen as specimen (a) and is typical of all the foils prepared. At this high (x 14,200) magnification, the specimen appears to have a fine-grained structure, and possesses a uniform grain size. No very large line discontinuities appear in the structure. In specimen (b) there are several light patches, which appear similar to light patches noticed at x 1000 magnification. When the dark and light patches at x 1000 were alternately magnified to x 10,000, they gave similar pictures of this fine-grained structure. Therefore, it can be thought that these light patches in specimen (b) will give a structure at higher magnifications. However at magnifications higher than x 15,000, there was a lot of electronic noise with the signal, and the images obtained were less reliable.

Specimen (c), which has a magnification of x 81, shows a flat nickel foil, curled at the end into a tight roll. The rough surface adjacent to the roll is a silver 'dag' solution added to make the specimen conduct the beam current of the microscope. In appearance this deposit on a non-activated surface is similar to those deposited on a palladium activated substrate.

Specimen (d) gives the same fine-grained structure as the deposits like specimen (b). Here there are no sharp boundaries and the structure is very homogeneous. Any further increase in magnification produced a picture with very little contrast over the prevailing electronic noise.

In general, the deposits of nickel were of a uniform fine grain size and were also characterised by rolls and curls at the edges of specimens. The appearance of foils deposited on glass activated by palladium and unactivated glass was not significantly different when examined under the scanning electron microscope.

5.4. Electron diffraction.

The results of depositing nickel on to various copper substrates are shown in Plate 5.3. All show ring patterns characteristic of f.c.c. nickel.

Patterns (a) and (b) are diffraction patterns of nickel deposited on the (110) face of a copper single crystal. (a) is the pattern of a thin layer of nickel, while (b) is the pattern of a thicker layer of nickel, deposited from the same solution. Thus (a) will represent the structure of (b) closer to the substrate, as the depth of penetration of 100 kV electrons is only a few atomic layers. Both show a ring pattern of polycrystalline f.c.c. nickel with no spots typical of single crystal structures. These patterns remained unchanged when the specimen was tilted with respect to the electron beam. Tilting was done to eliminate the possibility of the texture

(a) Nickel on (110) copper substrate

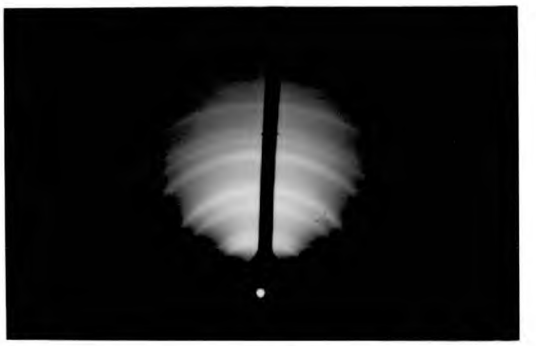

(b) Nickel on (110) copper substrate

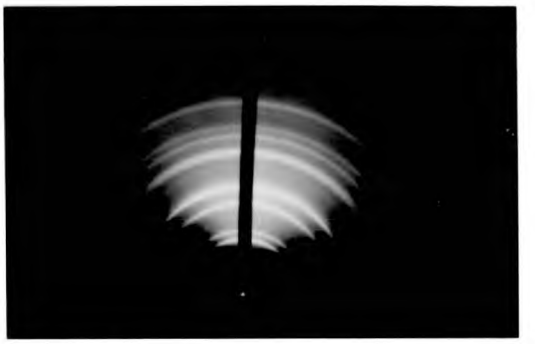

(c) Nickel on (100) copper substrate

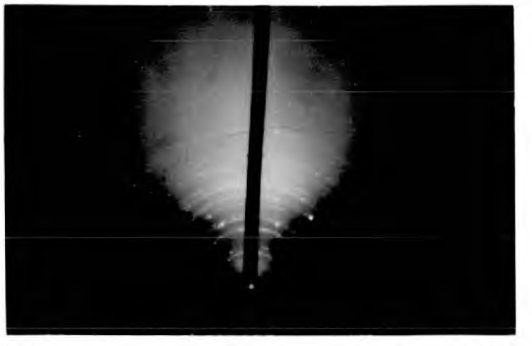

(d) Nickel on copper polycrystal

PLATE 5.3 ELECTRON DIFFRACTION

axis of the specimen being parallel to the electron beam.

Pattern (c) comes from a thick deposit of nickel, similar to (b), except that the substrate was a (100) face of the copper single crystal. Here again, the plate shows a series of uniform rings, whose intensities and appearance do not change with tilting the specimen. There were no spots characteristic of the single crystal structure in the pattern.

Pattern (d) is a nickel film deposited on a polycrystalline copper substrate. Compared with patterns (a) - (c), the rings, although characteristic of f.c.c. nickel, are not so sharp and there is a certain amount of "spottiness" in the pattern. However this pattern remains identical within the accuracy possible by inspection, when the specimen is tilted with respect to the electron beam. This kind of pattern was not typical of all deposits on polycrystalline nickel, the majority being of the uniform ring pattern described in (a) - (c).

In all the specimens, the lines were sharp and did not have diffuse edges. This indicates a large grain size and confirms the value of 10^{-4} - 10^{-5} cms. given in 4.3., as a reasonable estimate of the grain size.

Thus, electron diffraction shows there is no epitaxy in chemically deposited nickel, and that the deposited films have no preferred orientation. They are polycrystalline with a grain size greater than 1000 A^{o}, and the substrate has no effect on the structure of the deposit.

CHAPTER 6 DISCUSSION OF RESULTS

6.1. The chemistry of nickel deposition.

The chemistry of nickel deposition may be summarised under four heads:-

a) Energetics of reaction.

b) Spectral and other evidence about complexes in solution.

c) Kinetic results.

d) Spontaneous decomposition of the solution.

6.1.1. Energetics of reaction.

The hydrodynamics of and mass transfer to a rotating disc have been summarised by Levich (55). For a disc rotating with laminar flow of fluid toward the disc, the rate of flow of fluid is given by:

$$I \propto \omega^{0.5} \qquad (6.1.)$$

For a disc rotating with turbulent flow of fluid toward the disc, the rate of flow of fluid is given by:

$$I \propto \omega^{0.9} \qquad (6.2.)$$

The onset of turbulence comes when:

$$Re = \frac{r^2 \omega}{\nu} \sim 1 - 5 \times 10^4 \qquad (6.3.)$$

the higher figure applying to the case of a well-polished and centred disc.

Thus in the case of the experiments outlined in 3.1., there was laminar flow, except for the case of the two highest speeds, where the flow could have been turbulent.

In all cases, however, the rate of reaction was independent of the rotation speed of the disc, and this suggests that the rate of transport of the nickel ions to the surface of the disc was not the rate-controlling step of the reaction.

Another test for the presence of a transport-controlled reaction is the activation energy of the reaction. For laminar flow (55):

$$I \propto D^{2/3} \nu^{-1/6} \quad (6.3.)$$

and $D = D_o \exp(-E_D/RT)$ where $E_D \sim 3$ k.cal. mole^{-1} (6.4.)

$$\nu = \nu_o \exp(+E_\nu/RT) \text{ where } E_\nu \sim 3.6 \text{ k.cal. mole}^{-1} \quad (6.5.)$$

then $I = I_o \exp(-(4E_d + E_\nu)/6RT)$ (6.6.)

and the activation energy should be approximately 3 k.cal. mole^{-1}.

Similarly for turbulent flow (55):

$$I \propto D^{3/4} \nu^{-0.65} \quad (6.7.)$$

then $I = I_o \exp(-(0.75 E_D + 0.65 E_\nu)/RT)$ (6.8.)

and the activation energy should be approximately 4.5 k.cal. mole^{-1}.

In this work, the activation energy was measured as 18.3 $\pm$ 0.9 k.cals. mole^{-1} at higher temperatures and 34 $\pm$ 5 k.cals. mole^{-1} at lower temperatures. This confirms that the transport of nickel ions to the disc surface is not the rate-controlling step in the reaction. The value of 18.3 k.cals. mole^{-1} suggests that a chemical reaction at the catalytic surface of the disc is rate-controlling. At the lowest temperatures, where readings are more inaccurate due to the slow rate of deposition of metal, the estimated activation energy is 34 k.cals. mole^{-1}. This high activation energy barrier at lower temperatures has been noted in heterogeneous reactions, and is possibly due to there being an adsorption layer at the catalytic surface.

The rate dependence on the chemical reaction at the surface may be confirmed by estimating the rate of transport of nickel ions to the rotating disc and comparing this with the measured rate of reaction.

Extrapolating the upper section of Fig. 3.2. to a temperature of 25^{o}C. gives:

$$-\left[\frac{d(Ni^{2+})}{dt}\right]_{11} \sim 7 \times 10^{-11} \text{ moles } l^{-1} \text{ sec}^{-1} \text{ cm}^{-2} \quad (6.9.)$$

for the rate of chemical reaction.

Kakovsky (81) gives the rate equation for convective diffusion at 25^{o}C. as:

$$-\left[\frac{d(Ni^{2+})}{dt}\right]^{11} = K \cdot [Ni]_t \; w^{1/2} \qquad (6.10.)$$

where $K = 6.18 \times 10^{-4} \; D^{2/3} \; \nu^{-1/6}$ (6.11.)

and w is in revolutions per second.

The diffusion coefficient and viscosity for a solution of 0.02 M nickel chloride are not known but may be approximated to those of a 0.01 M solution of potassium nitrate. Thus:

$$D = 1.85 \times 10^{-5} \text{ cm}^2 \text{ sec}^{-1} \qquad (6.12.)$$

$$\nu = 8.98 \times 10^{-3} \text{ cm}^2 \text{ sec}^{-1} \qquad (6.13.)$$

Therefore for a speed of 700 r.p.m., similar to Fig. 3.2., one obtains:

$$-\left[\frac{d(Ni^{2+})}{dt}\right]^{11} = 6.5 \times 10^{-8} \text{ moles } l^{-1} \text{ sec}^{-1} \text{ cm}^{-2} \qquad (6.14.)$$

Thus the rate of transport of the nickel ions to the rotating disc is much faster than the rate of chemical reaction at the disc surface. The results of the activation energy plot and the variation of reaction rate with rotation speed are thus confirmed.

The activation energy for the reduction of nickel salts using hydrazine has been estimated as 11 k.cals. mole^{-1}, from the work of Dini and Coronado (48). A value of 15.7 k.cals. mole^{-1} has been reported for the cobalt-hydrazine system by Levy (47). Comparative results for the reduction of cobalt (II) ammines by gaseous hydrogen, obtained by Needes (62) give an activation energy of 16.4 - 19.6 k.cal. mole^{-1}, depending on the catalytic seed used to initiate the reaction. The activation energy of the reduction of nickel (II) ions by hypophosphite has been measured as 17.7 k.cal. mole^{-1} (82) and 14.5 k.cal. mole^{-1} (83) on an aluminium substrate, with a slightly higher value for an iron substrate (83). Thus it seems that the reactions:

$$Ni^{2+} \; (3d^8) \xrightarrow{+2e^-} Ni \; (3d^8, \; 4s^2) \qquad (6.15.)$$

and $Co^{2+} \; (3d^7) \xrightarrow{+2e^-} Co \; (3d^7, \; 4s^2)$ (6.16.)

have similar activation energies of approximately 16 k.cals. mole^{-1},

and the value obtained in this work of 18.3 k.cals. $mole^{-1}$ is consistent with these values.

The reduction of palladium (II) ions can be stated as:

$$Pd^{2+} (4d^8) \xrightarrow{+2e^-} Pd (4d^{10}) \qquad (6.17.)$$

As the 4d and 4s electrons are very similar in energy, the reduction of palladium (II) ions should have similar energetics to the reduction of nickel (II) ions, where electrons are transferred to the 4s shell. The activation energy of the homogeneous reaction of palladium (II) ions with hydrazine to form palladium powder has been measured (37) as 17.3 - 20.9 k.cals. $mole^{-1}$, depending on the complexing agents and concentrations of palladium used. This suggests that the reduction of nickel, cobalt and palladium ions have great similarities, and this is connected with the similar structure of the divalent ions.

6.1.2. Complexes in solution: Spectral and other data.

The study of the visible and ultra-violet spectra of solutions used in this work can give an insight into the complexes formed by the various chemical species. When nickel chloride and potassium sodium tartrate are mixed, their spectrum shows a peak at 390 nm, as shown in Fig. 3.13 (b). This peak probably corresponds to the bonding of the nickel ion and the tartrate ion in a complex, possibly a 1:1 complex as suggested by Bobtelsky (44). If nickel ions and hydrazine are mixed, the principal peak in the spectrum is at 244 nm (this happens to be close to the 239 nm peak for the palladium-hydrazine system (37)). Nickel-hydrazine complexes are known (84). These comprise the stepwise addition of six N_2H_4 ligands to the nickel (II) ion to form an octahedral complex with a stability constant $\log \beta_6 = 11.99$. The peak at 244 nm is probably due to these complexes. However, if hydrazine is added to the nickel and tartrate solution, the 390 nm peak is shifted to 360 nm. This

suggests that the presence of hydrazine affects the energy of the bond in the complex $\left[Ni(tar).\ nH_2O\right]$, and, since hydrazine forms complexes easily with the nickel (II) ion according to the equation:

$$\left[Ni.\ 6H_2O\right]^{2+} + nN_2H_4 = \left[Ni.\ nN_2H_4.(6-n)\ H_2O\right]^{2+} \qquad (6.18.)$$

a mixed nickel-hydrazine-tartrate complex does form according to the equation:

$$\left[Ni(tar).\ nH_2O\right] + x\ N_2H_4 = \left[Ni(tar).\ x\ N_2H_4.\ (n-x)H_2O\right] \qquad (6.19.)$$

Evidence for the formation of these mixed complexes comes from observations during the solution preparation. When the nickel chloride and potassium sodium tartrate have been dissolved in water and hydrazine added, a precipitate is formed which dissolves on the addition of further hydrazine. This precipitate was washed, dried and analysed. If one assumes that all the carbon is in the form of tartrate and all the nitrogen in the precipitate is in the form of hydrazine, then the empirical formula for the precipitate may be written as: $8Ni.\ 8N_2H_4.\ 5(tar).\ 3H_2O$. This has: Ni, 30.88; C, 15.79; H, 3.84; N, 14.74 and O (by difference), 34.72%. Found was Ni, 31.38; C, 15.74; H, 3.80; N, 14.19 and O (by difference), 34.89. Thus this precipitate may be regarded as a mixed complex of nickel (II), hydrazine and the tartrate ion.

At a pH of 10 - 13 copper (II) forms an anionic complex with the tartrate and hydroxyl ions (85) according to the equation:

$$\begin{array}{l} \left[Cu(tar)\right] + H_2O \rightarrow \left[Cu(tar)(OH)\right]^- + H^+ \\ \qquad\qquad\qquad\qquad\quad \downarrow + H_2O \\ \qquad\qquad\qquad\qquad\quad \left[Cu(tar)(OH)_2\right]^{2-} + H^+ \end{array} \qquad (6.20.)$$

To determine whether nickel forms such an anionic species, a solution of 0.02 M nickel chloride, 0.02 M potassium sodium tartrate and 1 M hydrazine was made up at a pH of 11. The solution was electrolysed and the migration of ions noted. Nickel was deposited at the cathode, presumably from $\left[Ni.\ nN_2H_4\right]^{2+}$ and free Ni^{2+} ions, while

there was no sign of migration of nickel complexes to the anode. Thus there were no anionic complexes of the type $\left[Ni(tar)(OH)_n\right]^{n-}$ in the working solutions.

6.1.3. Kinetics of reaction.

In this work, the parameters measured were the rate of metal deposition and the total concentrations of the reagents, nickel, tartrate, hydrazine, etc., used. The rate of nickel deposition can be considered to be proportional to the rate of loss of nickel ions from the solution. To derive a proper rate law, one must know the concentrations of the reacting species. These cannot be measured directly and there is not sufficient thermodynamic data to calculate their concentrations from the total concentrations of reagents used, except in an empirical manner. The results of the kinetic measurements may be summarised as follows:

$$\text{Rate} \propto -\left[\frac{d(Ni^{2+})}{dt}\right] \propto \frac{[Ni]_t}{[L]_t \{H\}^2} \qquad (6.21.)$$

This is not a true rate law, since the quantities on the right-hand side of the equation do not represent the actual reacting species.

Spectral and other evidence, outlined in 6.1.2., has indicated that the complexes in solution could be $\left[Ni.\ nN_2H_4\right]^{2+}$ and $\left[NiL.\ xN_2H_4\right]$. The concentration of free nickel ions is low. It seems more reasonable that the reaction takes place by the breakdown of a relatively long-lived complex at the substrate, rather than a collision mechanism between a nickel ion and a hydrazine molecule, via a short-lived intermediate.

In the case of the dissociation of tartaric acid, the stability constant for:

$$H^+ + L^{2-} = HL^- \qquad (6.22.)$$

is $$K_1 = \frac{[HL]}{[H^+][L^{2-}]} = 10^{4.4} \qquad (6.23.)$$

at 50°C. at zero ionic strength (86). This means at pH ~ 11, the solution can be regarded as containing L^{2-} ions only. Similarly the dissociation constant for malonic acid is log K_1 = 5.72 (87) at 35°C., and at pH ~ 11, the solution can be regarded as comprising L^{2-} ions only.

Considering the experiments with tartrate as the complexing agent, results can be derived over the range of conditions used, by assuming various values for the stability constants of:

$$K_1 = \frac{[NiL]}{[Ni^{2+}][L^{2-}]} \qquad (6.24.)$$

and $$\beta_n = \frac{[Ni.\ nN_2H_4]}{[Ni^{2+}][N_2H_4]^n} \qquad (6.25.)$$

These results can be compared with the measured rate equation.

(a) Effect of varying nickel concentration.

The experimental work was carried out under the following conditions:

$[Ni]_t$: 0.01 - 0.04 M $[L]_t$ = 0.02 M

$[N_2H_4]_t$: 1.0 M pH = 11.0

For values of $K_1 = 10^2$, 10^3 and 10^4, the graphs shown in Fig. 6.1. were obtained for the free nickel ion concentration, $[Ni^{2+}]$, over the range of nickel concentrations 0.01 - 0.04 M. Specimens of the calculations are shown in Appendix 4.

When the equilibrium between the free nickel ion and hydrazine is considered, the concentration of free nickel ion taken from Fig. 6.1. may be regarded as being equal to the concentration of $[Ni.\ nN_2H_4]^{2+}$ after equilibration for all $\beta_n > 10^2$. For calculations of this, see Appendix 4. Since the published stability constant (84) for nickel (II) and hydrazine is log β_6 = 11.99 (log β_2 = 5.20), the concentration of $[Ni^{2+}]$ plotted on Fig. 6.1. may be regarded as equal to the $[Ni.\ nN_2H_4]^{2+}$ concentration in the

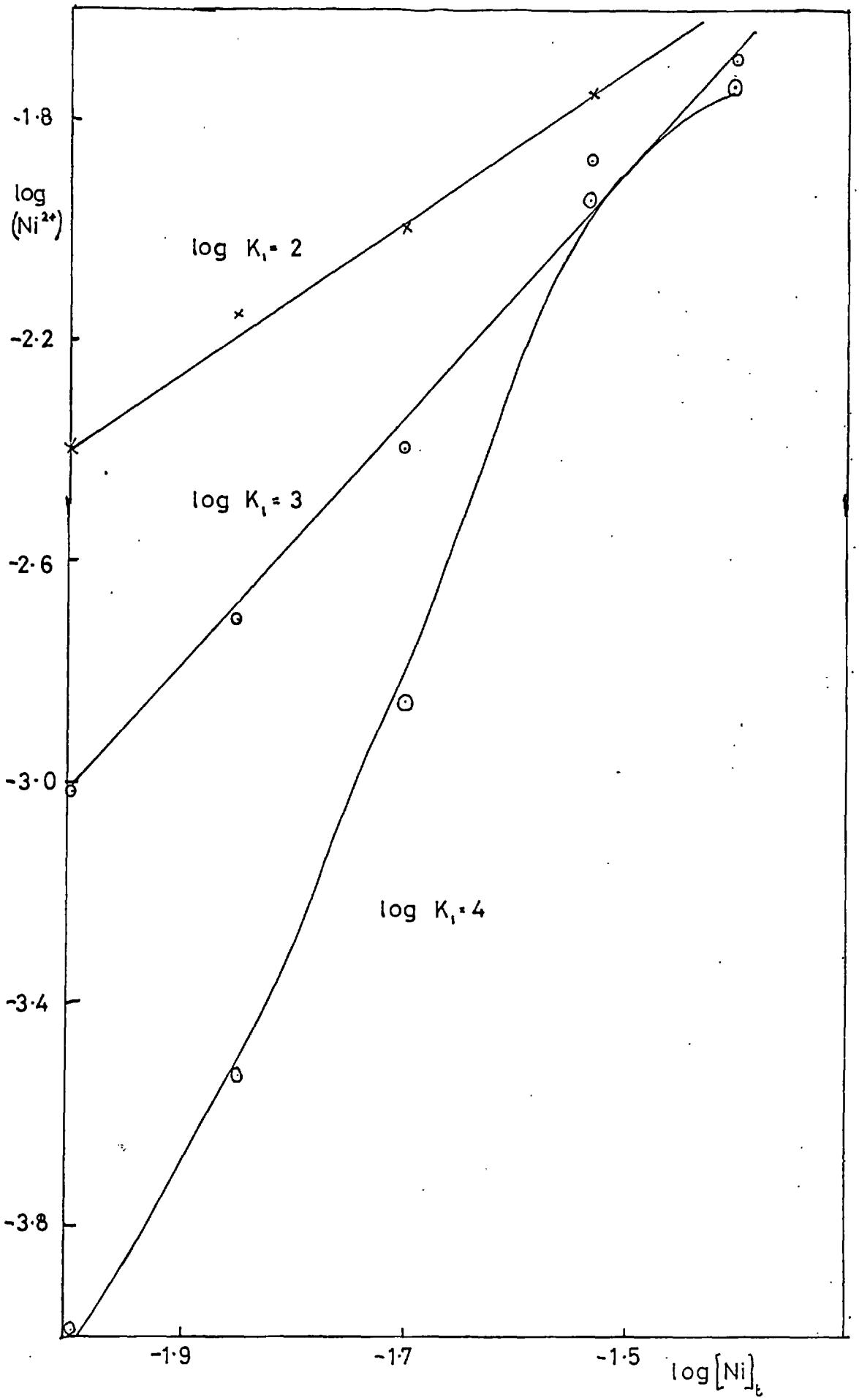

FIG. 6.1 CONCENTRATION OF FREE NICKEL ION AS FUNCTION OF NICKEL CONCENTRATION

deposition solution.

The values of K_1 assumed cover the probable value for the $[NiL]$ complex. The only data on complexes of the transition metals, Co, Ni, Cu, Zn with the tartrate ion are log K_1 = 3.2 for copper (II) (85) and log K_1 = 2.68 for zinc (II) (88). From data from the ammine systems from Bjerrum (89), the stability constants of the complexes are in the order:

$$Zn^{2+} < Cu^{2+} > Ni^{2+} > Co^{2+} \qquad (6.26.)$$

with copper being the most stable. Thus the stability constant for the complex $[NiL]$ may be estimated as log $K_1 \sim 2 - 3$.

Inspecting the graphs of Fig. 6.1., the graphs of log K_1 = 2 and log K_1 = 3 may be approximated to straight lines of slopes + 1.4 and + 2.2 respectively. The graph of log K_1 = 4 is an S-curve, often seen in solvent extraction studies. The experiments detailed in Fig. 3.3. give a slope for a log $\left[-\frac{d(Ni^{2+})}{dt}\right]$ 11 against log $[Ni]_t$ of + 1.12.

(b) Effect of varying tartrate ion concentration.

The experimental conditions used were:

$[Ni]_t$ = 0.025 M $[L]_t$ = 0.0125 - 0.05 M

$[N_2H_4]_t$: 1.0 M pH 11.0

Using a similar method to that described in (a), the calculations were repeated for these conditions, to give Fig. 6.2. of log $[Ni^{2+}]$ against log $[L]_t$. This again was taken as equal to the concentration of $[Ni.\ nN_2H_4]^{2+}$.

For log K_1 = 2 and log K_1 = 3, the graphs of Fig. 6.2. may be approximated to straight lines of slope - 0.7 and - 1.68 respectively. The graph of log K_1 = 4 is an S-curve similar to the one in Fig. 6.1. The experimental work detailed in Fig. 3.4. gives a slope of - 1.14.

If the concentration of a mixed complex $[NiL.\ nN_2H_4]$ is considered we have:

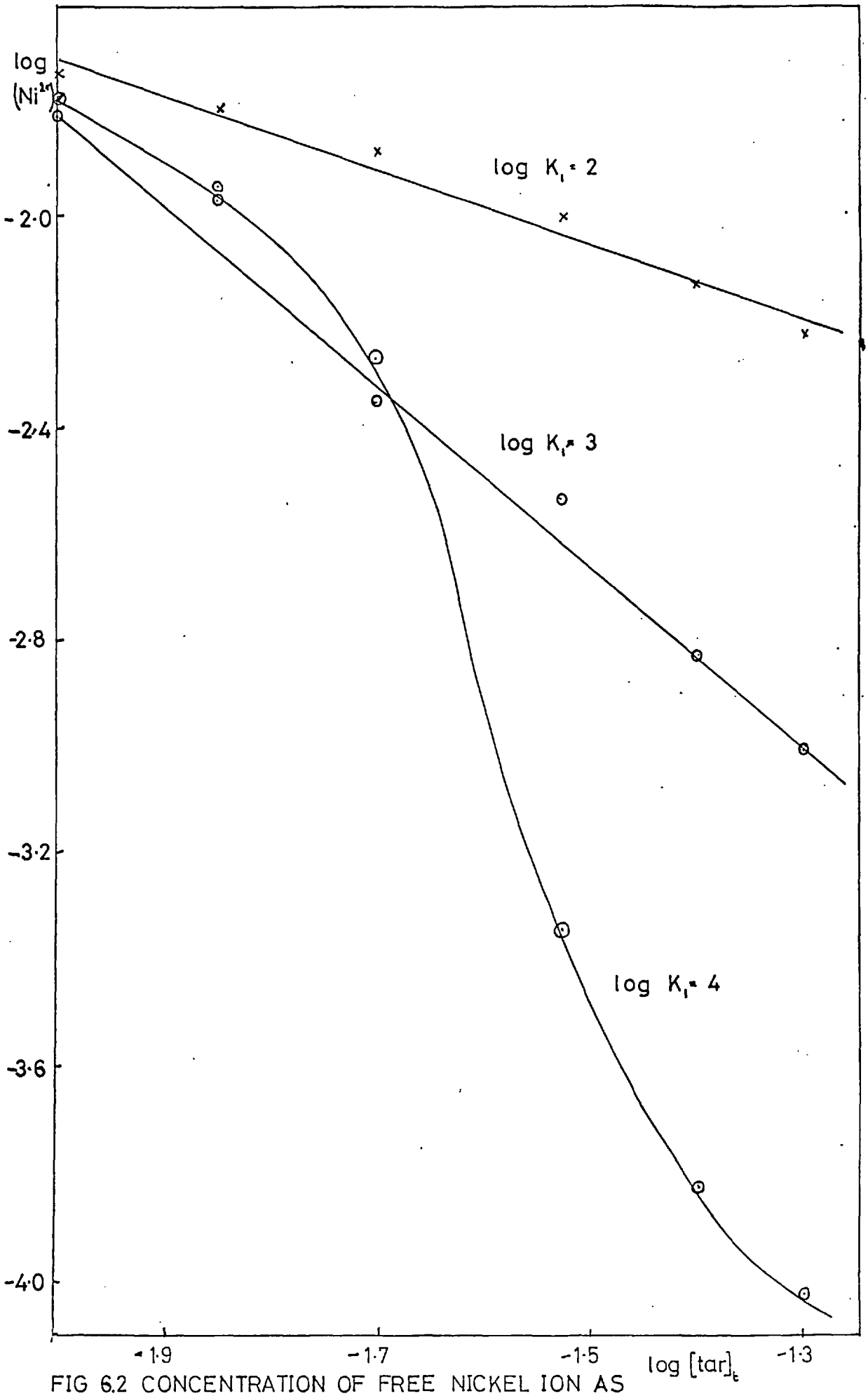

FIG 6.2 CONCENTRATION OF FREE NICKEL ION AS FUNCTION OF TARTRATE CONCENTRATION

$$Ni^{2+} + L^{2-} = NiL \qquad (6.27.)$$

$$K_1 = \frac{[NiL]}{[Ni^{2+}][L^{2-}]} \qquad (6.28.)$$

and $$NiL + nN_2H_4 = NiL.\ nN_2H_4 \qquad (6.29.)$$

$$\beta_n = \frac{[NiL.\ nN_2H_4]}{[NiL][N_2H_4]^n} \qquad (6.30.)$$

When the total concentration $[L]_t$ of tartrate is increased, the concentration of complex $[NiL]$ will increase, for log $K_1 \sim 2 - 3$, until the nickel is nearly all present as complex, when the concentration of complex $[NiL]$ will remain approximately constant. Assuming as before that $\log \beta_n > 2$, the concentration of $[NiL]$ taken from equation 6.28 may be approximated to the concentration of complex $[NiL.\ nN_2H_4]$ against $\log [L]_t$ should give a line of positive slope up to the point $[Ni]_t = [L]_t$ and of approximately zero slope at higher concentrations of tartrate ion. The experimental results give a negative slope for this plot, and this indicates that there is no direct relation between the rate of deposition and the concentration of the complex $[NiL.\ nN_2H_4]$.

(c) Effect of varying hydrazine concentration.

The experimental conditions were:

$[Ni]_t = 0.02\ \underline{M}$ $\qquad$ $[L]_t = 0.02\ \underline{M}$

$[N_2H_4]_t = 1.0 - 3.0\ \underline{M}$ $\qquad$ pH = 11.0

Considering the equilibrium:

$$Ni^{2+} + nN_2H_4 = Ni.\ nN_2H_4^{\ 2+} \qquad (6.31.)$$

$$\beta_n = \frac{[Ni.\ nN_2H_4^{\ 2+}]}{[Ni^{2+}][N_2H_4]^n} \qquad (6.32.)$$

The calculations, shown in Appendix 4, show that the concentration of complex $[Ni.\ nN_2H_4]^{2+}$, for $\log \beta_n > 2$, can be equated to the total nickel concentration of equation 6.32, i.e. $[[Ni^{2+}] + [Ni.\ nN_2H_4]^{2+}]$ over the range $[N_2H_4]_t = 1 - 3\ \underline{M}$. The accuracy of this approximation

improves with higher stability constant and higher hydrazine concentration.

Since the total nickel concentration and the total tartrate concentration remain constant, the concentration $\left[\left[Ni^{2+}\right] + \left[Ni.\ nN_2H_4\right]^{2+}\right]$ in equation 6.32 remains constant. Therefore the concentration of complex $\left[Ni.\ nN_2H_4\right]^{2+}$, is independent of the total hydrazine concentration, as a first approximation.

The experimental work outlined in Fig. 3.7. shows that the rate of nickel deposition is independent of the total hydrazine concentration.

(d) Effect of varying malonate ion concentration.

For the reaction:

$$Ni^{2+} + L = NiL \qquad (6.33.)$$

$$K_1 = \frac{[NiL]}{[Ni^{2+}][L^{2-}]} \qquad (6.34.)$$

$\log K_1$ for the malonate ion is 4.1 (90). Since this stability constant is valid only as an approximation in solutions other than the one in which the measurement was made, the values of $\log K_1 = 1$, 3 and 5 were taken. For the experimental conditions:

$[Ni]_t = 0.005\ \underline{M}$ $\qquad$ $[L]_t = 0.05 - 0.15\ \underline{M}$

$[N_2H_4]_t = 1.0\ \underline{M}$ $\qquad$ pH = 11.0

calculations similar to those in (a) and (b) were done to calculate the free $[Ni^{2+}]$ concentration. These are outlined in Appendix 4, and are plotted in Fig. 6.3. For $\log K_1 = 3$ and $\log K_1 = 5$, the slope can be taken as approximately -1. For $\log K_1 = 1$, the slope has a value of approximately - 0.3.

The experimental results detailed in Fig. 3.8. give a slope of - 0.98 for a plot of $\log \left[-\frac{d(Ni^{2+})}{dt}\right]^{11}$ against $\log [L]_t$.

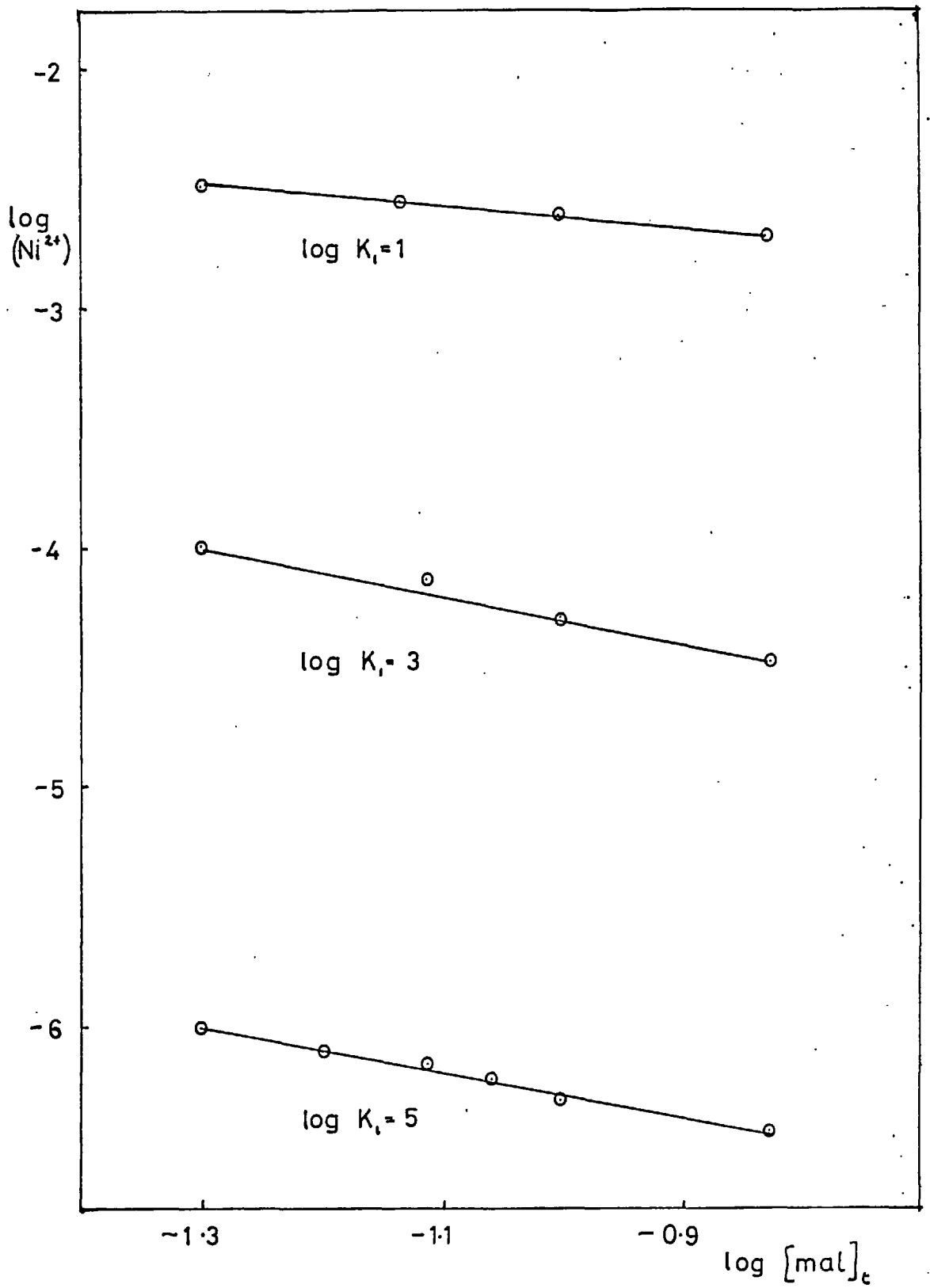

FIG. 6.3 CONCENTRATION OF FREE NICKEL IONS AS A FUNCTION OF MALONATE CONCENTRATION

(e) Effect of pH.

The analysis of the previous sections shows that the concentration of all species is unaffected by the pH of the solution, in the pH ranges used in this work. Therefore the variation of deposition rate with pH must be caused in a different way than the variation of deposition rate with reagent concentrations discussed in (a) - (d).

The oxidation of hydrazine to nitrogen and water has been described by Kirk and Browne (91). Their scheme is:

$$N_2H_4 \longrightarrow N_2H_2 + 2H^+ + 2e^- \qquad (6.35.)$$

with either

$$2\ H_2N.\ N \longrightarrow \underset{\text{tetrazene}}{N_4H_4} \longrightarrow N_2 + N_2H_4 \qquad (6.36.)$$

or

$$\underset{\text{di-imide}}{HN : NH} \longrightarrow N_2 + 2H^+ + 2e^- \qquad (6.37.)$$

Both give an overall reaction of

$$N_2H_4 \longrightarrow N_2 + 4H^+ + 4e^- \qquad (6.38.)$$

or

$$N_2H_4 + 4OH^- \longrightarrow N_2 + 4H_2O + 4e^- \qquad (6.39.)$$

as outlined in 1.2.1. Thus hydrazine species tend to be oxidised, and these oxidation reactions involve the liberation of hydrogen ions. Therefore for the reaction:

$$A = B + H^+ \quad \text{Rate constants } k_1,\ k_{-1} \qquad (6.40.)$$

$$-\frac{d[A]}{dt} = k_1 A - k_{-1}[B][H^+] \qquad (6.41.)$$

Thus the rate will be slowed if there is an increased concentration of hydrogen ions, provided that $k_1[A]$ and $k_{-1}[B][H^+]$ are comparable in magnitude.

Although the rate is dependent on the concentration of hydrogen ions, and pH is a measure of the activity of hydrogen ions, it can be assumed that the concentration of hydrogen ions is higher at a lower pH than at a higher pH. Therefore the rate should be faster at a high pH and slower at a low pH.

Experimentally, this is what happens and Fig. 3.6 gives

$$-\left[\frac{d(Ni^{2+})}{dt}\right]^{11} \propto \frac{1}{\{H^+\}^{1.76}} \qquad (6.42.)$$

The results of (a) - (d) seem to suggest that the rate equation could be stated as:

$$-\left[\frac{d(Ni^{2+})}{dt}\right]^{11} = K[Ni.\ nN_2H_4] \qquad (6.43.)$$

but a difficulty arises when the results for the two complexing ligands, tartrate and malonate, are compared. In the tartrate case, the concentration of complex, $[Ni.\ nN_2H_4]$ is 10^{-2} to 10^{-3} M, while in the malonate case, assuming a stability constant log $K_1 = 4$, the concentration of complex is 10^{-5} - 10^{-6} M. Although there are three orders of magnitude difference in these concentrations, the deposition rates are comparable in magnitude. Other evidence against the simple equation 6.43 are the results of varying the ligand : metal ratio in Fig. 3.5. With $[Ni]_t$ = 0.01 M and $[Ni]_t$ = 0.02 M, runs were made varying the tartrate concentrations. Both sets of results were fitted into Fig. 3.5, and within experimental scatter, fit on the same straight line in Fig. 3.5. The concentrations of the complex $[Ni.\ nN_2H_4]$ would be different for the two sets of results, but their deposition rates are approximately the same.

Thus it seems that no definite reaction mechanism can be proposed, since the thermodynamic data required to determine the species present and their concentrations is not available. The most reasonable explanation of the reactions would be the formation in the bulk of the solution of a nickel-hydrazine complex. This complex would diffuse to the substrate, react at the substrate via a short-lived intermediate and a two-electron transfer, the metallic

substrate acting as a sink for electrons, to produce nickel metal and products of hydrazine oxidation.

6.1.4. Bath decomposition.

The spontaneous decomposition of nickel solutions always takes place at the container walls, unlike the platinum group metals, which form metal powders in suspension. This is probably due to the fact that nickel does not form dimers in solution to produce the two-atom nuclei needed for powder production.

Although in 3.9 - 3.12, the results are reported as "decomposition on walls" and "decomposition on substrate", this is a rather oversimplified picture. Some solutions that have a low [ligand]:[metal] ratio will decompose on to the walls before the bath has reached temperature, while others with higher [ligand]:[metal] ratios will not decompose until nearly the end of the experimental run of two hours. Thus the heterogeneous reaction at the container walls appears to have kinetics of its own, and these have not been determined.

Bath decomposition seems to be represented by the following equation:

$$\frac{[L]_t}{[Ni]_{t\ crit}} \propto \frac{1}{\{H\}^2} \qquad (6.44.)$$

If $\frac{[L]_t}{[Ni]_t} \propto \frac{[L]_t}{[Ni]_{t\ crit}}$ decomposition will take place on the substrate only during a two-hour experimental run. This critical ratio is an order of magnitude higher for the malonate ion than the tartrate ion.

There seems to be a minimum concentration of hydrazine required. Another feature of bath decomposition is that very small concentrations of substances like thiourea can slow the kinetics of decomposition reactions very markedly. Concentrations of 2 p.p.m.

have been reported as stabilisers (54). Thus the concentration of intermediate required to start deposition on glass must be small, to be affected by such a small concentration of stabiliser. A possible form of reaction at the glass surface is that the concentration of a nickel-hydrazine intermediate determines the rate of electron transfer to the intermediate to produce nickel metal. The rate of electron transfer at a glass substrate, which is an insulator, would be much lower, even if chemisorption of hydrogen took place, than the rate of electron transfer at a metal substrate. So decomposition on to glass would only occur when decomposition on to metal takes place quickly. This happens to be the case in this work, except for the effect of hydrazine concentration on bath decomposition. Why there is a minimum concentration of hydrazine of 0.85 M, i.e. a ratio of $[Ni]_t : [N_2H_4]_t$ of 1 : 40, is inexplicable. Complexes between nickel ions and hydrazine would have formed and taken up all the nickel, at much lower [ligand] : [metal] ratios than 40 : 1.

6.2. Presence of hydrogen in the deposited metal.

The lattice parameter of the nickel deposited has been measured as 3.5282 ± 0.001 A°, compared with the value of 3.5238 A° (61) for pure nickel. This discrepancy suggested that some gas had entered the nickel lattice and had extended the lattice parameter. To test this hypothesis, palladium was deposited as outlined in 4.2. The deposition of palladium on to a catalytic substrate is a slow reaction, similar to the deposition of nickel. If the lattice parameter of this palladium is increased, it shows the solubility of hydrogen in the palladium, since hydrogen dissolves easily in palladium and affects the lattice parameter, while nitrogen is sparingly soluble in palladium at room temperature. The results,

shown in Fig. 4.2, show that palladium, deposited on to a catalytic substrate, has a lattice parameter of 3.8962 ± 0.001 A^{o}, compared with the lattice parameter of pure palladium of 3.8907 A^{o} (61). In addition, the lattice parameter of palladium, produced by a homogeneous reaction with hydrazine, was found to be 3.8893 ± 0.001 A^{o}, as shown in Fig. 4.2. This is in good agreement with the lattice parameter of pure palladium.

The palladium-hydrogen system has been one of the most studied metal-gas systems. Work by Owen and Jones (92) at 100°C., on the lattice parameters of palladium alloys, charged with hydrogen, showed that there were two phases, α - Pd and β - Pd. α - Pd was formed at low hydrogen pressures, as a dilute solution of hydrogen in the pure palladium lattice, while β - Pd was a separate phase with an f.c.c. structure, the lattice parameter being extended by about 3%. Their results are shown in Fig. 6.4. Later work by Maeland and Gibb (93) showed that the addition of hydrogen to palladium gave the α - and β - phases, except at temperatures above 300°C., where there was a continuous increase in the lattice parameter of α - Pd up to values of 3.997 A^{o}. These results are shown in Fig. 6.5.

For the palladium-hydrogen system at temperatures near room temperature, the following structural changes can be noted with increasing hydrogen concentration:

a) For hydrogen concentrations from zero up to $[H]:[Pd] \sim 0.015$ (94) the lattice parameter increases gradually from 3.890 to 3.893 - 3.895 A^{o}.

b) For hydrogen concentrations from $[H]:[Pd] \sim 0.015$ to $[H]:[Pd] \sim 0.58$ (95), the α - phase exists with the β - phase which has a lattice parameter of 4.025 A^{o} (95 - 97).

c) At higher concentrations of hydrogen, the α - phase disappears and a single β - phase structure remains. The lattice parameter increases to 4.040 A^{o} at $[H]:[Pd] \sim 0.7$ (95), which corresponds to the

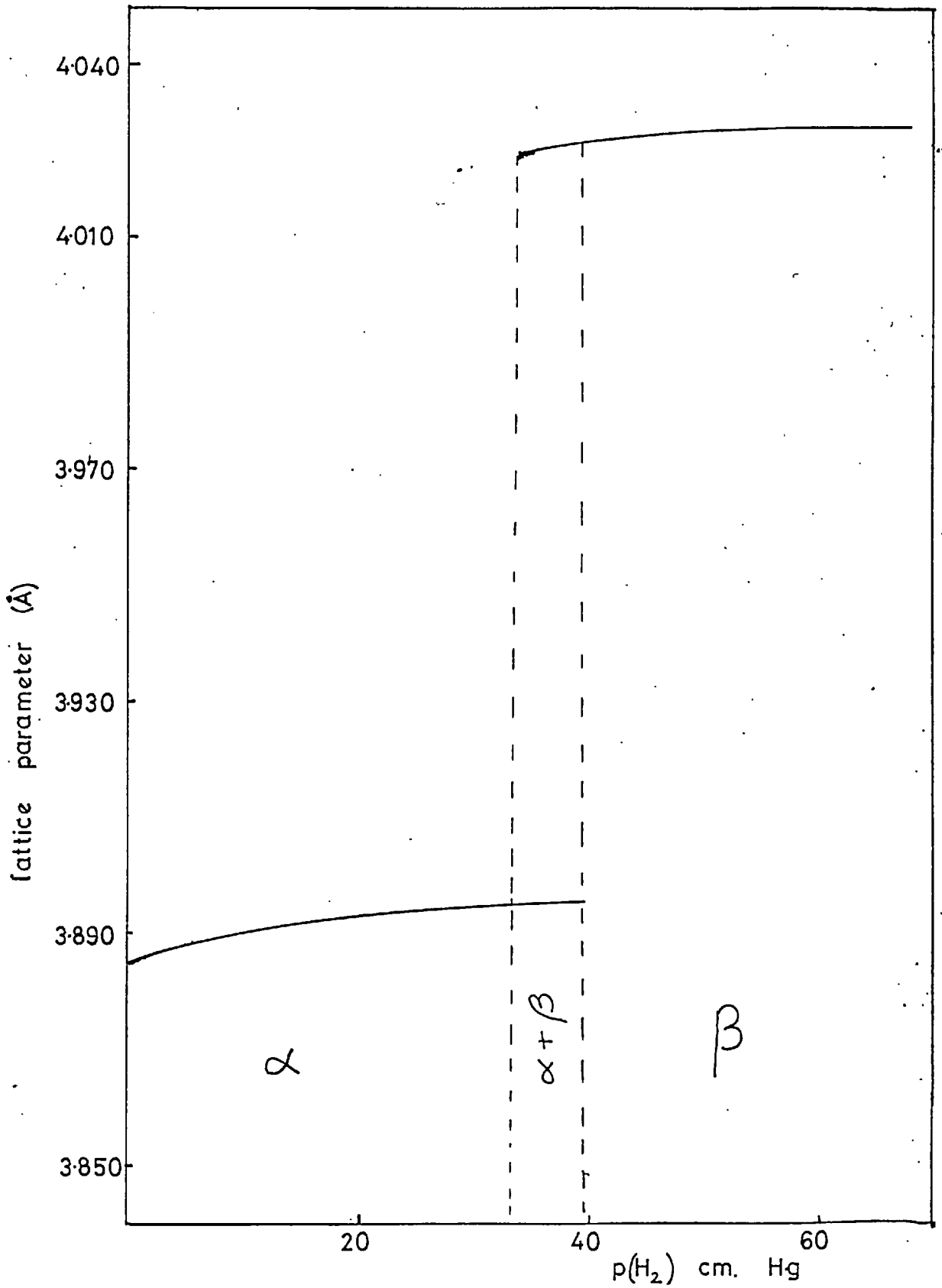

FIG 6.4 LATTICE PARAMETERS OF THE PALLADIUM-HYDROGEN SYSTEM AT 100°C AFTER OWEN AND JONES (92)

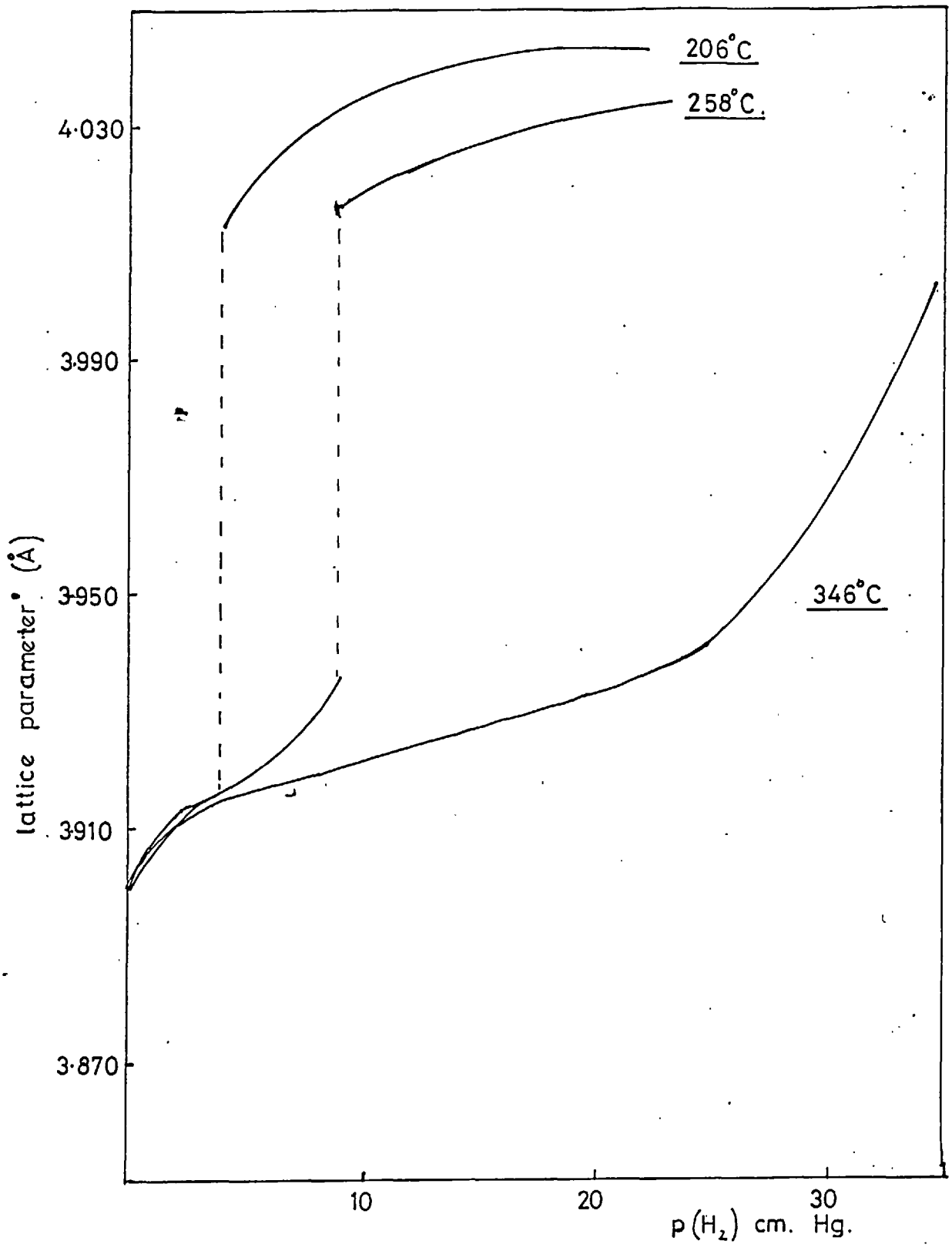

FIG. 6.5 ISOTHERMS IN THE PALLADIUM - HYDROGEN SYSTEM AFTER MAELAND AND GIBB (93)

hydrogen content of palladium in equilibrium with 1 atm. H_2. With even higher concentrations of hydrogen, lattice parameters as high as 4.08 A^o have been measured (98).

From this, it can be seen that the palladium deposited heterogeneously, is an α - phase solid solution of hydrogen in palladium with a hydrogen content [H]:[Pd] of approximately 0.015.

The system nickel-hydrogen shows similarities to the palladium-hydrogen system. There is evidence of an f.c.c. hydride of nickel similar to the β- phase in the palladium-hydrogen system. For this β- nickel, the lattice parameter has been measured as 3.70 A^o (99), 3.71 - 3.735 A^o (100) and 3.721 A^o (101). All these nickel hydrides were formed by the electrolytic charging of nickel with hydrogen. The [H]:[Ni] ratio was given as approximately 0.8 (101). The β - phase in the nickel-hydrogen system is, however, unstable at room temperature (102). Work on the position of hydrogen in the β- phase palladium-hydrogen alloy (103) showed that the hydrogen occupied octahedral sites and a similar occurrence in the nickel-hydrogen β - phase has been noted (102).

From these similarities between the behaviour of both nickel and palladium with hydrogen, it is suggested that the nickel deposited by hydrazine has hydrogen dissolved in it. The lattice parameter of 3.5282 $\pm$ 0.001 A^o, compared with 3.5238 A^o (61) for pure nickel, suggests that the nickel is in the α- phase, and, by analogy with palladium, has a maximum hydrogen content of [H]:[Ni] $\sim$ 0.015. The exact hydrogen content of the alloy is difficult to assess, but the estimate is near the maximum.

The work of Needes (62) on the reduction of nickel salts by hydrogen gas, showed that the lattice parameter of his nickel powder was 3.5236 - 3.5240 A^o. This was using pressures of 500 p.s.i. of hydrogen. From this, it is suggested that the hydrogen gas does not appreciably dissolve into nickel at moderate (100 - 250^{o}C.)

temperatures, and the mechanism of hydrogen dissolution in the foils of this work must be different. It is suggested that at the formation of nickel atoms at the substrate, hydrogen atoms are formed at the same time, by a similar electron transfer process. These atoms which are far more reactive than hydrogen molecules, attach themselves to the growing nickel lattice on the substrate. Evidence for this suggestion comes from the measurements of the lattice parameters of palladium produced at a substrate, which shows an increase, and palladium produced as powder, which is substantially pure palladium with no increase in lattice parameter.

6.3. Physical characteristics of the deposited metal.

The results of the electron probe microanalysis show that the nickel forms a layer on top of the copper substrate. There is no penetration of nickel into the copper, which would occur if the bonding between the coating and substrate were a diffusion bonding. Considering the temperature of deposition of about 90°C., significant diffusion of nickel into the copper should not be expected and, in fact, did not occur. Since the sections shown in plate 5.1. were prepared by cutting a transverse section, mounting and polishing, the adhesion between deposit and substrate was very strong, because there was no sign of the nickel peeling away from the copper. The deposit was uniform in thickness, and this suggests that there was a large number of nucleation sites on the polycrystalline copper substrate.

Plate (c) of the scanning electron micrographs of plate 5.2., shows a "roll" of nickel metal deposited on a catalytically activated glass substrate. Bending of thin foils because they have been stressed is a common occurrence, and was noted by Stoney (104) in nickel electrodeposits. It is suggested that this "roll" has occurred because the nickel metal has a high internal stress. Dini and Coronado (48) measured the stress in their nickel deposits, with

hydrazine as a reducing agent, as a tensile stress of 2100 kg. cm^{-2} which is high compared to the 112 kg. cm^{-2} of a proprietary hypophosphite bath. These authors attributed the internal stress to the high gas content of their nickel deposits. Since the hydrogen content of the nickel produced in this work was sufficient to alter the lattice parameter, it would seem reasonable to expect a highly stressed deposit. In the case of nickel deposited on to glass, rolling and peeling of the deposited metal away from the substrate was frequently noticed. For nickel deposited on to iron, stainless steel or copper, the deposits remained adherent, although occasionally cracked in appearance.

In previous work on the deposition of cobalt-phosphorus alloys (78) and on electroplated nickel-phosphorus alloy (105, 106), amorphous structures have been unambiguously produced. It has been suggested (107) that under practical conditions, the deposition during electroplating of nickel at a cathode requires an activation overvoltage (energy) due to a slow step in the process between:

$$Ni^{2+} + 2e^{-} \rightarrow Ni \qquad (6.45.)$$

and:

$$Ni \rightarrow Ni \text{ (in lattice)} \qquad (6.46.)$$

If there is not sufficient energy available to surmount the activation energy for the second step, the metal deposited is deposited in an amorphous state. For a complex alloy, such as the metastable nickel-phosphorus alloys, the activation energy of lattice formation is likely to be higher than for a pure metal. This analysis has been stated in terms of electroplating, but since the reaction involved in chemical plating is also an electron transfer process, the same reasoning can be used for chemical plating. As a mechanism to explain the occurrence of amorphous structures, this is more reasonable than one based on the deposits being supercooled liquids or glasses, as the temperatures of the deposition baths are less than $100^{o}C$.

Previous work on the hydrazine-reduced nickel by Levy (46) has shown that thin foils (100 A^{o} thick) had a crystallite size of 1000 A^{o}. One film showed an amorphous structure. Dini (48) found line broadening of X-ray diffraction patterns, consonant with a small grain size. This work, both in the thin films examined by electron diffraction and in the thicker films examined by pin-hole X-ray diffraction, found that the grain size was 10^{3} - 10^{4} A^{o}, with the thicker deposits having the larger grain size. Thus there seems general agreement that the product of reduction of nickel salts by hydrazine is a fine-grained polycrystalline nickel, with a grain size of about 1000 A^{o}. Work done on cobalt (53), produced by the hydrazine reduction of cobalt salts, gives a grain size of 200 A^{o}, somewhat smaller than the results for nickel.

The experiments to determine preferred orientations showed that all the nickel was in the form of randomly oriented polycrystals. This occurred on all substrates, whether single crystals or not, and for all thicknesses of deposit. In this work, solutions were sometimes made oxygen-free by bubbling nitrogen through but sometimes left in contact with air. In neither case did it have any effect on the orientation of the deposit.

According to the Pangarov theory (71), the only time when a thick deposit shows a random orientation is when the overvoltage is exceptionally high, while the occurrence of marked textures has been uncommon in chemically deposited metals. Indeed in the deposition on catalytic substrates of pure nickel or cobalt no textures have been reported. Deposition takes place at a surface which has a large number of discontinuities of structure (dislocations, impurity atoms etc.) and cannot be regarded as the flat defect-free structure of the theory. The solution carrying the metal ions is a turbulent, moving fluid where the ions have many different energies and possibilities of nucleation and growth. Thus theories that base

themselves on the uniform building up of layers of atoms separately cannot explain the growth of metal deposits. Marton and Schlesinger (9) found that, depositing nickel-phosphorus on to a palladium sensitised substrate, growth started from nuclei less than 10 A^{o} in diameter. These nuclei grew in three dimensions and the deposit was not continuous until it was 300 - 1000 A^{o} in thickness. In their work, the deposit grew in hemispheres, in three dimensions. In the present work, the surfaces have been examined under the scanning electron microscope (Plate 5.2.) and found to be fairly rough and curved in shape. This again seems more compatible with three-dimensional rather than two-dimensional growth.

CHAPTER 7 CONCLUSIONS

The reduction of nickel salts to nickel metal, using hydrazine, is a practical proposition for plating materials only in narrow ranges of reagent concentrations. Outside these ranges, there is either a very slow rate of reaction or the reduction will take place at any solid substrate. The rate of reaction is dependent on the chemical reaction at the substrate and not on the transport of reactants to the substrate. The probable mechanism of the reaction is the decomposition of a nickel-hydrazine complex at the substrate, with electron transfer forming nickel metal. Since the nickel ion forms complexes with hydrazine very readily and the concentration of free nickel ions is very low, it is highly improbable that a collision mechanism between nickel ions and hydrazine would be the reaction mode.

The nickel produced was substantially pure, with hydrogen as the main impurity. It seemed to be an α- solid solution of hydrogen in nickel, with a maximum hydrogen content of $[H]:[Ni] \sim 0.015$. Possibly because of the high gas content, the deposits appeared to be highly stressed. From the properties measured, it would not seem to be justified to use this method, instead of other methods of coating, such as the hypophosphite method or vapour deposition of very thin films. This is because of the difficulty of maintaining stable plating baths.

ACKNOWLEDGEMENTS

I would like to thank my supervisor, Dr. A.R. Burkin, for his help, advice and encouragement throughout the whole period of this work. I would also like to thank the technical staff for their help, especially Mr. J. Burgess, Mr. F. Huggins, Mr. P. Monk and Mr. J. Robertson. In the preparation of this thesis, I acknowledge the help of the photographic section of the department and the library staff, both of the department and the Lyon Playfair Library. I would like to thank my colleagues for useful discussions and helpful suggestions.

Financial support for the author came from the Science Research Council and Rolls-Royce Limited, who also granted leave of absence for this work. I am grateful for both.

Finally I wish to thank Miss Frances Webb for typing this thesis.

Department of Metallurgy,
Imperial College.

January 1970.

REFERENCES

1. Fisher R.D. and Chilton W.D. J. Electrochem. soc. (1962), 109, 485.
2. Brenner A. and Riddell G.E. J. Research. Nat. Bur. Standards. (1946), 37, 31.
3. Wurtz A. Compt. rend. (1845), 21, 149.
4. Paal C. and Friederici L. Ber. deut. chem. Ges. (1931), 64, 1766.
5. Latimer W.M.: "The Oxidation States of the Elements and their Potentials in Aqueous Solution"; 2nd edition, Prentice Hall, N.Y. (1962).
6. Krieg A.: "Symposium on Electroless Nickel Plating"; Spec. Tech. Publication 265, 21, A.S.T.M. Philadelphia (1959). Cited in ref. 10.
7. Marton J.P. and Schlesinger M. J. Electrochem. soc. (1968), 115, 16.
8. Goldenstein A.W., Rostoker W., Schlossberger F. and Gutzeit G. J. Electrochem. soc. (1957), 104, 104.
9. Marton J.P. and Schlesinger M. J. Phys. Chem. Solids (1968), 29, 188.
10. Graham A.H., Lindsay R.W. and Read H.J. J. Electrochem. soc. (1965), 112, 401.
11. Lang K. Metalloberfläche (1965), 19, 257.
12. Sullivan E.A. U.S. Patent (1960), 2 942 990
13. McLeod H.G. U.S. Patent (1962), 3 062 666
14. Stockmeyer W.H., Rice D.W. and Stephenson C.C. J. Am. Chem. soc. (1955), 77, 1980.
15. Winkler L. Draht, (1967), 18, 647.
16. Schlesinger H.I. and Brown H.C. U.S. Patent (1949), 2 461 661
17. Curtius Th. and Schrader F. J. Prakt. Chem. (2), (1894), 50, 311.

18. Jannek J. and Meyer J. Ber. deut. chem. Ges. (1913), 46, 2876.

19. Jannasch P. and Muller W. Ber. deut. chem. Ges. (1898), 31, 2393-4.

20. Gutbier A. Z. Anorg. Chem. (1902), 32, 106.

21. Montignie E. Bull. soc. Chim. France (4), (1932), 51, 127.

22. Gutbier A. Z. Anorg. Chem. (1902), 32, 51.

23. Jannasch P. and Stephan C. Ber. deut. chem. Ges. (1904), 37, 1980.

24. Jannasch P. and Muller W. Ber. deut. chem. Ges. (1904), 37, 2210.

25. Paal C. and Amberger C. Ber. deut. chem. Ges. (1907), 40, 1378.

26. Krauss F. and Mahlmann K. Z. Anorg. Allgem Chem. (1929), 184, 298.

27. Galatzky A. Bull. soc. Chim. France Memoires (5), (1935), 2, 1801.

28. Purgotti A. Ann. ist. super. agrar Partici (3), (1929), 3, 47. Cited in Chemical Abstracts, 25, 3259.

29. Davidoff C. U.S. Patent, (1966), 3 271 135.

30. Ivanov V.P. and Shestakov I.M. Zh. Prikl. Khim. (1961), 34, 1154.

31. Paal C. and Friederici L. Ber. deut. chem. Ges. (1932), 65, 19.

32. Sharov V.A. and Krylov E.I. Zh. Neorg. Khim. (1966), 11 (7), 1725.

33. Sharov V.A. and Krylov E.I. Zh. Prikl. Khim. (1967), 40 (1), 201.

34. Reveillaud R. French Patent (1958), 1 168 715.

35. Pearlstein F. Metal Finishing (1955), 53 (8), 59.

36. Rhoda R.N. and Madison A. U.S. Patent (1959), 2 915 406.

37. Singh I.P. Ph.D. Thesis, University of London (1968).

38. International Nickel Ltd. British Patent (1965), 994 560.

39. Rhoda R.N. and Vines R.F. British Patent (1967), 1 097 010.

40. Gostin E.L. and Swan S.D. U.S. Patent (1962), 3 032 436.

41. Levy D.J. French Patent (1965), 1 399 847.

42. Luce E.M. U.S. Patent (1967), 3 300 328.

43. Cwen J.T. U.S. Patent (1957), 2 801 935.

44. Bobtelsky M. and Jordan J. J. Am. Chem. soc. (1945), 67, 1824.

45. Barmashenko I.B. and Voronin M.M. Legka. Prom. Nauk - Tekn. Zb. (1963)(2), 16. Cited in Chemical Abstracts, 59, 8450e.

46. Levy D.J. Electrochemical Technology (1963), 1, 38.

47. Levy D.J. Unpublished work. Cited in D.J. Levy, 50th Ann. Tech. Proc. Amer. Electroplaters Soc. (1963), 29.

48. Dini J.W. and Coronado P.R. Plating (1967), 54, 385.

49. Latatnev V.I., Denisov A.D. and Peshkov O.L. Vestn. Mashinostr. (1964), 44, (8), 32.

50. Latatnev V.I., Denisov A.D., Kazakova V.P. and Peshkov O.L. Vysshikh. Uchebn. Zavednii Khim i Khim. Tekhnol. (1964), 7 (6), 973.

51. Koslova N.I. and Korovin N.V. Zh. Prikl. Khim. (1967), 40 (4), 902.

52. Koslova N.I. and Korovin N.V. Zh. Prikl. Khim. (1967), 40 (2), 446.

53. Takano O., Shiigata T. and Ishibashi S. Kinzoku Hyomen Gijitsu. (1967), 18 (8), 299. Cited in Chemical Abstracts 68, 15405.

54. Takano O., Shiigata T. and Ishibashi S. Kinzoku Hyomen Gijitsu. (1967), 18 (12), 466. Cited in Chemical Abstracts 68, 62135.

55. Levich V.G. "Physicochemical Hydrodynamics", Prentice-Hall, N.J. (1962).

56. Vogel A.I. "A Text-book of Quantitative Inorganic Analysis" 3rd ed. p. 479. Longmans, London (1961).

57. Sandell E.B. "Colorimetric Determination of Traces of Metals" 3rd ed. p. Interscience, N.Y.

58. Vogel A.I. "A Text-book of Quantitative Inorganic Analysis" 3rd ed. p. 380. Longmans, London (1961).

59. Thornton P.R. Scanning Electron Microscopy: Applications to materials and device science. Chapman and Hall, London (1968).

60. Taylor A. "X-ray Metallography" Wiley, N.Y. (1961).

61. Pearson W.B. "A Handbook of Lattice Spacings and Structures of Metals and Alloys", 2, Pergamon (1967).

62. Needes C.R.S. Ph.D. Thesis, University of London (1969).

63. Newman R.C. and Pashley D.W. Phil. Mag. (1955), 46, 917.

64. Newman R.C. Phil. Mag. (1957), 2, 750.

65. Grunbaum E. Proc. Phys. Soc. (London), (1958), 72, 459.

66. Pashley D.W. Adv. in Physics, (1965), 14, 327.

67. Schulz L.G. Acta Cryst. (1951), 4, 487.

68. Schulz L.G. Acta Cryst. (1952), 5, 130.

69. Pangarov N.A. J. Electroanal. Chem. (1965), 9, 70.

70. Matthews J.W. Phil. Mag. (1965), 12, 1143.

71. Pangarov N.A. Electrochim. Acta. (1962), 7, 139.

72. Pangarov N.A. Electrochim. Acta. (1964), 9, 721.

73. Bliznakov G. Ann. Rev. Polytech. (Sofia), (1950), 3, 187.

74. Pangarov N.A. and Rashkov S. Compt. rend. Acad. Bulgar. Sci. (1960), 13, 555.

75. Pangarov N.A. and Mihailova W. Dokl. Acad. Nauk SSSR, (1963), 153, 1117.

76. Rashkov S. and Pangarov N.A. Electrochim. Acta, (1969), 14, 17.

77. Evans D.M. and Wilman H. Acta Cryst. (1952), 5, 731.

78. Fisher R.D. and Koopman D.E. J. Electrochem. soc. (1964), 111, 263.

79. Frieze A.D., Sand R. and Weil R. J. Electrochem. soc. (1968), 115, 586.

80. Morton V. and Fisher R.D. J. Electrochem. soc. (1969), 116, 188.

81. Kakovsky I.A. 6me Congres International de la Preparation des Minerais 1963; Compte Rendu Scientifique Societe de l'Industrie Mineral. St. Etienne (1964).

82. Gutzeit G. Plating (1959), 46, 1158, 1275, 1377, (1960), 47, 63.

83. Moser Z. Rudy i. Metale Niezelazne (1967), 12, 507.

84. Schwarzenbach G. and Zobrist A. Helv. Chim. Acta (1952), 35, 1291.

85. Lefebvre J. J. Chim. Phys. (1957), 54, 601.

86. Bates R.G. and Canham A.G. J. Res. Nat. Bur. Standards (1951), 47.

87. Gelles E. and Nancollas G.H. J. Chem. Soc. (1956), 4847.

88. Cannan R.K. and Kibrick A. J. Am. Chem. Soc. (1938), 60, 2314.

89. Bjerrum J. "Metal Ammine Formation in Aqueous Solution", Haase, Copenhagen (1957).

90. Nair V.S.K. and Nancollas G.H. J. Chem. Soc. (1961), 4367.

91. Kirk B.E. and Browne A.W. J. Am. Chem. Soc. (1928), 50, 337.

92. Owen E.A. and Jones J.I. Proc. Phys. Soc. London (1937), 49, 603.

93. Maeland A.J. and Gibb T.R.P. J. Phys. Chem. (1961), 65, 1270.

94. Simons J.W. and Flanagan T.B. J. Phys. Chem. (1965), 69, 3581, 3773.

95. Aben P.C. and Burgers W.G. Trans. Faraday Soc. (1962), 58, 1989.

96. Axelrod S.D. and Makrides A.C. J. Phys. Chem. (1964), 68, 2154.

97. Maeland A. and Flanagan T.B. J. Phys. Chem. (1964), 68, 1419.

98. Andrews J.N. and Ubbelhode A.R. Proc. Roy. Soc. A, (1959), 253, 6.

99. Janko A. and Michel P. Comptes rend. (1960), 251, 1001.

100. Janko A. Bull. de l'acad. polon. des sciences ser. chim. (1960), 8, 131.

101. Boniszewski T. and Smith G.C. J. Phys. Chem. Solids (1961), 21, 115.

102. Wollan E.O., Cable J.W. and Koehler W.C. J. Phys. Chem. Solids (1963), 24, 1141.

103. Worsham J.E., Wilkinson M.K. and Schull C.G. J. Phys. Chem. Solids (1957), 3, 303.

104. Stoney G.G. Proc. Roy. Soc. A. (1909), 82, 172.

105. Brenner A., Couch D.E. and Williams E.K. J. Res. Nat. Bur. Stan. (1950), 44, 109.

106. Bagley B.E. and Turnbull D. J. Appl. Phys. (1968), 39, 5681.

107. Boldt J.R. and Queneau P. "The Winning of Nickel", Methuen, London, p. 345 (1967).

108. Cullity B.D. "Elements of X-ray Diffraction", Addison Wesley, London (1959).

109. Nelson J.B. and Riley D.P. Proc. Phys. Soc. (London), (1945), 57, 160.

110. Brandes H. J. Phys. Chem. (1927), 126, 196.

111. Stranski I.N. and Kaishev R. Z. phys. chem. (1934), B 26, 114.

Appendix 1 : List of symbols.

A	absorbance	
A_{hkl}	function in equation 5.1.	
B	line broadening (chap. 4.1.)	
B_o	measured line broadening	
B_{hkl}	function in equation 5.1.	
D	grain size (chap. 4.1.)	
D	diffusion coefficient (chap. 6.1.1.)	$cm^2\ sec^{-1}$
E_D	activation energy for diffusion	$k.cal.\ mole^{-1}$
E	activation energy for viscosity	k.cal. mole
I	rate of flow of fluid by convective diffusion	moles sec^{-1}
K_1	stability constant for A + L = AL	
L	ligand (either tartrate or malonate)	
L_i	length of edge i (appendix 3)	
M	metal	
M^{z+}	metal ion with z positive charges	
N	Avogadro number	
R	gas constant	
Re	Reynolds number	
T	absolute temperature	
V	volume of solution	
W_{hkl}	work needed to build two dimensional nucleus on plane (hkl)	
a	lattice parameter	
a_i	activity of species	
b	instrumental broadening	
d	interplanar spacing	
e^-	electron	
k, k_1	rate constant	

k_{-1}	reverse rate constant	
m	number of atoms in a gas molecule	
r	radius of disc	
β_n	stability constant of $A + nL = AL_n$	
ν	kinematic viscosity	$cm^2\ sec^{-1}$
κ_i	specific edge energy of edge i (appendix 3)	
$\overline{\psi}$	average work of separation of an atom from an edge row (appendix 3)	
ψ_i	work needed to separate an atom from its i th neighbour	
ψ_o	work needed to separate atom from substrate	
w	rotation speed	revs. min^{-1}
λ	wavelength	m or nm.
θ	Bragg angle	
μ	chemical potential of vapour above two-dimensional nucleus	
μ_o	chemical potential of vapour above infinite three-dimensional nucleus	
μ_{hkl}	chemical potential of vapour above infinite plane (hkl)	
ΔG	Gibbs free energy	
ΔG^o_T	standard free energy at temperature T	
(hkl)	the face of a crystal with Miller indices hkl	
[hkl]	direction in a crystal	
$\{H^+\}$	hydrogen ion activity given by: $pH = -\log \{H^+\}$	
[i]	concentration of species i	
$[Ni]_t$	total concentration of nickel	
$[Ni^{2+}]$	concentration of free nickel ion	
$[L]_t$	total ligand concentration	
$[N_2H_4]_t$	total hydrazine concentration	
$[mal]_t$	total malonate concentration	

$[tar]_t$	total tartrate concentration
$\left[\frac{d(Ni^o)}{dt}\right]^{11}$	rate of deposition of nickel metal per unit area of substrate moles sec^{-1} cm^{-2}
$-\left[\frac{d(Ni^{2+})}{dt}\right]^{11}$	rate of loss of all nickel species from solution per unit area of substrate moles $litre^{-1}$ $sec^{-1}cm^{-2}$
ϕ_i	work required to break bond between ith neighbour atoms.
ϕ_o	work required to break atom from substrate

Appendix 2 : The Nelson-Riley function

The values of θ obtained from the diffraction pattern may be used to calculate values of a_o from the Bragg equation:

$$\lambda = 2d \sin\theta \qquad (A2.1)$$

where d is based on the cell geometry.

For cubic structures:

$$\frac{1}{d^2} = \frac{h^2 + k^2 + l^2}{a_o^2} \qquad (A2.2)$$

The values of a_o obtained in this way are not constant but increase as θ approaches $\frac{\pi}{2}$, since the error Δa_o decreases as θ approaches $\frac{\pi}{2}$.

Errors arising from specimen absorption, film thickness, specimen eccentricity and beam divergence have been analysed (108). The contribution of each source of error has been analysed in terms of the Bragg angle(θ.) Error functions, thus obtained have the property that they tend to zero as θ tends to $\frac{\pi}{2}$. The most accurate function is due to Nelson and Riley (109):

$$F(\theta) = \frac{1}{2}\left(\frac{\cos^2\theta}{\theta} + \frac{\cos^2\theta}{\sin^2\theta}\right) \qquad (A2.3)$$

The precision of a_o obtained by linear extrapolation of a_o against $F(\theta)$ is claimed to be as good as 1 part in 10^5. For cases where there are 3 or less lines in the back-reflection region, the precision falls to 1 part in 10^4.

Appendix 3 : Two-dimensional nucleation theory.

The theory developed for the analysis of preferred orientations in electrodeposits by Pangarov (71) may be stated as follows:

Work of formation of a two-dimensional nucleus W_{hkl} of the lattice plane (hkl) os (110):

$$W_{hkl} = \frac{1}{2}\sum_i \kappa_i L_i \qquad (A3.1)$$

The equilibrium between the vapour and the two dimensional crystal formed on the face of a crystal, depends on the average work of separation, $\overline{\psi}$, of an atom out of an edge row, calculated from evaporation of that row. At equilibrium, the average work of separation must be the same for all edges of the two dimensional crystal. The form of the two dimensional nucleus depends on the condition that every atom on the periphery of the nucleus must be so strongly bonded with the other atoms, that its separation needs work at least equal to the average work of separation.

For the (100) plane of the f.c.c. lattice (Fig. A3.1), the work of separation of an atom at the periphery (shown shaded) is:

$$\psi^{o}_{(100)} = 2\phi_1 + 2\phi_2 + \phi_o \qquad (A3.2)$$

The equilibrium form of the two-dimensional nucleus will be an octagon with four type I edges and four type II edges (Fig. A3.1).

The average work of separation of one atom from a row of type I, $\overline{\psi}_I$, calculated by evaporation of this row is:

$$\overline{\psi}_I = \frac{2n_I\phi_2 + n_I\phi_1 + (n_I-1)\phi_1 + n_I\phi_o}{n_I} \qquad (A3.3)$$

$$= \psi^{o}_{(100)} - \frac{\phi_1}{n_I} \qquad (A3.4)$$

Similarly for type II edges:

$$\psi_{II} = \psi^{o}_{(100)} - \frac{\phi_2}{n_{II}} \qquad (A3.5)$$

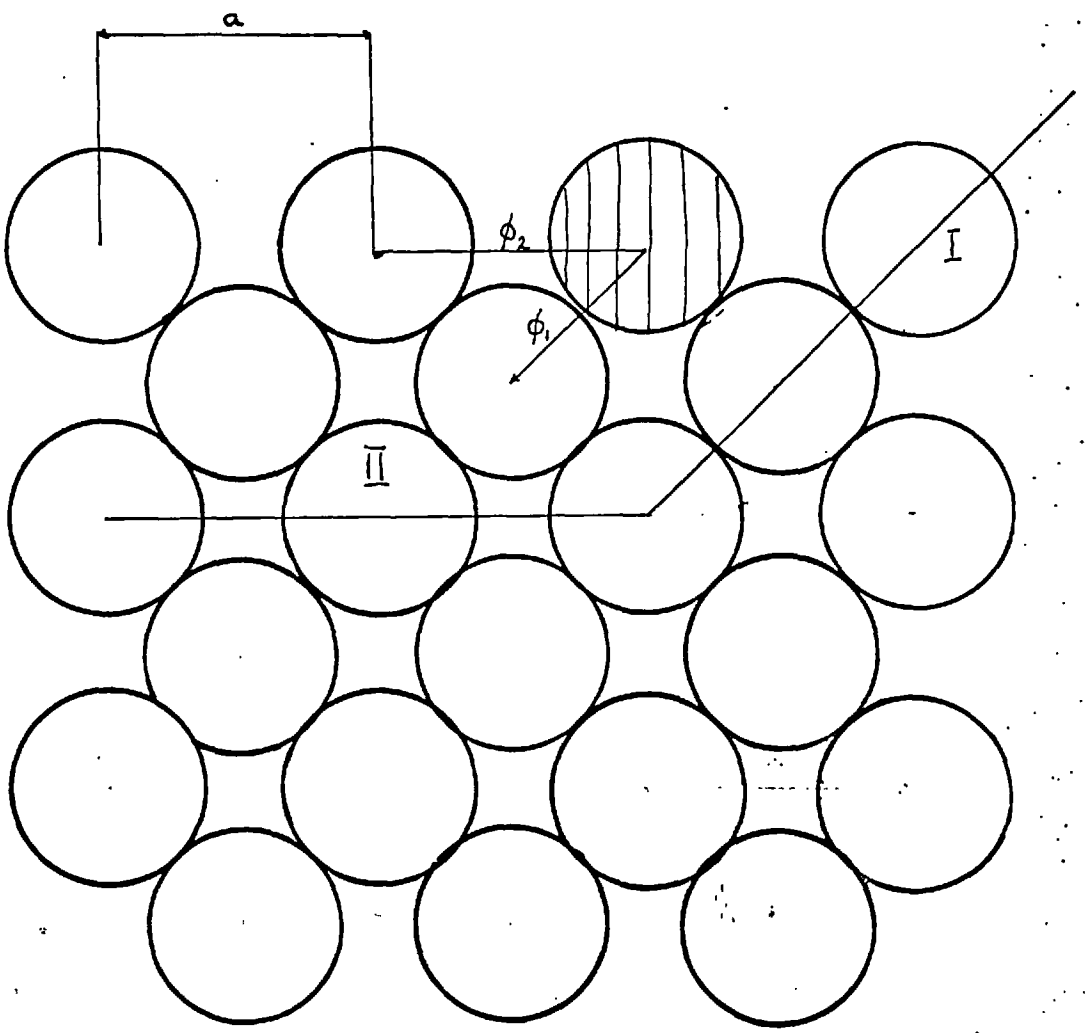

FIG A3.1 (100) TWO DIMENSIONAL NUCLEUS OF A FACE CENTERED CUBIC METAL (71)

The number of atoms in the edge rows may be calculated from a form of the Gibbs-Thomson equation (111):

$$\frac{1}{mN}(\mu - \mu_{hkl}) = \psi^{o}_{hkl} - \bar{\psi} \qquad \text{(A3.6)}$$

At equilibrium:

$$\bar{\psi}_{I} = \bar{\psi}_{II} \qquad \text{(A3.7)}$$

and

$$n_{I} = \frac{\phi_1}{\frac{1}{mN}(\mu - \mu_{100})} \qquad \text{(A3.8)}$$

and

$$n_{II} = \frac{\phi_2}{\frac{1}{mN}(\mu - \mu_{100})} \qquad \text{(A3.9)}$$

So the length of the edge rows will be:

$$L_{I} = \frac{a\phi_1}{\frac{\sqrt{2}}{mN}(\mu - \mu_{100})} \qquad \text{(A3.10)}$$

and

$$L_{2} = \frac{a\phi_2}{\frac{1}{mN}(\mu - \mu_{100})} \qquad \text{(A3.11)}$$

The specific edge energies are:

$$\kappa_1 = \frac{\phi_1 + 2\phi_2}{a\sqrt{2}} \qquad \text{(A3.12)}$$

$$\kappa_2 = \frac{2\phi_1 + \phi_2}{2a} \qquad \text{(A3.13)}$$

Substituting κ and L in (A3.1)

$$w_{100} = \frac{B_{100}}{\frac{1}{mN}(\mu - \mu_0) - \frac{1}{mN}(\mu_{100} - \mu_0)} \qquad \text{(A3.14)}$$

where $B_{100} = \phi_1^{2} + \phi_2^{2} + 4\phi_1\phi_2$

and μ_0 is the chemical potential of the vapour of an infinite three-dimensional crystal at equilibrium.

But:

$$\frac{1}{mN}(\mu_{100} - \mu_0) = \psi^{o} - \psi^{o}_{(100)} \qquad \text{(A3.15)}$$

$$= \Lambda_{100}$$

where $\psi^{o} = 6\phi_1 + 3\phi_2 + 12\phi_3$ and is the work of separation of an atom from the periphery of a three-dimensional f.c.c. crystal.

$$A s\psi^{o}_{100} = 2\phi_1 + 2\phi_2 + \phi_o \qquad (A3.2)$$

$$\underline{A_{100} = 4\phi_1 + \phi_2 + 12\phi_3 - \phi_o} \qquad (A3.16)$$

Thus for any crystal lattice Eq. 5. is obtained:

$$w_{hkl} = \frac{B_{hkl}}{\frac{1}{mN}(\mu - \mu_o) - A_{hkl}}$$

For different planes in the f.c.c. system B_{hkl} and A_{hkl} are as follows (71):

$A_{(100)} = 4\phi_1 + \phi_2 + 12\phi_3 - \phi_o$; $B_{(100)} = \phi_1^2 + \phi_2^2 + 4\phi_1\phi_2$

$A_{(110)} = 5\phi_1 + 2\phi_2 + 10\phi_3 - \phi_o$ $B_{(110)} = \phi_1\phi_2 + 2\phi_1\phi_3 + 2\phi_2\phi_3 + \phi_3^2$

$A_{(111)} = 3\phi_1 + 3\phi_2 + 12\phi_3 - \phi_o$ $B_{(111)} = 3\phi_1^2$

Appendix 4 : Specimen calculations.

a) Effect of varying nickel concentration.

Take $[Ni]_t = 0.01$, $\log K_1 = 2$, $[L]_t = 0.02$

$$K_1 = \frac{[NiL]}{[Ni^{2+}][L^{2-}]} = 10^2 \qquad (A4.1)$$

By iteration $[Ni^{2+}] = 4 \times 10^{-3}$ $[NiL] = 6 \times 10^{-3}$ and $[L^{2-}] = 14 \times 10^{-3}$

$$\underline{K_1 = 1.07 \times 10^{+2}}$$

This value for $[Ni^{2+}]$, 4×10^{-3} is plotted on Fig. 6.1.

Similar methods may be used to calculate the free nickel ion concentration at various values of $[Ni]_t$ and for various values of the stability constant K_1. These values are plotted on Fig. 6.1.

Considering the equilibrium:

$$Ni^{2+} + nN_2H_4 \rightarrow Ni.\ nN_2H_4^{\ 2+} \qquad (A4.2)$$

$$\beta_n = \frac{[Ni.\ nN_2H_4]}{[Ni^{2+}][N_2H_4]^n} \qquad (A4.3)$$

Assume a value of $\left[[Ni.\ nN_2H_4] + [Ni^{2+}] \right]$ of 4×10^{-3} from above, $[N_2H_4]_t = 1$ and a value of $\log \beta_1 = 2$, then

$$\frac{[Ni.\ N_2H_4]}{[Ni^{2+}]} = 100 \qquad (A4.4)$$

which means that for $[Ni^{2+}]$ plotted on Fig. 6.1. as 4×10^{-3} can be taken as equal to the concentration of $[Ni.\ N_2H_4]^{2+}$ without much error.

For the full $\log \beta_6 = 12$ and $n = 6$:

$$\frac{[Ni.\ 6N_2H_4]}{[Ni^{2+}]} = 10^{12} \qquad (A4.5)$$

and the error is much less.

In this analysis it is assumed that the hydrazine concentration of 1 M is all involved in the reaction of equation A4.2. This is not

so but even if all the NiL was complexed with the maximum of six hydrazine molecules, the free hydrazine concentration would be reduced to about 0.8 M as a minimum. If the value of 0.8 M is substituted in A4.4. the ratio $\frac{[Ni.nN_2H_4]}{[Ni^{2+}]}$ would be reduced to 80 and in A4.5. the ratio would be reduced to 2.6×10^{11}, so the error involved is negligible.

b) Effect of varying hydrazine concentration.

Take the case of $[Ni]_t = 0.02$ M, $[tar]_t = 0.02$ M then with $\log K_1 = 2$, the free nickel ion concentration will be 0.01 M from Fig. 6.1.

$$Ni^{2+} + nN_2H_4 = [Ni.\ nN_2H_4]^{2+} \qquad (A4.6)$$

$$\beta_n = \frac{[Ni.\ nN_2H_4]}{[Ni^{2+}][N_2H_4]^n} \qquad (A4.7)$$

For $\log \beta_1 = 2$ we have:

$$[N_2H_4]_t = 1 \qquad 100 = \frac{[Ni.\ nN_2H_4]}{[Ni^{2+}].\ 1}$$

$$\frac{[Ni.\ N_2H_4]}{[Ni^{2+}]} = 100 \qquad (A4.8)$$

$$[N_2H_4]_t = 3 \qquad \frac{[Ni.\ N_2H_4]}{[Ni^{2+}]\ 3} = 100$$

$$\frac{[Ni.\ N_2H_4]}{[Ni^{2+}]} = 300 \qquad (A4.9)$$

For $\log \beta_6 = 12$ then:

$$[N_2H_4]_t = 1 \qquad \frac{[Ni.\ 6N_2H_4]}{[Ni^{2+}]\ .\ 1^6} = 10^{12}$$

$$\frac{[Ni.\ 6N_2H_4]}{[Ni^{2+}]} = 10^{12} \qquad (A4.10)$$

$$[N_2H_4]_t = 3 \qquad \frac{[Ni.\ 6N_2H_4]}{[Ni^{2+}]\ 3^6} = 10^{12}$$

$$\frac{[Ni.\ 6N_2H_4]}{[Ni^{2+}]} = 7 \times 10^{14} \qquad \text{(A4.11)}$$

A4.7 - A4.11 show that for a constant $[Ni]_t$ and $[tar]_t$, the concentration of nickel-hydrazine complex may be regarded as constant, since practically all the free nickel ion from (A4.1) is converted into complex.

c) Effect of varying malonate concentration.

Take $[Ni]_t = 0.005$ M , $\log K_1 = 3$ and $[L]_t = 0.05$

$$K_1 = \frac{[NiL]}{[Ni^{2+}][L^{2-}]} \qquad \text{(A4.12)}$$

By iteration $[Ni^{2+}] = 1 \times 10^{-4}$ $[NiL] = 49 \times 10^{-4}$

and $[L^{2-}] = 451 \times 10^{-4}$

then $K_1 = 1.08 \times 10^3$

Similar calculations can be done to calculate the free nickel ion concentrations at various values of $[L]_t$ and for various values of the stability constant K_1. These values are plotted on Fig. 6.3.